Mines and Minerals Division

Ontario Geological Survey
Open File Report 5689

Ontario Geoscience Research Grant Program

Grant No. 193

Geological Setting, Structure and Alteration Associated With Gold - Pyrite Mineralization in Mafic Volcanic Rocks at Cameron Lake, Wabigoon Subprovince, Northwestern Ontario

1988

Ontario

Ministry of
Northern Development
and Mines

©Queen's Printer for Ontario 1988
Printed in Ontario, Canada

MINES AND MINERALS DIVISION

ONTARIO GEOLOGICAL SURVEY

Open File Report 5689

Ontario Geoscience Research Grant Program
Grant No. 193

Geological Setting, Structure, and Alteration Associated With Gold-Pyrite Mineralization in Mafic Volcanic Rocks at Cameron Lake, Wabigoon Subprovince, Northwestern Ontario

by

D.R. Melling

1988

Parts of this publication may be quoted if credit is given. It is recommended that reference to this publication be made in the following form:

Melling, D.R.

1988: Ontario Geoscience Research Grant Program, Grant No. 193, Geological Setting, Structure, and Alteration Associated With Gold-Pyrite Mineralization in Mafic Volcanic Rocks at Cameron Lake, Wabigoon Subprovince, Northwestern Ontario; Ontario Geological Survey, Open File Report 5689, 112 p., 24 figures, 7 plates, 3 tables, and 4 appendices.

Ontario
Ministry of
Northern Development
and Mines

Ontario Geological Survey

OPEN FILE REPORT

Open File Reports are made available to the public subject to the following conditions:

This report is unedited. Discrepancies may occur for which the Ontario Geological Survey does not assume liability. Recommendations and statements of opinions expressed are those of the author or authors and are not to be construed as statements of government policy.

This Open File Report is available for viewing at the following locations:

(1) Mines Library
Ministry of Northern Development and Mines
8th floor, 77 Grenville Street
Toronto, Ontario M7A 1W4

(2) The office of the Regional or Resident Geologist in whose district the area covered by this report is located.

Copies of this report may be obtained at the user's expense from a commercial printing house. For the address and instructions to order, contact the appropriate Regional or Resident Geologist's office(s) or the Mines Library. Microfiche copies (42x reduction) of this report are available for $2.00 each plus provincial sales tax at the Mines Library or the Public Information Centre, Ministry of Natural Resources, W-1640, 99 Wellesley Street West, Toronto.

Handwritten notes and sketches may be made from this report. Check with the Mines Library or Regional/Resident Geologist's office whether there is a copy of this report that may be borrowed. A copy of this report is available for Inter-Library Loan.

This report is available for viewing at the following Regional or Resident Geologists' offices:

All Resident Geologists' Offices

The right to reproduce this report is reserved by the Ontario Ministry of Northern Development and Mines. Permission for other reproductions must be obtained in writing from the Director, Ontario Geological Survey.

V.G. Milne, Director
Ontario Geological Survey

ONTARIO GEOSCIENCE RESEARCH GRANT FUND

Final Research Report

Foreword

This publication is a final report of a research project that was funded under the Ontario Geoscience Research Grant Program. A requirement of the Program is that recipients are to submit final reports within six months after termination of funding.

A final report is designed as a comprehensive summary stating the findings obtained during the tenure of the grant, together with supporting data. It may consist, in part, of reprints or preprints of publications and copies of addresses given at scientific meetings.

It is not the intent of the Ontario Geological Survey to formally publish the final reports for wide distribution, but rather to encourage the recipients of grants to seek publication in appropriate scientific journals whenever possible. The Survey, however, also has an obligation to ensure that the results of the research are made available to the public at an early date. Although final reports are the property of the applicants and the sponsoring agencies, they may also be placed on open file. This report is intended to meet this obligation.

No attempt has been made to edit the report, the content of which is entirely the responsibility of the author(s).

V.G. Milne
Director
Ontario Geological Survey

Table of Contents.

		Page
	Contents	vii
	List of Figures	ix
	List of Tables	xv
	List of Plates	xv
	List of Appendices	xv
	Acceptance Sheet	xvii
	Acknowledgements	xix
	Abstract	xxiii
1.0	Introduction	1
2.0	Regional Geological Setting and Its Influence on Gold Mineralization	4
3.0	Local Geology of The Cameron Lake Property	9
4.0	Deposit Structure	15
	4.1 Shear Zone Structure	15
	4.2 Vein Geometry and Paragenesis	21
	4.3 Ore Deposit Geometry and Gold Distribution	24
	4.4 Structural Interpretation	29
5.0	Alteration of Basaltic and Gabbroic Rocks	37
	5.1 Petrography of Sulfide Minerals in The Altered Rocks	41
6.0	Lithogeochemistry	48
	6.1 Sampling and Analytical Proceedures	48
	6.2 Interpretation of Results	49
7.0	Discussion	58
	7.1 Significance of The Cameron Lake Shear Zone	58
	7.2 Structural Control of The Cameron Lake Deposit	59
	7.3 Alteration in Gold-bearing Rocks	61
	7.4 Gold Transport and Precipitation	63
	7.5 Model For Gold Precipitation At Cameron Lake	64
8.0	Conclusions	66
9.0	Selected Bibiliography	68
	Appendix 1	77
	Appendix 2	87
	Appendix 3	90
	Appendix 4	107

List of Figures.

		Page
1.	Location of the Cameron Lake gold deposit (star) within the Wabigoon Subprovince of northwestern Ontario and the distribution of supracrustal rocks (modified after Blackburn et al., 1985).....	2
2.	Geology of the Kakagi-Cameron-Rowan Lakes area and the location of the Cameron Lake deposit. A - A' and B - B' stratigraphic sections are shown in Figure 3.....	Pocket
3.	Stratigraphic sections from the Cameron-Rowan Lakes area. See Figure 2 for the location of the sections.....	7
4.	Jensen cation plot of samples taken from the Cameron-Rowan Lakes area. Open symbols and closed symbols represent the Rowan Lake and Cameron Lake Volcanic successions respectively. Squares are basaltic rocks, diamonds are pyroclastic rocks, triangles are mafic intrusions, and circles are quartz-feldspar porphyry dikes and sills.....	8
5.	Geology of the Cameron Lake property (modified after Hunter, 1981).....	10
6.	Local geology of the Cameron Lake gold deposit. Letters refer to: Discovery outcrop (A), North trench (B), Vic's trench (C), and NC-19 trench (D).....	Pocket
7.	Equal area stereographic projections of structural data from the Cameron Lake deposit. Contours represent percentage of points per 1% unit area. (A) Poles to cleavage, Cameron Lake Shear Zone; great circle represents the mean. (B) Poles to cleavage, North trench splay; great circle represents the mean. (C) Lineations, Cameron Lake Shear Zone; great circle represents mean cleavage from (A). (D) Poles to type 3 vein orientations; great circle represents the mean.	16
8.	Diamond drill cross-section A - A', 3+50 E.....	Pocket
9.	Diamond drill cross-section B - B', 0+50 E.....	17
10.	Diamond drill cross-section C - C', 2+50 W.....	Pocket
11.	Diamond drill cross-section D - D', 4+50 W.....	Pocket
12.	Level plan datum 0+00.....	18

13. Frequency versus gold assay histogram plot of assay data from the Cameron Lake deposit. Two distinct gold-bearing rock types are present: pyritiferous, deformed altered basaltic rocks (0.08 to 0.19 oz/ton Au) and breccia-veins (greater than 0.19 oz/ton Au)..... 26

14. Longitudinal section dipping 65° N from the baseline. Contours represent the value of grade times thickness (eg. 0.2 oz/ton Au over 50 feet = 10). The contours are based on approximately 75 drill hole piercing points..... 28

15. Simplified stereographic projection illustrating the coincidence of the pitch of the ore shoots with the line of intersection of the Cameron Lake Shear Zone and bedding-controlled shear zone splays..... 31

16. Diagramatic representation of the spatial relationship between gold zones and the northwest striking Cameron Lake Shear Zone and the northeast to east striking bedding-plane splays..... 31

17. Schematic diagram of Cameron Lake Shear Zone illustrating the paragenesis of vein formation in relation to progessive deformation. (17a) Type 1 en-echelon extension veins. (17b) The inital buckling of the type 1 veins and the initiation of irregular and multi-plane fractures parallel to the shear zone boundaries. (17c) Dilation of the type 2 veins in response to incremental displacement along the cracks and subsequent rock bursts due to extreme fluid pressure differentials. (17d) Close-up view of a portion of a breccia-vein formed in 17c. CO_2 effervesces as the hydrothermal fluid depressurizes upon entering the vein. Gas bubbles adhere to the breccia fragments and coalesce during rapid ascent. (17e) Further buckling of the type 1 veins, intensification of cleavage along the type 2 breccia-veins, and the initiation of the type 3 veins during the waning stages of deformation..... 33

18. Alteration assemblage profiles from DDH NC-29 illustrating the spatial relationships between hydrothermal alteration and deformation at Cameron Lake. Data correspond to X-ray diffraction peak heights normalized to quartz. Absolute peak heights for quartz are used. Shear zone boundaries are indicated by the fault symbols. The gold-bearing zone is centred on 500 ft. In conjunction with core logging and petrography, four symmetrical alteration zones are defined based on these data. The assemblages characteristic of these zones include: 1) Quartz-albite-chlorite-calcite-ankerite-epidote-actinolite, 2) Quartz-albite-ankerite-sericite-chlorite-calcite-rutile 3) Quartz-albite-ankerite-sericite-siderite-chlorite-pyrite-rutile, 4) Quartz-albite-ankerite-ankerite-sericite-siderite-pyrite-rutile. The

latter assemblage is spatially associated with pyritic, quart-albite breccia-veins. Within the gabbroic rocks Fe-rich magnesite is developed in contrast to the Mg-rich siderite in the basalts. Dots correspond to sample locations. Quartz = Qtz, Albite = Ab, Chlorite = Chl, Calcite = Cal, Ankerite = Ank, Siderite = Sd, Sericite = Ser. Mineral abbreviations after Kretz (1983)..... 40

19. Jensen cation plot of samples taken from the Cameron Lake deposit. Half filled squares are weakly altered basalt, solid squares are pervasively altered basalts and diamonds are breccia-veins. Triangles are gabbro, and circles are quartz-feldspar porphyry dikes..... 50

20. Lithogeochemical profiles for samples taken from DDH NC-29 and breccia veins at surface which illustrate the broad alteration envelopes which surround the gold deposit and the dilution effect of silica in the breccia-veins. Analyses of major oxides recalculated to 100% (volatile free)..... 52

21. Scatter plots of geochemical data from the Cameron Deposit. (A) CO_2 against Log Au. (B) CO_2 against S. (C) CO_2 against K_2O. (D) CO_2 against CaO. (E) SiO_2 against CO_2. (F) CO_2 against Fe_2O_3. (G) SiO_2 against Na_2O. (H) SiO_2 against K_2O. Half filled squares are weakly altered basalt, solid squares are pervasively altered basalts. Diamonds are breccia-veins, circles are quartz-feldspar porphyry dykes, and triangles are gabbros. Fields are specified for weakly altered basalts (light dots), pervasively altered basalts (dark dots), and breccia veins (crosses)..... 55

22. Schematic diagram of a hypothetical shear zone where metamorphic fluid derived from mineral dehydration reactions are focused during movement to higher levels within the crust. Gold deposition is likely to occur in the region A - B where the fluid enters chemically favorable host rocks. Such a model could apply to the Cameron Lake deposit (modified after Fyfe and Henley, 1973)..... 65

23. Location map of regional lithogeochemical sampling sites..... Pocket

24. Location map of lithogeochemical sampling sites from trench workings..... 108

List of Tables.

		Page
I.	Petrographic summary of least altered basaltic rocks.....	14
II.	Classification of principal vein types in the Cameron Lake deposit.....	22
III.	Summary of sulfide petrography: mineralogy, and textures...	43

List of Plates.

1.	Photographs of polished core samples representing the major stratigraphic units encountered in drilling at Cameron Lake	93
2.	Photographs of polished core samples and slabs of altered rocks and breccia-veins encountered in drilling and on surface at Cameron Lake.....	96
3.	Photographs of deformed rocks and vein types exposed in the excavated outcrops at Cameron Lake.....	98
4.	Photomicrocraphs of altered basaltic rocks in thin section.	100
5.	Photomicrographs of sulfides, oxides and gold in polished section.....	102
6.	Photomicrographs of deformation textures in sulfides in polished section.....	104
7.	Photomicrographs of deformation textures, rutile, and an inclusion in a quartz-feldspar porphyry dyke.....	106

List of Appendicies.

I.	Analytical data for samples taken from the Cameron-Rowan Lakes area.....	77
II.	Detection limits and methods of chemical analyses.....	87
III.	Plates 1, 2, 3, 4, 5, 6, and 7.....	90
IV.	Analytical data for samples taken from DDH NC-29 and breccia-veins on surface.....	107

The undersigned recommend to the Faculty

of Graduate Studies and Research

acceptance of the thesis

"Geological Setting, Structure and Alteration Associated With Gold-Pyrite Mineralization in Mafic Volcanic Rocks at Cameron Lake, Wabigoon Subprovince, Northwestern Ontario"

submitted by David Rigby Melling, B.Sc.,

in partial fulfilment of the requirements

for the degree of Master of Science.

.....
Thesis Supervisor

.....
Thesis Supervisor

.....
Chairman, Department of Geology

Carleton University

April 9, 1986

Acknowledgements.

I wish to thank Mr. H.D. Hume and Mr. G.F. Archibald of Nuinsco Resources Limited for allowing this study to be undertaken and providing unrestricted access to data on the Cameron Lake gold deposit. Mr. A.D. Hunter suggested this project and provided valuable insight into the geology of the area.

I am indebted to Dr. L.B. Chorlton, Dr. H.K. Poulsen, and Dr. D.H. Watkinson for guiding this research. Throughout this study they provided assistance, encouragement, and quick critical reviews of my work. Grateful appreciation is extended to Mr. C.E. Blackburn (Ministry of Northern Development and Mines, Resident Geologist, Kenora) for visiting the field area and initiating lively discussions.

Thanks are due to Mr. V. Petrie and Mr. L. Tomalty for providing the excavated exposures of the deposit. Assistance and discussions with Mr. M. Bucke, Mr. P.L. Jones, and Mr. M. Wade in the field have helped with the geological interpretation of the area. Mr. R. Westendorp was an amiable and conscientious field assistant.

Enlightening discussions were held with many of my fellow graduate students, principally among them Ms. S. Carr, Dr. L.S. Lane, Dr. D. Murphy, and Mr. C.E. Rees. They made significant contributions to my understanding of deformation mechanisms and shear zone kinematics. Ms. S.V. Thompson of the Geological Survey of Canada performed the X-ray diffraction analysis, and Mr. P.C. Jones of Carleton University completed numerous electron microprobe analyses.

This project was financially supported by Ontario Geoscience Research Grant Award 193 to Dr. D.H. Watkinson and through the generosity of Nuinsco Resources Limited.

It is with deep gratitude that I acknowledge the contribution of my wife Fay; her encouragement, love, and patience have made this possible.

Abstract

The Cameron Lake gold deposit is an epigenetic, structurally-controlled, vein-type deposit which occurs in deformed metabasaltic rocks of the Cameron Lake Shear Zone. The deposit occurs within a mixed succession of tholeiitic flows and calc-alkaline pyroclastic rocks of the Cameron Lake Volcanics near the transition from the stratigraphically lower, tholeiitic subaqueous flow succession of the Rowan Lake Volcanics. The Cameron Lake Shear Zone is a discordant, brittle-ductile system which exhibits evidence of dextral, strike-slip shear.

The shear zone consists of several branches which form both anastamosing and **en echelon** shears whose orientations are in part controlled by lithologic anisotropies. The pitch of the deposit appears to be controlled by the intersection of bedding-controlled sympathetic splays with the Cameron Lake Shear Zone. The paragenesis and geometry of veins, and mechanics of their formation are all related to deformation in the enveloping shear zone.

Four distinct, symmetrical zones of hydrothermal alteration envelop the deposit. From the least altered metabasaltic rocks inward, these alteration assemblages include:

(1) Quartz-albite-chlorite-calcite-ankerite-epidote-actinolite-magnetite;
(2) Quartz-albite-ankerite-sericite-chlorite-calcite-rutile;
(3) Quartz-albite-ankerite-sericite-siderite-chlorite-pyrite-rutile;
(4) Quartz-albite-ankerite-sericite-siderite-pyrite-rutile.

The latter assemblage is spatially associated with pyritic, quartz-albite breccia-veins which contain the greatest gold concentrations.

The alteration is chemically expressed by the addition of major amounts of CO_2, K, Ca, and S, and minor amounts of Ag, As, Au, B, Hg, Rb, Sr, and W to the metabasalts. Carbonatization and sericitization appear to have occurred early, followed by sulfidation and gold precipitation.

Geological Setting, Structure, and Alteration Associated With Gold-Pyrite Mineralization in Mafic Volcanic Rocks at Cameron Lake, Wabigoon Subprovince, Northwestern Ontario.

by

David Rigby Melling, B.Sc.

A thesis submitted to the Faculty of
Graduate Studies and Research in partial
fulfilment of the requirements for the degree of
Master of Science

Department of Geology

Carleton University
Ottawa, Ontario
April 9, 1986

© copyright

1986 David R. Melling

Manuscript approved for publication by V.G. Milne, Director, Ontario Geological Survey, July 8, 1988.

This report is published with the permission of V.G. Milne, Director, Ontario Geological Survey, Toronto.

1.0 Introduction.

The Cameron Lake gold deposit is located in northwestern Ontario about 80 km southeast of Kenora (Latitude 49° 17'N, Longitude 94° 44'W) (Figure 1). It was originally discovered in 1960 by two prospectors working for Noranda Mines; however, low gold prices at that time as well as the complex subsurface geometry (drill-indicated) and poor outcrop exposure, discouraged investment and development. Four separate diamond drilling programs were conducted on the property prior to the discovery of a major gold zone in 1983 by Nuinsco Resources Limited. Proven reserves presently total 1,625,202 short tons grading 0.16 oz/ton Au, including 1,006,704 short tons grading 0.20 oz/ton Au (Archibald, 1985). Complete and colourful histories of mining in the Kenora-Fort Frances region and exploration in the vicinity of Cameron Lake are given by Beard and Garret (1976) and Hunter (1985), respectively.

Sparked by the spectacular rise in the price of gold during the last decade and recently depressed base metal prices, precious metal exploration has been the focus of the mining industry since the late 1970's. Accordingly, research on the origin of Canadian Archean lode gold deposits has increased dramatically, resulting in several volumes devoted to their genesis (Pye and Roberts, 1981; Petruk and Hodder, 1982; Colvine, 1983; Colvine et al., 1984). Although several workers have characterized the gold occurrences in the Kenora-Fort Frances region (Blackburn, 1982; Blackburn and Janes, 1983; Mackasey et al., 1974; Poulsen, 1983; Thompson, 1935; Trowel et al., 1980), few detailed studies have focused directly on descriptive and genetic models of gold emplacement in this promising region. Before this study began, the

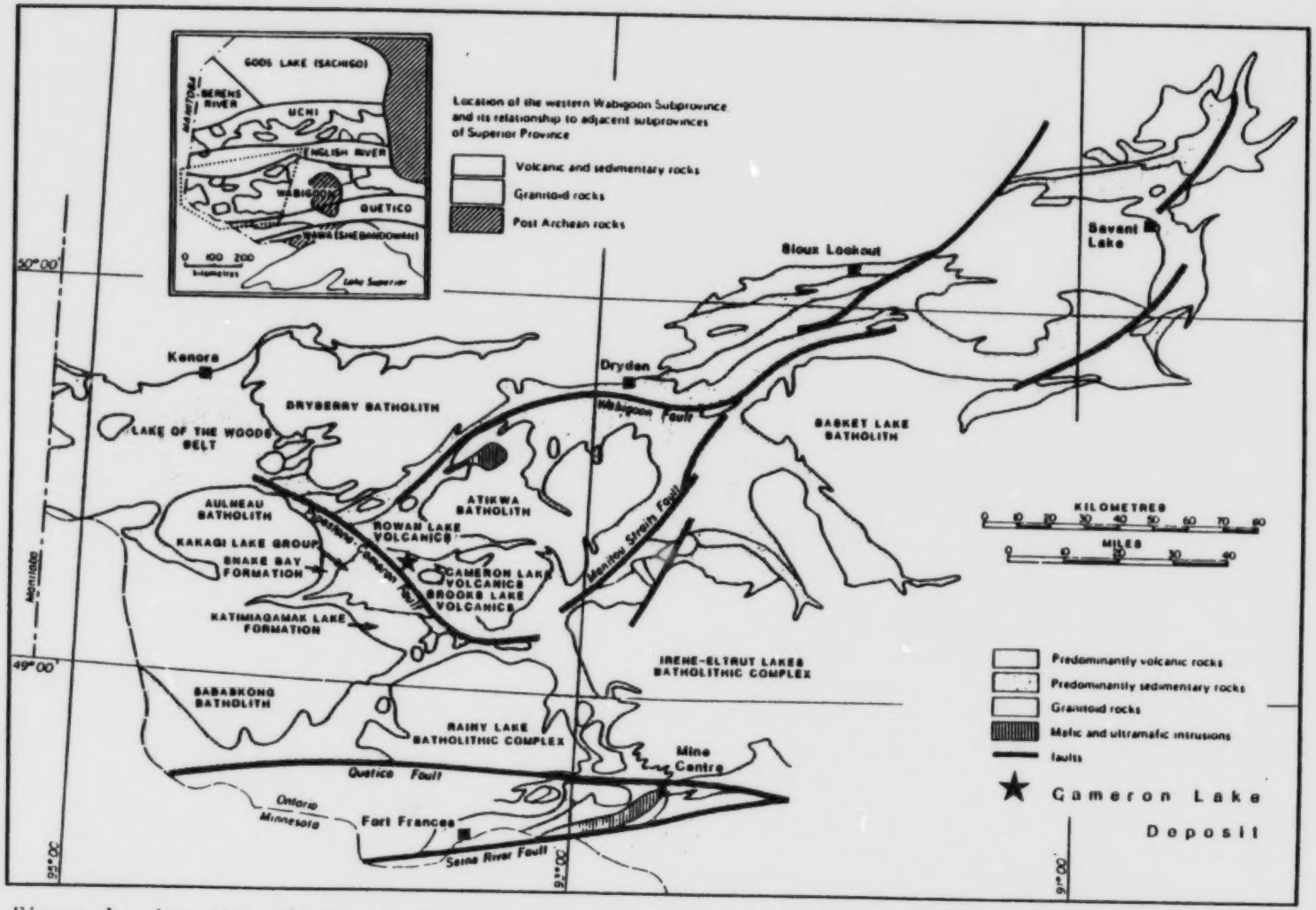

Figure 1. Location of the Cameron Lake gold deposit (star) within the Wabigoon Subprovince of northwestern Ontario and the distibution of supracrustal rocks (modified after Blackburn et al., 1985).

genetic model favored for the origin of gold enrichment at Cameron Lake involved stratiform, volcanogenic exhalations (Esson, 1982).

The purpose of this study is to document the basic geologic features associated with the Cameron Lake gold deposit. Emphasis is placed on three aspects of the deposit: geologic setting, structure, and alteration. Geological setting is important in all ore deposits research because the identification of favourable host lithologies, and tectonic environments conducive to gold deposit formation constrains the regional parameters involved in genetic modeling. Documenting the structural controls on gold emplacement is critical to the understanding of ground preparation processes which focus hydrothermal fluid flow and concentrate gold in economic quantities. Ore deposit form, gold distribution, paragenetic significance, geometry and the mechanics of vein formation are all influenced by deformation processes. Alteration studies provide constraints on the processes of gold mineralization and illustrate features which may be used to recognize and predict other areas of potential gold enrichment. Lithogeochemistry not only supports lithologic and alteration studies but helps identify the elemental associates of gold and define the geochemical signature of the deposit.

This thesis summarizes three field seasons of work at Cameron Lake, and forms part of a broader study on the geologic setting and genesis of gold occurrences in the Cameron-Rowan Lakes area funded by the Ontario Geological Survey. The data presented here are based on limited regional mapping, detailed mapping (1:60 scale) of excavated exposures of the deposit, and diamond drill core logging. To date, 89,450 ft (27,264 m) of drilling have been completed in delineating

the deposit, and 17,805 ft (5,427 m) have been done in exploration drilling elsewhere on the property.

2.0 Regional Geologic Setting and its Influence on Gold Mineralization.

Cameron Lake lies at the western extremity of the Archean, Savant Lake-Crow Lake metavolcanic-metasedimentary belt (Trowell et al., 1980) in the Wabigoon Subprovince of the Canadian Shield, northwestern Ontario (Figure 1). The region is divided geologically by the southeast-striking, northeast-dipping Pipestone-Cameron Fault (Figure 2), a major zone of deformation and displacement similar to the Larder Lake-Kirkland Lake, Destor-Porcupine, and the Cadillac-Malartic Lake Breaks recognized in other Canadian Archean gold camps. The Pipestone-Cameron Fault has been defined over 100 km of strike length, although its exposure in the Cameron Lake area is often obscured by lakes and low swampy depressions. Southwest of the fault lies the topographically high, north- to east-facing, Kakagi Lake greenstone terrain (Schwerdtner et al., 1979) and, to the northeast, the south-facing Rowan Lake greenstone terrain which contains the Cameron Lake gold deposit. Correlation of lithologies across the fault, although suspected, has not been possible to date (Trowell et al., 1980).

The structural geology of the Rowan Lake greenstone terrain is dominated by the Shingwak Lake Anticline. The axial surface of the fold has a east-northeast strike and the plunge is steep toward the southwest (Kaye, 1973). The anticline is asymmetric, with an east-southeast vergence. The Rowan Lake Volcanics, a thick, predominantly pillowed, subaqueous mafic flow succession are exposed in the core of the Shingwak Lake Anticline. These rocks are overlain by the Cameron Lake Volcanics, a mixed succession of southward facing subaqueous

FIGURE 2 - SEE BACK POCKET

pillowed and massive basaltic rocks, and intermediate to felsic pyroclastic rocks. The transition between volcanic cycles is marked by the first appearance of intermediate to felsic pyroclastic rocks which characterize the Cameron Lake Volcanics, as well as a change from dominantly pillowed basalt to a succession consisting of pillowed and massive basalts (Figure 3).

Subvolcanic gabbroic sills were emplaced at all levels in the succession before folding. Felsic porphyry sills and dykes, and quartz monzonite stocks intrude all of the earlier strata. All rocks have been metamorphosed to greenschist facies assemblages.

Blackburn and Hailstone (1984) defined the lower succession (Rowan Lake Volcanics) as geochemically tholeiitic, mainly magnesium-rich, and the upper succession (Cameron Lake Volcanics) as tholeiitic to calc-alkaline. The most significant gold occurrences within the Rowan Lake greenstone terrain (including the Cameron Lake deposit) are located within the Cameron Lake Volcanics (Figure 2).

Field mapping, petrography and lithogeochemical sampling were carried out to refine the volcanic stratigraphy. Figure 4 is a Jensen diagram (Jensen, 1976) of rock analyses from the Cameron-Rowan Lakes area. Sample grouping is designed to distinguish rocks from the two volcanic cycles and between mafic flows, mafic sills, felsic intrusions, and intermediate to felsic pyroclastic rocks. Most of the rocks from the Rowan Lake Volcanics plot within the tholeiitic field (79%), the majority as high-iron tholeiites. There is no suggestion of high magnesium content. Approximately 18% of the tholeiitic rocks are classified as andesitic. The remaining 21% all project within the calc-alkaline basalt field. The Cameron Lake Volcanics plot as a

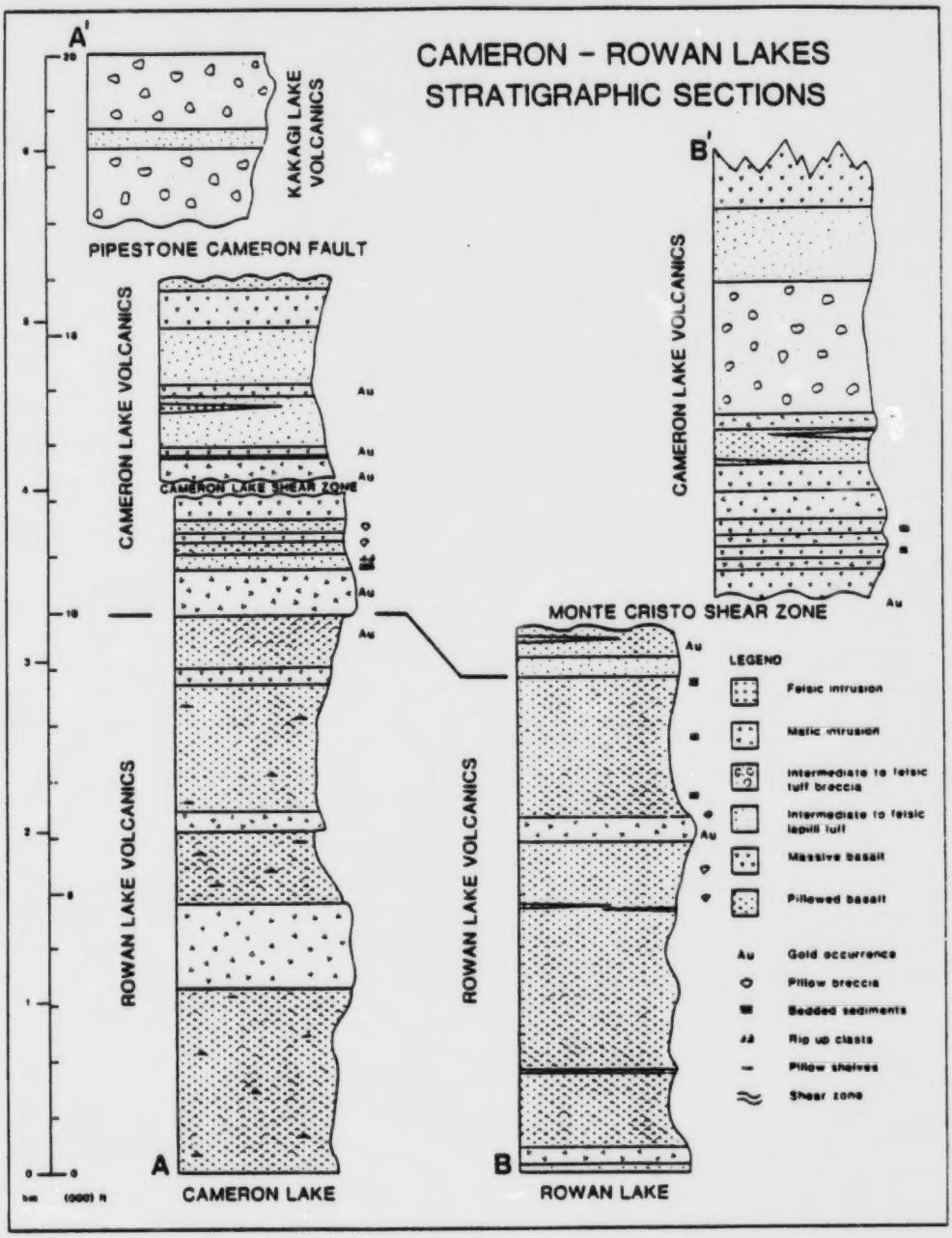

Figure 3. Stratigraphic sections from the Cameron-Rowan Lakes area. See Figure 2 for the location of the sections.

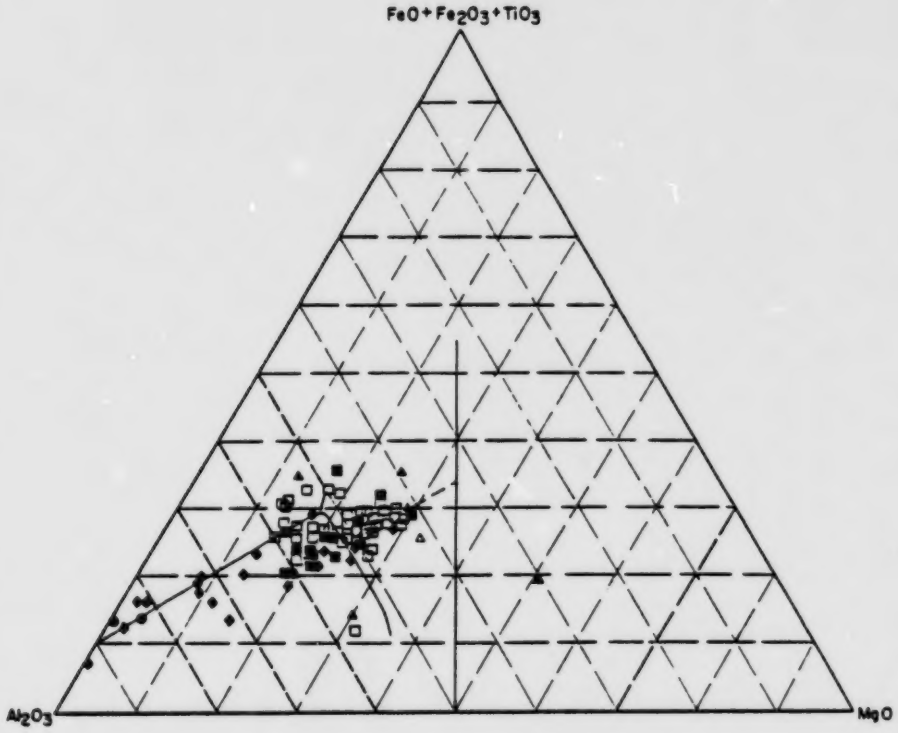

Figure 4. Jensen cation plot of samples taken from the Cameron-Rowan Lakes area. Open symbols and closed symbols represent the Rowan Lake and Cameron Lake Volcanic successions respectively. Squares are basaltic rocks, diamonds are pyroclastic rocks, triangles are mafic intrusions, and circles are quartz-feldspar porphyry dikes and sills.

mixed succession of tholeiitic and calc-alkaline rocks as shown by previous workers. The rocks range from high magnesium mafic intrusions to rhyolitic felsic pyroclastics. Regional lithogeochemical data used in Figure 4 are listed in Appendix I.

Gold occurrences within the Rowan Lake greenstone terrain tend to be associated with zones of high strain (Figure 2), several of which are situated at or near gabbroic-volcanic rock contacts. Two gold-bearing high strain zones, previously unnamed, are referred to here as the Cameron Lake Shear Zone (CLSZ) and Monte Cristo Shear Zones (MCSZ). They are subconcordant with respect to lithologic contacts (Melling et al., 1985; Wade, 1985) and occur within an arcuate belt of Cameron Lake Volcanics, on the southern limb of the Shingwak Lake Anticline. The volcanic rocks were intruded by the Nolan Lake Stock to the south and truncated by the Pipestone-Cameron Fault to the east. The CLSZ and MCSZ have attitudes of 315/70°N and 246/80°N respectively. Despite the presence of these two structural breaks, major displacements have not been recognized, and stratigraphic correlations may be made within the belt (Figure 3).

3.0 Local Geology of The Cameron Lake Gold Deposit.

The Cameron Lake deposit is situated about 700 m from the north shore of Cameron Lake (Figure 5). The property, comprising 61 mining claims held in good standing by Nuinsco Resources Ltd., was originally mapped in 1981 by A.D. Hunter. Drill data and additional field mapping have been incorporated into the updated map.

Outcrop exposure in the western half of the property is poor; however, ridges and generally higher topography to the east provide some exposure. Since 1981, 32,691 m of diamond drilling have been

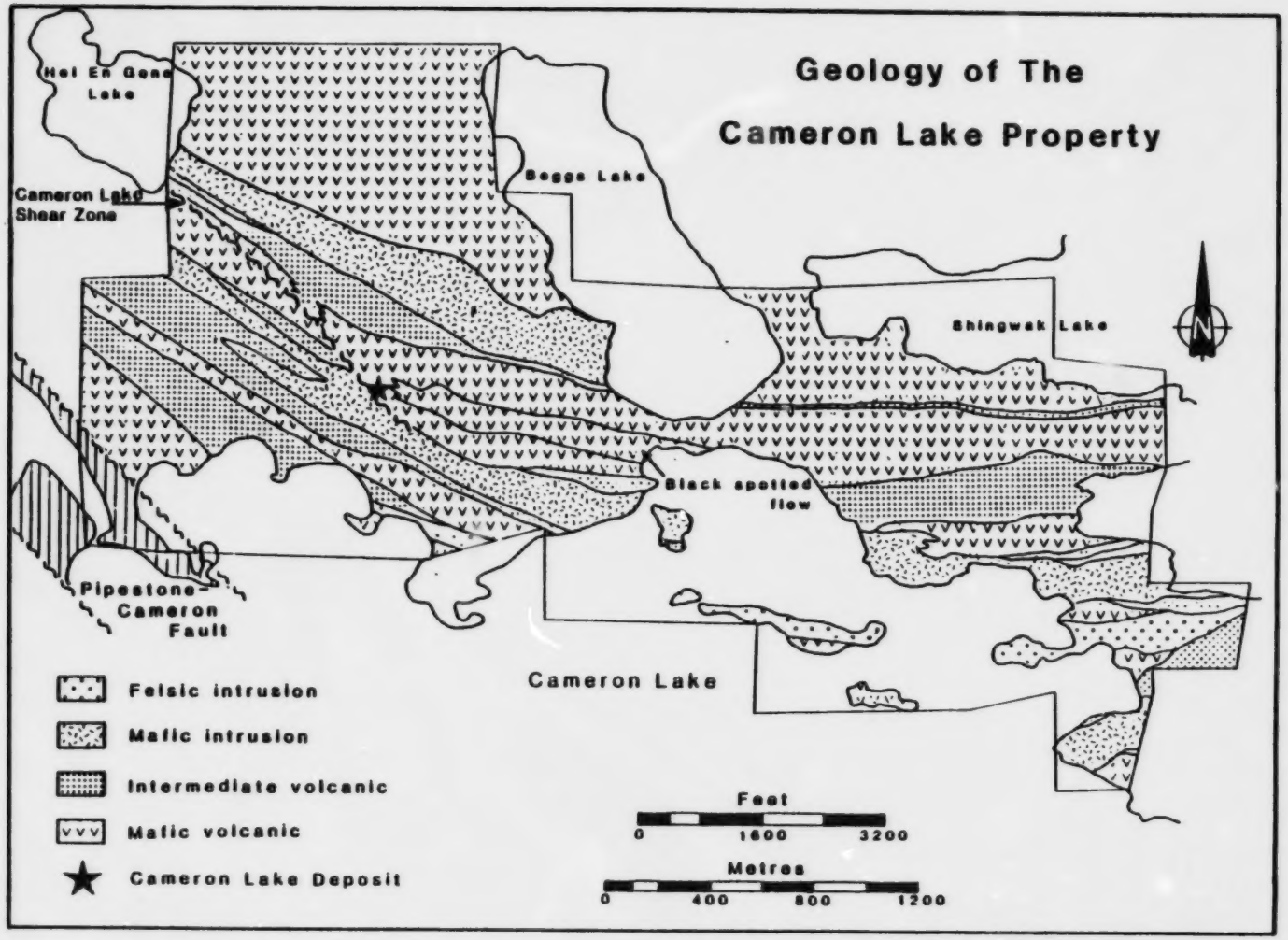

Figure 5. Geology of the Cameron Lake property (modified after Hunter, 1981).

completed on the property. Core logging emphasizing lithologies as well as alteration, structure, and veining has permitted detailed documentation of the stratigraphy surrounding the deposit.

The property (Figure 5) is underlain by basaltic rocks and interbedded intermediate to felsic volcaniclastic rocks of the Cameron Lake Volcanics. Two subconcordant gabbroic sills intruded the volcaniclastic units and are interpreted as subvolcanic intrusions related to large masses of mafic to ultramafic rock to the northwest of the map area (Kaye, 1973). A large concordant quartz-feldspar porphyry sill is present, as well as numerous thin dykes of similar composition which are markedly discordant.

The Cameron Lake gold deposit occurs in sheared mafic volcanic rocks adjacent to their highly deformed contact with a gabbroic sill. The basaltic rocks are predominantly massive and pillowed flows with minor (<10%) pillow breccia. The pillowed flows are aphyric, amygdaloidal, and have well defined chloritic pillow selvages (Plates 1b and 1c). Locally, pyrite, magnetite and minor hyaloclastite are concentrated between pillows. Individual pillowed units range from 3 m to 175 m in thickness.

Massive flow units may be subdivided into fine-grained aphyric and distinctly medium- to coarse-grained porphyritic types. The coarser-grained flows locally display up to 3% irregularly shaped chloritic clots interpreted as amygdules (Plate 1d), which impart a distinctive black spotted texture. One flow, about 130 m thick, has been traced 1.2 km northeast along strike from the CLSZ where it terminates against pillowed flows near the deposit (Figure 5). Flow unit thicknesses vary from 2 m to 200 m, and flows are commonly recognized by thin (<1 m)

brecciated flow tops and amygdule concentrations at contacts. Locally the massive flows may contain as much as 35% amygdules composed of assemblages of quartz-carbonate-chlorite-epidote-actinolite (Plate 1e).

Pillow breccia units 2 m to 20 m thick occur interbedded with the massive and pillowed flows (Plate 1f and 1g). Foliation within the pillowed and pillow breccia units is more prominent than in the massive flows.

Three distinctive intermediate to felsic volcaniclastic units occur on the property (Figure 5). The first marks the contact between the Rowan Lake and overlying Cameron Lake Volcanics (Figure 3). It consists of well-bedded pyroclastic (Plates 1j) and epiclastic rocks (Plates 1h and 1i), and laminated, muddy graphitic sedimentary rocks. The presence of numerous graphitic rip-up clasts within the epiclastic beds may indicate either shallow water conditions above storm wave base or reworking due to gravity flows. Local thickening of this unit along strike may reflect deposition on an irregular erosional surface, which would suggest a possible hiatus in volcanism coincident with the transition in volcanism.

The second volcaniclastic unit is a distinctive intermediate lapilli-crystal tuff averaging 50 m thick (Plates 1k and 1l). The unit is crudely bedded, monolithologic and contains as much as 50% euhedral feldspar laths, and 1-5% quartz phenocrysts. In general, finer grain sizes occur toward the west suggesting a more distal location from the vent. Thin (<1 m) chert beds occur locally within it. The unit is considered to be an ash flow (Hunter, 1981) and it is intruded by a gabbroic sill. The gabbroic sill, approximately 100 m thick, consists of fine- to medium-grained rocks locally containing quartz megacrysts

(Plate 1a). Its contacts are always sheared, carbonatized and variably sericitized.

The third volcaniclastic unit underlies the north shore of Cameron Lake and consists of reworked heterolithic lapilli-tuff (Plate 1m, 1n, and 1o). The rocks are bedded; however, deformation is intense due to the proximity to the Pipestone-Cameron Fault and commonly the unit is a fine-grained carbonate-sericite schist.

Thin discordant quartz-feldspar porphyry dykes, 1 cm to 3 m in thickness intrude the volcanic succession, and have been traced by drilling for several hundred metres along strike. Locally, they occur within the zones of shearing, but they are fractured and display a complex internal quartz-carbonate vein-network rather than penetrative foliation (Plate 1p). They contain inclusions of sheared and altered rock fragments similar in texture and mineralogy to those containing anomalous gold concentrations (Plate 7d) and these dykes are interpreted to post-date the formation of the deposit.

All rock units have been metamorphosed to greenschist facies assemblages. The most common mineral assemblage in the mafic volcanic rocks away from the deposit is quartz-albite-chlorite-epidote-actinolite-calcite. Petrography of the least altered host rocks to the deposit is summarized in Table I.

Table 1. Petrographic summary of least altered rocks.

Rock Type	Sample #	Primary Assemblage	Primary Textures	Secondary Assemblage	Secondary Textures
Massive basalt	NC-15-73 NC-27-174 NC-36-110 NC-36-207	-plagioclase -pyroxene -sphene -magnetite -pyrite	-holocrystalline -phaneritic -medium-grained -subophitic -amygdaloidal	-chlorite -carbonate -actinolite -epidote -quartz -muscovite	-foliation weak to absent -pressure fringes on opaques
Pillowed basalt	NC-22-185 NC-28-246 NC-36-435	-plagioclase -quartz -magnetite -pyrite -devitrified glass	-hypocrystalline -aphanitic -cryptocrystalline -amygdaloidal	-chlorite -carbonate -quartz -epidote -actinolite -muscovite	-foliation weak to moderate -pressure fringes on opaques
Gabbro	NC-8-452 DM-84-24 NC-81-1146	-plagioclase -pyroxene -quartz -sphene -magnetite -pyrite	-holocrystalline -medium-grained -phaneritic -chilled margins	-chlorite -carbonate -actinolite -epidote -quartz -muscovite	-foliation weak to moderate -sheared contacts
Quartz feldspar porphyry dyke	NC-29-495 NC-31-555 NC-31-587 NC-21-225 NC-28-687	-quartz -plagioclase	-holocrystalline -fine- to coarse-grained -porphyritic -chilled margins	-carbonate -muscovite	-foliation weak to absent -fractured and veined -sheared contacts
Intermediate tuff	NC-33-87 NC-33-99 NC-33-193	-quartz -plagioclase	-holocrystalline -fine-grained -fragmental -monolithologic	-carbonate -muscovite -chlorite	-foliation moderate to strong

4.0 Deposit Structure.

Exposure of the CLSZ in the vicinity of the deposit occurs in an area approximately 100 m by 350 m. Most outcrops have been enlarged, or discovered and subsequently stripped, since 1983. As no other exposures of the CLSZ occur on the property, its location and orientation have been established through exploration diamond drilling.

Detailed mapping at 1:60 scale was conducted on all excavated exposures. A map of part of the trenched area is shown in Figure 6 at 1:120 scale; structural measurements are summarized in Figure 7. This area contains significant gold-pyrite occurrences at the junction of two distinct zones of deformation.

During mapping particular emphasis was placed on the morphology, mineralogy, orientation, and textures of the veins, as well as fabrics and structures in the wall rocks. The objectives were to interpret the kinematics of the CLSZ and establish the vein paragenesis. Further understanding of structure was gained by logging diamond drill core, preparing cross-sections, and from these deriving level plans to illustrate the subsurface geology. Where possible, surface observations were used to constrain the interpretation of cross-sections. The results are illustrated by typical cross-sections (Figures 8, 9, 10, and 11) and one level plan (Figure 12). These data have been used to describe the geometry of the deposit.

4.1 Shear Zone Structure.

The CLSZ is a zone of high strain indicated by the pronounced flattening of primary features such as pillows and amygdules, and intense penetrative cleavage development in aphanitic to fine-grained massive basalts, pillowed basalts, and medium-grained gabbroic rocks

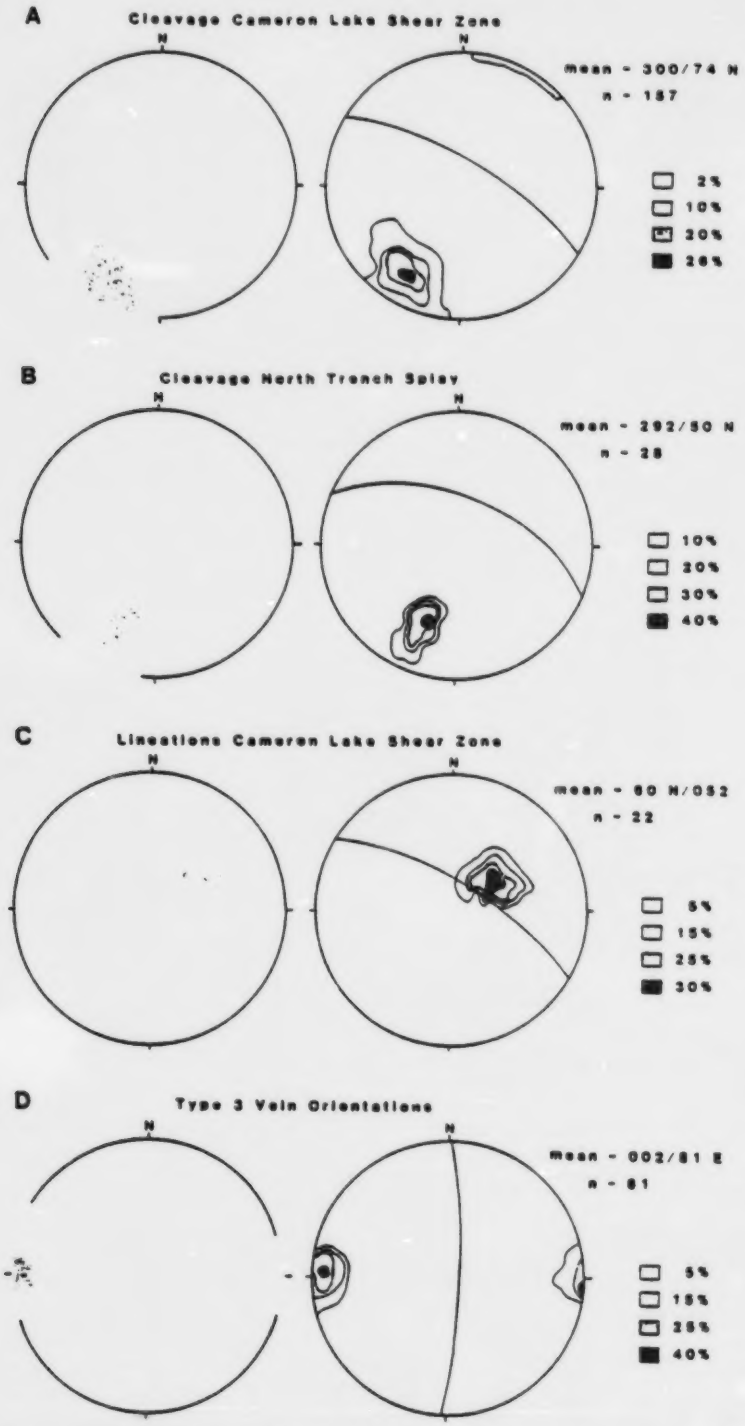

Figure 7. Equal area stereographic projections of structural data from the deposit. Contours represent percentage of points per 1% unit area. (A) Poles to cleavage, CLSZ; great circle represents the mean. (B) Poles to cleavage, North trench splay; great circle represents the mean. (C) Lineations, CLSZ; great circle represents mean cleavage from (A). (D) Poles to type 3 vein orientations; great circle represents the mean.

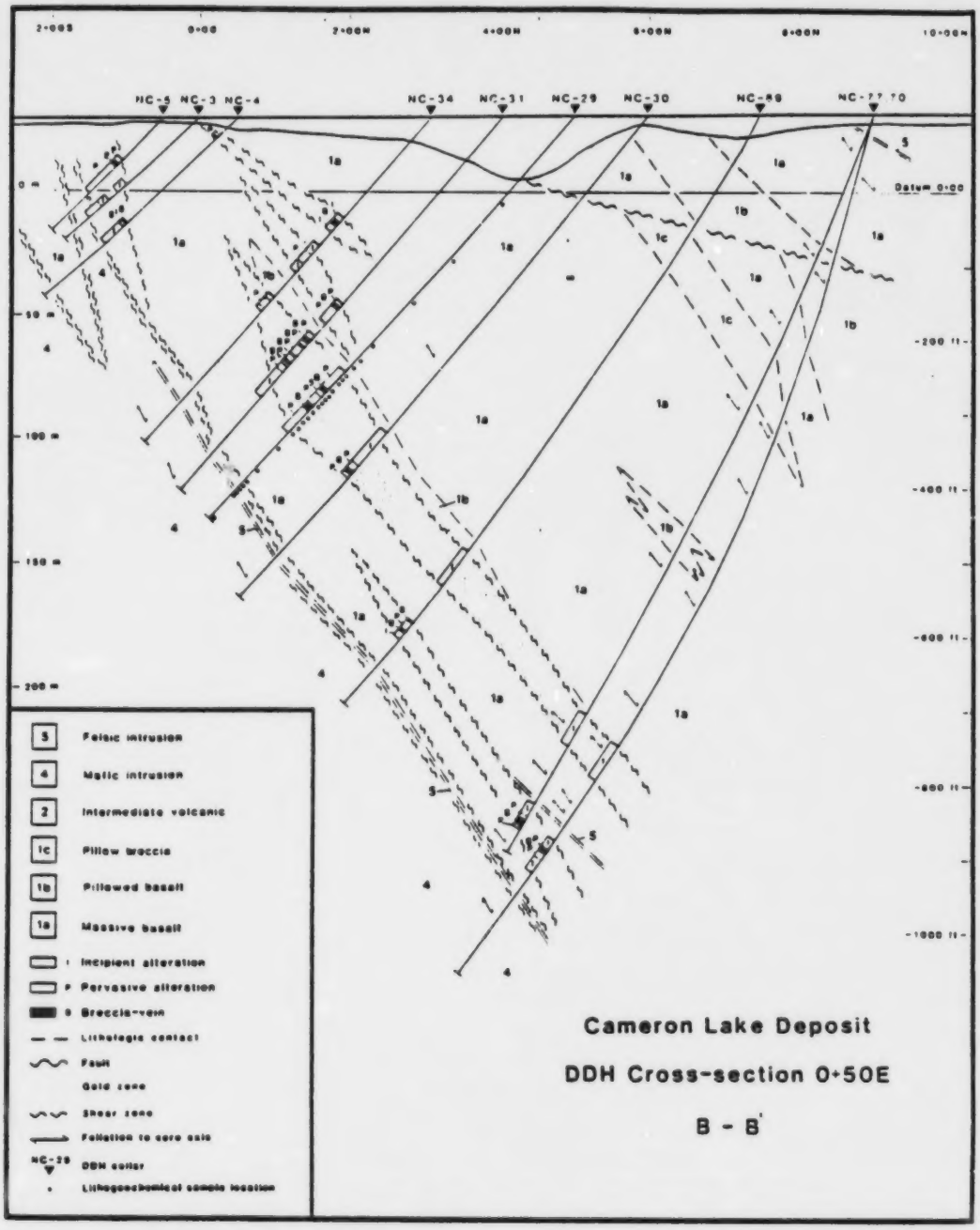

Figure 9. Diamond drill cross-section B - B', 0+50 E.

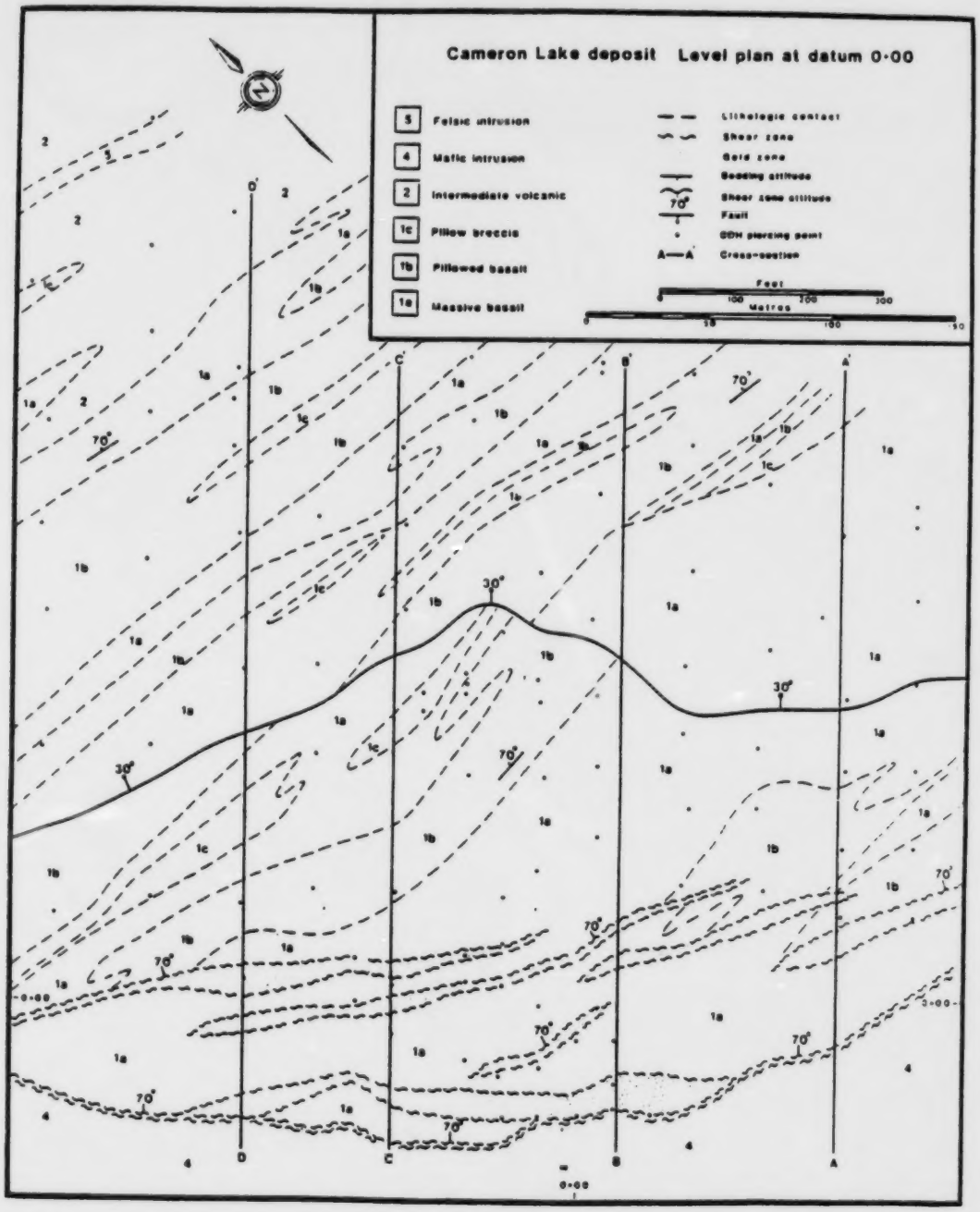

Figure 12. Level plan datum 0+00.

(Plates 3a and 3b). The rocks are intensely weathered and fissile in the excavated outcrops. They weather rusty-brown in areas of hydrothermal alteration and medium green in unaltered areas. Cleavage within the CLSZ is defined by the planar alignment of sheet silicates (chlorite and sericite). The mean foliation 300°/74° N (Figure 7a) measured within the zone of deformation occurs at a low angle to the shear zone boundaries which trend 315°/70° N. Two planar fabrics are locally present in the zone; a spaced cleavage parallel to the shear zone, and a more continuous planar mineral alignment inclined at angles less than 45° to the shear zone boundaries. The latter is represented by the measurements in Figure 7a. The intersecting planar fabrics yield somewhat uneven products which resemble those of phyllonitic rocks (Higgins, 1971).

A steeply plunging lineation, formed by the intersection of the two cleavages, is recognized in outcrop and drill core. Its mean attitude is 60° N/052° (Figure 7c). No stretching lineation was identified in the foliation plane.

During surface mapping a thin unit of interflow sediment was found on the northeastern edge of the Discovery outcrop near the boundary of the CLSZ (Figure 6). This unit represents a passive marker which is transposed into the plane of the shear zone. In addition, within the zone of deformation exposed on surface, two distinct massive flows occur within the pillowed succession (Figure 6). Both flows have been rotated toward the plane of shear and are transected by narrow zones of intense deformation and cleavage development. One flow exhibits a dextral offset of about 3.5 m across one of these discontinuities and transposition of the flow is seen in the adjacent walls. Foliation,

elsewhere oblique to these discrete shears, becomes increasingly parallel as the shear discontinuities are approached. Rare Z-folds are observed on this foliation (Figure 6).

The CLSZ is actually composed of several branches as shown by the orientation of the splay which bifurcates from the main zone of deformation in the North trench (Figure 6, trench B). Its orientation (285/70° N) is similar to that of bedding measured in the Discovery outcrop (Figure 6, trench A). This geometric relationship is seen on surface at scales from 1 m (Figure 6, trench D), to tens of metres (Figure 6, trench B).

The CLSZ has been traced by exploration diamond drilling over 1000 m to Hel En Gone Lake on the western boundary of the property (Figure 5). An average strike of 315/70° N and a width between 11 m and 60 m has been established based on these data (Melling et al., 1985). In detail the CLSZ consists of both anastamosing and en echelon shears with their orientations in part controlled by lithologic anisotropies. The gabbroic sill in the structural footwall to the deposit exerts the greatest influence on the orientation of the CLSZ in the vicinity of the deposit. The contact between the gabbroic sill and the volcanic rocks is always sheared. At intermediate depths (200 m) a branch of the shear zone is located about 50 m in the footwall and appears to parallel the main zone of gold enrichment (Figure 9). However, mapping and additional drilling data indicate that these two structures merge along strike in both directions, at surface, and probably at depth (Figures 8, 10, 11, and 12).

As illustrated in cross-sections and level plans through the deposit (Figures 8, 9, 10, 11, and 12) a general trend of 275/70° N is

observed for bedding in the conformable units of massive, pillowed, and brecciated pillow basalt outside the zone of deformation. Level plans constructed through the deposit illustrate that in some places the CLSZ consists of several **en echelon** shears oriented about 295/70° N (Figure 12). This trend is equivalent to that in the transposed bedding along the shear zone boundaries. This geometry, at the deposit scale, is similar to that seen in outcrop (Figure 6, trenches B and D).

4.2 Vein Geometry and Paragenesis.

Three distinct vein types are present in the CLSZ: (1) early barren, extensional, quartz-carbonate veins which have been buckled (Plates 3c and 3d), (2) a major system of gold-bearing pyritic, quartz-albite-rich breccia-veins (Plates 3e and 3f), and (3) a late group of straight, cross-cutting, locally **en echelon** extension veins which contain a quartz-carbonate-chlorite-hematite-gold assemblage (Plates 3g and 3h). Vein dimensions, orientations, and mineralogy are summarized in Table II, and their spatial distribution is illustrated in Figure 6. Mineralogy and petrography of the breccia-veins are discussed further in Chapter 5.

The type 1 veins were buckled during progressive deformation resulting in up to 63% shortening, and are locally dismembered (Plates 2b, 3c, and 3d). Cleavage within the foliated host rocks to the veins is approximately axial planar to the buckles which locally display Z - fold asymmetry. The veins dip subvertically to easterly and enveloping surfaces strike about 340°. These buckled veins have no associated iron carbonate or pyrite alteration envelopes.

The breccia-veins (type 2 veins) display a wide range of morphologies and textures. Where weathered they have a thick (4 cm)

Table II. Classification of principal vein types in the Cameron Lake deposit.

Type	Dimensions	Geometry	Textures / Mineralogy	Age / Significance
1	Less than 10 cm thick and 3 to 4 m in unfolded length (63% shortening).	Commonly display buckled Z-fold asymmetry, with pointed terminations. Rarely dismembered. Veins trend about 340° and dips are generally subvertical. Occur within sheared, carbonatized basalts with cleavage approximately axial planar to fold hinges.	Quartz crystals normal to vein walls. Contain a thin (< 3 mm) median seam of rusty weathering carbonate.	Interpreted as tension gashes formed early and propagated normal to the least principal stress direction. Subsequently buckled during progressive deformation.
2	As much as 4 m thick and 175 m long, but most commonly 1 m thick and 10 to 20 m in length.	Approximately planar and parallel to the high strain zones in which they occur (315°/70°N or 292°/70°N). Locally pinch and swell, and may terminate abruptly. Margins are often the sites of pronounced shearing.	Veins contain angular, commonly elongate fragments of carbonatized, sheared basalt which range in size from 1 mm to 0.5 m. Fragments are separated by a matrix of quartz (10% to 70%) with minor carbonate and albite. Vein minerals display massive or fibrous textures perpendicular to the fragment boundaries. Pyrite rarely exceeds 10%, concentrated within fragments and forming envelopes surrounding the breccia-veins.	Interpreted as formed in response to high pore fluid pressures and/or high differential stresses. Represent major conduits which facilitated fluid circulation. Contain highest gold values.
3	Maximum width of 3.5 cm and 1 to 2 m in length.	Planar veins which occur in arrays. Individual veins are spaced at fairly regular intervals (6 to 10 cm). They cut the breccia-veins and carbonatized basalts, and have an attitude of 002°/84°E.	Carbonate crystals normal to vein margins with fibrous quartz centres. Aggregates of chlorite and specular hematite are locally present. Gold is locally present where these veins cut breccia-veins	Interpreted to have formed during the later stages of progressive deformation and have propogated normal to the least principal stress direction.

rind of buff coloured siliceous rock mottled by rusty recessive pits (Plates 3g and 3h), resulting from selective weathering of pyritic, carbonatized fragments (Plate 2g). Internally the veins consist of angular to subrounded, pervasively altered fragments in a matrix of quartz with lesser albite and carbonate. The breccias may be either framework or matrix supported. Fragments display a wide range in shapes and sizes and generally have internal cleavages which predate brecciation (Plates 2c and 2k). Groups of fragments commonly have shapes suggesting that by removing the vein material they could be fitted together like pieces in a jigsaw puzzle (Plates 2d and 3c). Some fragments were veined prior to fracturing and incorporation into the breccia-vein (Plate 2d). The angularity, lack of communition of fragments, and the fit of breccia fragments indicate that minimal movement of fragments after brecciation and fracturing has occurred. Rarely vein walls grade through fracture zones into vein breccia (Plate 2e), but most commonly their margins are curvi-planar and the sites of pronounced shearing. Individual breccia-veins exhibit a continuum of megascopic deformation textures from undeformed (Plate 2c, 2d, 2e, and 2g) to ribbon textures produced by the smearing of sheared and altered fragments resulting from ductile deformation postdating brecciation and vein formation (Plate 2f, 2h,and 2i).

Pyrite is concentrated within and rimming the altered fragments, but not in the siliceous matrix and along with carbonate it forms mappable alteration envelopes surrounding the breccia-veins (Figure 6). Drilling data indicate that a gold bearing shear may contain one or several breccia-veins depending on its width. Wider shear zones, which in cross-section contain several breccia-veins, display wide

intervals of deformed, pyritic, altered rocks between the veins.

The stage (3) veins form arrays of the type described by Roering (1967), Beach (1975), and Ramsay and Graham, (1970). In the North trench (Figure 6) they are spaced at fairly regular intervals of 6 to 10 cm (Plates 3g, and 3h) and oriented 002/81°E. They cut the breccia-veins (Plates 2j and 2l) and the altered, foliated rocks of the shear zone. Internal fibrous quartz-carbonate textures (Plate 7c) and included vein-parallel slivers of wall rock suggest that these veins formed by crack seal-mechanisms (Ramsay, 1980a). No alteration envelopes are seen adjacent to the veins and the quartz-carbonate-chlorite-hematite-gold assemblage infilling the veins (Plate 2i) is thought to be locally derived by solution transfer.

4.3 Ore Deposit Geometry and Gold Distribution.

Before the 1983-84 trenching program a genetic model involving statiform volcanogenic exhalations was influencing exploration strategy and very little was known about the structural controls on gold distribution in the deposit. Correlations of features among drill holes was difficult and further development was discouraged even though 17 shallow holes (averaging 100 m in depth) were drilled on 16 m centres in the immediate area (Figure 6), all intersecting highly anomalous gold concentrations. Since then, detailed mapping of surface exposures integrated with additional drilling data has permitted definition of the ore body geometry in relation to other structural and stratigraphic features. Systematic sampling of drill core and surface exposures have allowed those features most commonly associated with gold enrichment to be identified. In the following discussion of deposit form the terminology of Colvine et al., (1984) is adopted; ore

shoot is defined as gold concentrations occurring on the smallest scale (tens of centimetres), ore zone in the range of tens of metres, and ore body as the entire deposit.

The significance of the breccia-veins cannot be understated. Core, grab, and channel samples indicate that they contain highly anomalous gold concentrations. A 7 m composite channel sample of breccia-vein from the North Trench averaged 0.273 oz/ton Au (Archibald, 1984). Grab sample locations and results are presented in Figure 6. The breccia-veins represent a specific gold-bearing rock type which commonly contains greater than 0.3 oz/ton Au. Enveloping them and occupying a large volume of the CLSZ are lower-grade, pyritic, foliated altered rocks. The subdivision of gold-bearing rock types is readily visible in surface exposures of the deposit and diamond drill core. Figure 13 is a frequency plot of assay results from drill holes intersecting zones of gold concentration. Note the bimodal character of the assay data. The lower values correspond to the sheared and altered rocks, whereas the higher grades are from the breccia-veins.

Mapping and assay data indicate that the principal locus of gold-pyrite mineralization occurs at the junction of the two distinct structures located at the western end of the North trench (Figure 6, trench B). The trend of the breccia-vein, which is central to and parallels the splay, is similar to bedding orientations measured in the volcanic rocks exposed in the Discovery outcrop (Figure 6, trench A).

The geometrical relationship between the CLSZ, bedding in the volcanic rocks, and the orientation of gold-bearing shoots and zones is reflected in cross-sections and level plans through the deposit. Shoots commonly occur in the structural hanging wall and footwall to

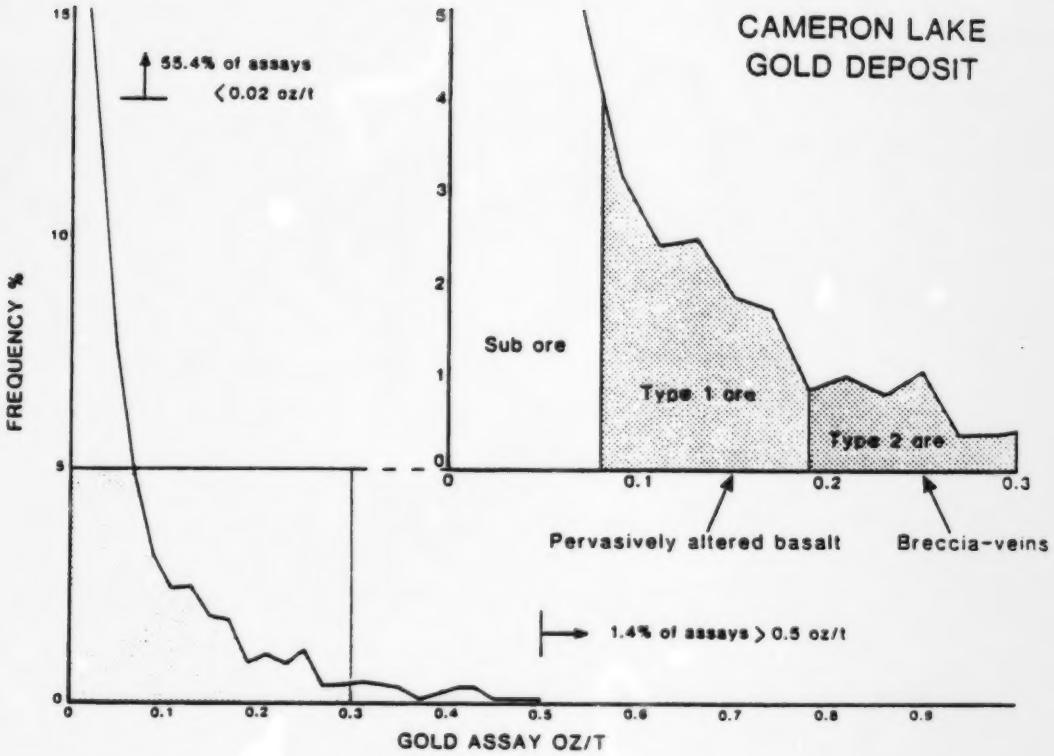

Figure 13. Frequency versus gold assay histogram plot of assay data from the Cameron Lake deposit. Two distinct gold-bearing rock types are present: pyritiferous, deformed altered basaltic rocks (0.08 to 0.19 oz/ton Au) and breccia-veins (greater than 0.19 oz/ton Au).

the main zones of gold enrichment (Figures 8, 10, and 11). They are in general narrower (<3 m), apparently of shallower dip, and of lesser lateral and vertical extent than the main zones of gold mineralization. Drill cross-sections drawn perpendicular to the CLSZ reflect the true dip of the ore body; however, gold shoots which occur in bedding-controlled splays are oblique to both the CLSZ and the drill cross-sections. Consequently only apparent dips and not true dips of the gold shoots are reflected in drill cross-sections.

Level plans clearly illustrate the lateral extent of the gold shoots and the control of bedding on their orientation (Figure 12). They diverge from the main zone of gold enrichment toward the east where they pinch out, thus accounting for their discontinuous nature. In general the gold shoots follow the trend of bedding in the volcanic rocks which is transposed into the plane of the CLSZ and are therefore arranged **en echelon**, oblique to the overall trend of the CLSZ.

The sheared contact of the mafic volcanic rocks and gabbroic rocks in the structural footwall to the deposit is, in general, barren of gold. Only locally, near surface and at depth (Figures 8, and 11), where the main zone of deformation and the sheared lithologic contact merge, are gold concentrations encountered.

The overall geometry of the deposit is illustrated using a longitudinal section of contoured gold grade times intersection thickness values of data compiled from drilling (Figure 14). The section is drawn within the plane of the CLSZ dipping 65° toward north from the base line (Figure 6). All gold-bearing intersections are projected onto the diagram. Note the 70° W pitch of the deposit, defined by linking the zones of highest gold contents, and their

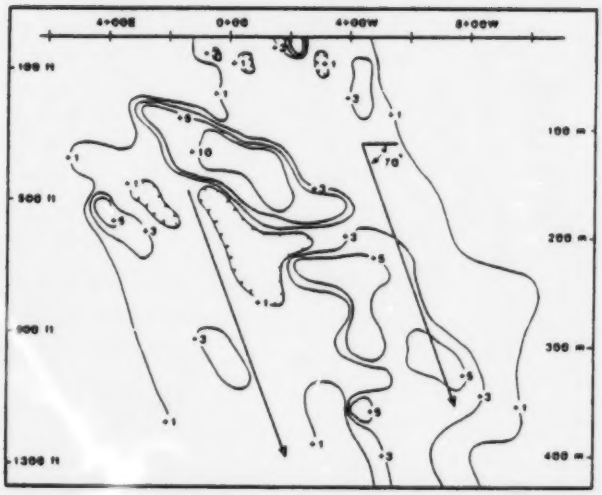

Figure 14. Longitudinal section dipping 65° N from the baseline. Contours represent the value of grade times thickness (eg. 0.2 oz/ton Au over 50 feet = 10). The contours are based on approximately 100 drill hole piercing points. Section looking south. Modified after Archibald, 1985.

periodicity.

4.4 Structural Interpretation.

The following features are relevant to the kinematic interpretation of the CLSZ. (1) Within the high strain zones primary structures are flattened (pillows, amygdules). (2) Passive bedding markers outside the CLSZ are transposed into parallelism at the boundaries of the zone. (3) Passive bedding markers within the CLSZ are offset across discrete zones of high strain in a dextral sense. (4) Continuous cleavage developed within the CLSZ occurs at a low angle (15^{o}) to the boundaries of the CLSZ. This sense of cleavage asymmetry has been shown to be indicative of dextral shear (Ramsay and Graham, 1970; Berthe et al., 1979; Ramsay, 1980b; Simpson and Schmid, 1983). (5) This oblique foliation is transposed into the plane of the late shears and rare Z-folds of the foliation are developed. (6) Locally two cleavages are present within the CLSZ. These are tentatively interpreted as C- and S-fabrics respectively, described by Berthe et al., 1979. (7) The lineation observed in rocks from the CLSZ is interpreted as the intersection of shear (C) and flattening plane (S) foliations. This implies a subhorizontal displacement vector perpendicular to the intersection lineation within the plane of shear. (8) The 45^{o} inclination of the type 3 extensional veins to the boundaries of the shear zone is considered indicative of dextral shear as shown by Roering (1968), Ramsay and Graham (1970), Hancock (1972), and Beach (1975). (9) Type 1 veins acted as nonpassive markers which were buckled and shortened by as much as 63 percent. They are rarely dismembered and therefore have remained within the fields of shortening during most of their deformational history. The enveloping surfaces of

the type 1 veins strike appoximately north-south. The orientation is similar to that measured for the later type 3 veins.

All these features indicate that there are components of dextral simple shear within the CLSZ; however the lack of an identifiable stretching lineation is problematic, particularly in the high strain zones. A possible solution is that there is a significant pure shear or flattening component to deformation in the CLSZ. This is supported by the apparent lack of rotation on the type 1 veins. Estimates of the amount of displacement on the CLSZ are uncertain for the following reasons: inadequate exposure, lack of distinctive marker units, poor strain markers, heterogenous distribution of strain, primary lithologic anisotropies, and unknown ratio of pure shear to simple shear strain.

The location of highly anomalous quantities of gold along the CLSZ corresponds, in part, to the development of oblique, secondary, sympathetic shear zones. These splays, which bifurcate from the CLSZ, are apparently controlled by bedding in the mafic volcanic rocks which is transposed into the plane of shear. Figure 15 is a stereographic projection of the CLSZ and the oblique, bedding-controlled, sympathetic splays. The pitch of the deposit, as defined by drilling, is coincident with the intersection of these two shear systems. The relationship between the two shear systems and the deposit is illustrated in Figure 16. This model serves to explain the complex subsurface geometry of the deposit, as well as the existence of hanging wall and footwall ore shoots on either side of the main zone of gold enrichment. At this stage of investigation the periodicity of the high grade gold zones can not yet be adequately explained.

The CLSZ may be classified as a brittle-ductile shear zone

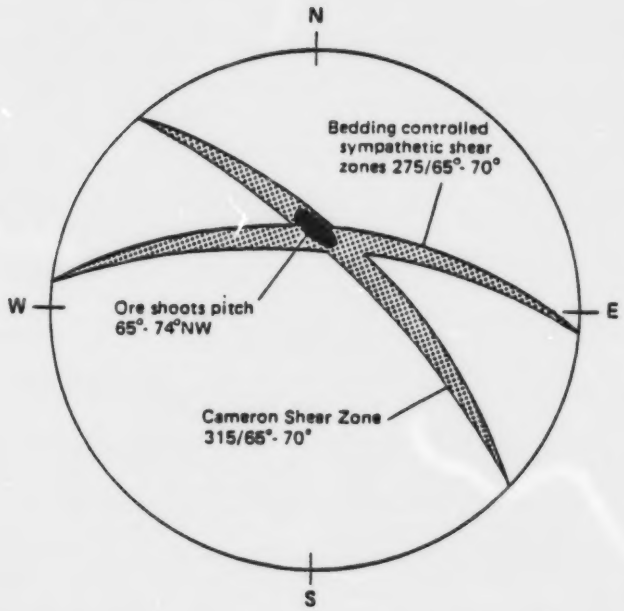

Figure 15. Simplified stereographic projection illustrating the coincidence of the pitch of the ore shoots with the line of intersection of the Cameron Lake Shear Zone and bedding-controlled shear zone splays.

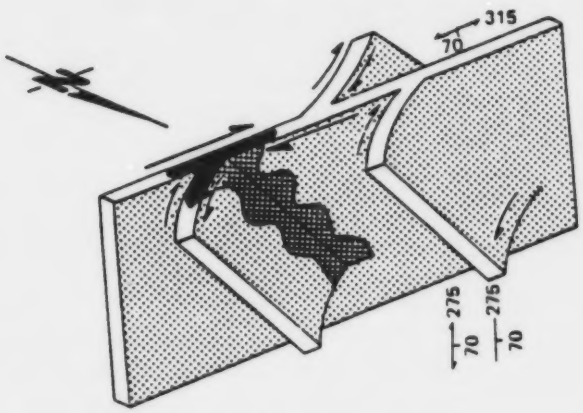

Figure 16. Diagramatic representation of the spatial relationship between gold zones and the northwest striking Cameron Lake Shear Zone and the northeast to east striking bedding-plane splays.

(Ramsay, 1980b). Brittle deformation within ductile shear zones may be conveniently thought of as having two modes of occurrence. The first corresponds to shear fracturing parallel to the plane of shear, and the second to the initiation of extension fractures normal to the least principal stress direction. Deformation within the CLSZ was dominantly ductile; however, the formation of extension veins and vein-breccias attests to the sporadic transiton to brittle processes. These changes in deformation regime may have been achieved by fluctuations in several variables such as temperature, lithostatic pressure, strain rate, and pore fluid pressure (Price, 1975). Petrography of least deformed, least altered rocks, and sheared, altered rocks (chapter 5) indicate that both brittle and ductile deformation, and hydrothermal alteration occurred near greenschist facies metamorphic conditions. Furthermore brittle faults attributable to high strain rates are not present.

The influence of pore fluid pressure on the mechanical and chemical behaviour of rocks undergoing deformation is extremely important. High pore fluid pressures promote higher strain rates and change the absolute values of each differential stress in the rock by reducing the shear stress required for failure (Hobbs, Means, and Williams, 1976; Jaeger and Cooke, 1979; Phillips, 1972; Price, 1975; and Ramsay, 1967).

The conditions under which fracturing and vein formation is envisaged to have occurred are represented in Figure 17. Schematic diagrams of the shear zone are drawn to illustrate the stages of vein formation and assist in a qualitative discussion of the role of hydrothermal fluid pressure during the transition from ductile to

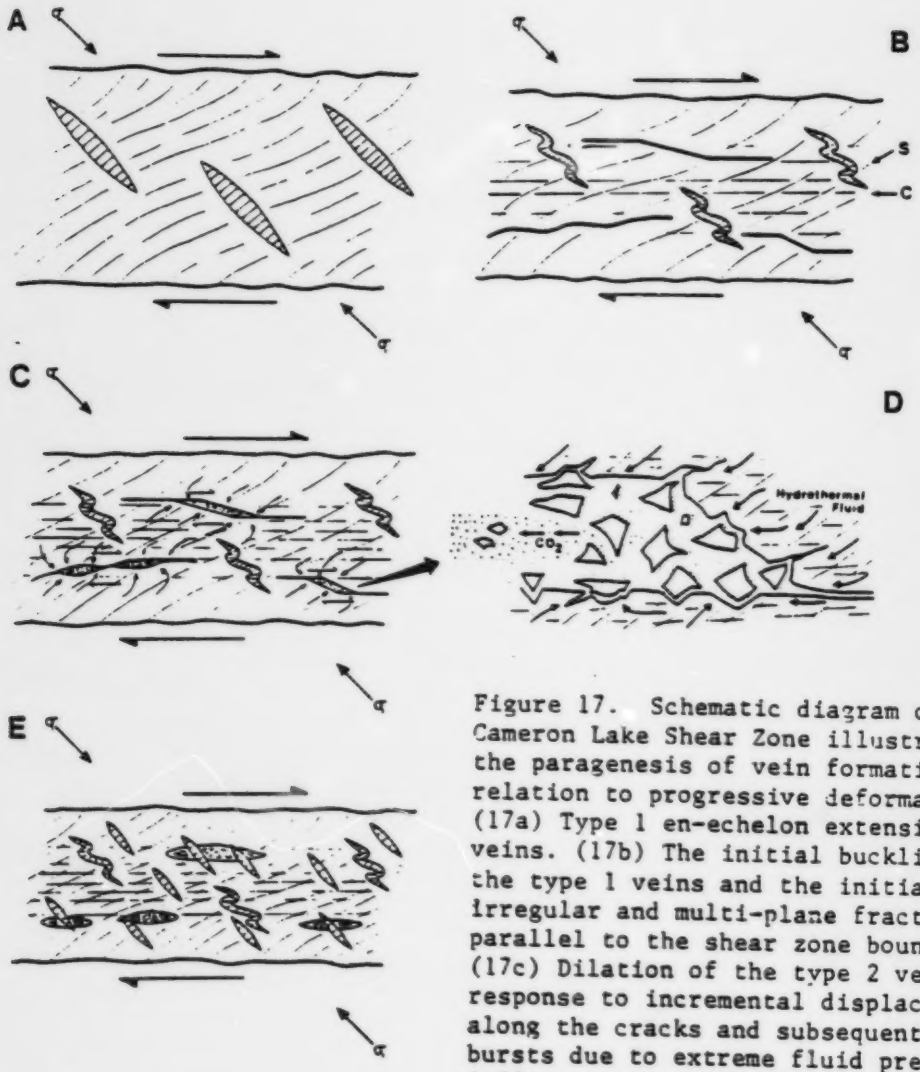

Figure 17. Schematic diagram of the Cameron Lake Shear Zone illustrating the paragenesis of vein formation in relation to progressive deformation. (17a) Type 1 en-echelon extension veins. (17b) The initial buckling of the type 1 veins and the initiation of irregular and multi-plane fractures parallel to the shear zone boundaries. (17c) Dilation of the type 2 veins in response to incremental displacement along the cracks and subsequent rock bursts due to extreme fluid pressure differentials. (17d) Close-up view of a portion of a breccia-vein formed in 17c. CO_2 effervesces as the hydrothermal fluid depressurizes upon entering the vein. Gas bubbles adhere to the breccia fragments and coalesce during rapid ascent. (17e) Further buckling of the type 1 veins, intensification of cleavage along the type 2 breccia-veins, and the initiation of the type 3 veins during the waning stages of deformation.

brittle behavior. The shear zone model presented here follows that of Ramsay (1980b) and involves a planar zone of deformation in which the internal fabric is defined by the extension of mineral components at 45° to the shear zone walls. The body of rock in the undeformed state is assumed to be isotropic and the shear zone propagates at about 45° to the maximum principal stress direction.

Figure 17a is an interpretation of the conditions under which the type 1 veins may have formed. In order to initiate extension fractures normal to the least principal stress direction the differential stress must be equal to or less than 4 times the tensile strength of the rock. If the pore fluid pressure exceeds the minimum principal stress by an amount equal to the tensile strength of the rock the failure criteria for crack growth and extension fracturing are identical and fluid filled tension gashes develop by hydraulic fracture (Phillips, 1975).

The conditions under which type 2 veins form are illustrated in Figure 17b and 17c. As simple shear displacement increases the flattening plane foliation intensifies and the angle between it and the shear zone walls becomes smaller (Ramsay, 1980b). Because ductile shear zones generally display a maximum displacement gradient in the zone centre, tectonically induced fabrics within shear zones generally display a sigmoidal form. The formation of C-surfaces (Berthe et al., 1979; Simpson and Schmid, 1983) would enhance the degree of anisotropy developed parallel to the shear zone boundaries. Contemporaneous with cleavage development there occurs a loss of cohesion and a progressive lowering of tensile strength in a direction normal to the cleavage, which at this stage is beginning to parallel the shear zone walls. In such anisotropic rocks the geometrical relationships between the principal stress directions are more complex than those shown in Figure

17a. A lower tensile strength in the rock, across the cleavage, will require lower critical shear stresses to initiate failure parallel to cleavage. When the differential stress rises to about 8 times or greater than the tensile strength of the rock across the cleavage a sufficient rise in pore fluid pressure will initiate shear fractures parallel to the shear zone boundaries.

During the first incremental stages of displacement along the shear fractures, small dilatant openings are created due to irregularities in the crack walls (Guha et al., 1983) and multiplane fractures (Mitcham, 1974). These openings become local low pressure areas relative to the rocks permeated with high pressure fluids adjacent to the fracture. A decrease in hydrothermal fluid pressure on these dilatant fracture surfaces would create high fluid pressure differentials resulting in rock bursts adjacent to the fractures (Phillips, 1972). During brecciation tectonic stress would be relieved by brittle failure, and rapid flow of fluid into the brecciated fracture surface would result in a reduction of fluid pressure in the surrounding rocks (Sibson et al., 1975). Thus brittle fracture would cease locally and ductile deformation would resume.

These processes may be envisaged as occurring in different locations at different times, with each breccia-vein having its own drainage area. Fracturing and brecciation could form permeable conduits into which gold-bearing hydrothermal fluids would percolate. The breccia-veins would become self-propagating by focussing the fluid flux and extending the fractures. Within the centre of brecciated zones, the upward rate of fluid flow may have been sufficiently high to carry fragments which would be abraded and result in sub-rounded

breccias. Brecciation increases the rock surface area exposed to the hydrothermal fluids enhancing metasomatism and gold precipitation. A model involving brecciation and hydrothermal fluid influx as related processes represents a first attempt to explain their origin. Models involving brecciation and hydrothermal activity as unrelated processes would not account for many of the features observed in breccia-veins.

This mechanism of breccia-vein formation would result in lens-like breccia-veins whose walls would grade through fracture zones into angular vein breccias. The common observation of matrix-supported breccias suggests that the matrices began to crystallize immediately after brecciation while the fragments were suspended in the fluid which may have resulted from boiling and the attachment of gas bubbles to the fragments (Figure 17d). The angular nature of the veins indicates that minimal displacement occurred along the fracture surfaces. Locally strained quartz grains occur in the matrix interstitial to the breccia-fragments (Plates 17a and 17b) which indicates that ductile deformation continued after vein formation.

The conditions under which the type 3 veins form are illustrated in Figure 17e. These veins are interpreted to occur late in the deformational history of the CLSZ. When the differential stress is less than four times the tensile strength of the rock, and pore fluid pressures exceed the minimum principal stress by an amount equal to the tensile strength of the rock the conditions of fracture are met and fluid filled tension gashes develop by hydraulic fracture (Phillips, 1972). Extension fractures are initiated normal to the least principal stress direction. The type 3 veins are in general planar features which indicate that little or no progressive displacement along the shear zone occurred after their formation.

5.0 Alteration of Basaltic and Gabbroic Rocks.

The delineation of different alteration facies in the excavated exposures of the deposit was attempted during mapping, but the intensely weathered and fissile nature of some of the rocks prevented detailed subdivision. The three types of alteration mapped, in order of increasing proximity to the deformed gold-bearing rocks (Figure 6), include:

1) Disseminated carbonate rhombs;
2) Pervasive carbonate±sericite;
3) Pervasive carbonate-sericite-pyrite.

Least altered rocks are defined as those rich in chlorite and containing no carbonate porphyroblasts or sericite.

The disseminated carbonate rhomb type of alteration is restricted to most chloritic basaltic and gabbroic rocks outside, but adjacent to, the zones of high strain (Figure 6). It is characterized by rusty-weathering carbonate euhedra up to 2 mm in size. The abundance of carbonate rhombs increases with proximity to the zones of high strain. This type of alteration forms envelopes at the scale of tens of metres in the rocks adjacent to wide foliated zones of gold-enrichment, but occurs over several metres near the smaller gold shoots.

The pervasive carbonate-sericite type of alteration is confined to the foliated basaltic rocks which occur within the zones of high strain (Figure 6). It is characterized by abundant, rusty-weathering, fine-grained carbonate with lesser light buff to tan sericite aggregates and laminae. Chlorite content is diminished (<20%) or absent in zones of this type of alteration. In areas of less intense deformation, flow contacts and relict pillow selvages are locally preserved (Plate 3b).

Sericite abundance is greatest in strongly foliated rocks.

The pervasive carbonate-sericite-pyrite type of alteration is in general spatially associated with the breccia-veins which occur in the shear zone (Figure 6). It is characterized by disseminated pyrite euhedra (<2 mm) in foliated, pervasive, carbonate-sericite altered basaltic rocks. Pyrite abundance rarely exceeds 10% and occurs in highest concentrations adjacent to the breccia-veins. Locally, diffuse patches of disseminated pyrite occur in areas where breccia-veins have not been located (Figure 6). These patches do, however, occur either along the strike extension of breccia-veins or adjacent to unexposed areas, where breccia-veins may be concealed.

Detailed mineralogical study of the alteration assemblages was restricted to drill core which is unaffected by surface weathering and provides complete cross-sections through the deposit. Data presented are based on thin section and X-ray diffraction studies; mineral compositions were further verified by electron microprobe analysis. These methods permitted recognition of four symmetrical zones of hydrothermal alteration which envelop the deposit. Proceeding inward from the least altered basaltic rocks the following assemblages were observed:

1) Quartz-albite-chlorite-calcite-ankerite-epidote-actinolite-magnetite;
2) Quartz-albite-ankerite-sericite-chlorite-calcite-rutile;
3) Quartz-albite-ankerite-sericite-siderite-chlorite-pyrite-rutile;
4) Quartz-albite-ankerite-sericite-siderite-pyrite-rutile.

The distribution of these alteration assemblages with respect to gold concentration and the shear zone are illustrated in Figure 18.

The first assemblage is recognized in the least altered basaltic rocks in the hanging wall to the deposit (Plate 4a). It is considered, in part, to be the result of regional greenschist facies metamorphism.

Alteration assemblage 2 is restricted to basaltic rocks which lie outside but adjacent to the zones of high strain. It is characterized by diminished chlorite and calcite, increased ankerite, and the appearance of sericite. This assemblage is equivalent to the carbonate rhomb alteration mapped on surface. Assemblage 2 forms a zone of alteration about 8 m wide in the hanging wall to the deposit but is more extensive in the footwall to the zone of gold-enrichment where it occurs in a lozenge of undeformed basaltic rocks in sheared contact with the gabbroic sill (Figure 18). The carbonate porphyroblasts are more abundant in the medium-grained basaltic rocks (Plate 4b) and are locally associated with flow contacts.

Alteration assemblage 3 occurs in both strongly foliated basaltic rocks on the fringes of the high strain zones and the sheared gabbroic rocks in the footwall to the deposit (Figure 18). It is characterized, in the basaltic rocks, by the absence of calcite, further diminished chlorite, the occurrence of siderite, and high ankerite and sericite content (Plates 4c and 4d). Pyrite may be present. This assemblage is similar to that in the chloritic patches occurring within pervasive carbonate-sericite alteration zones as mapped on surface. This alteration assemblage was logged in drill core as "incipient" on the basis of >20% chlorite. The term incipient will be retained in further discussion. This assemblage contains low grades of gold concentration (<300 ppm), and forms zones, 8 to 10 m, wide on the edges of the shear zone. In sheared gabbroic rocks of the footwall to the deposit

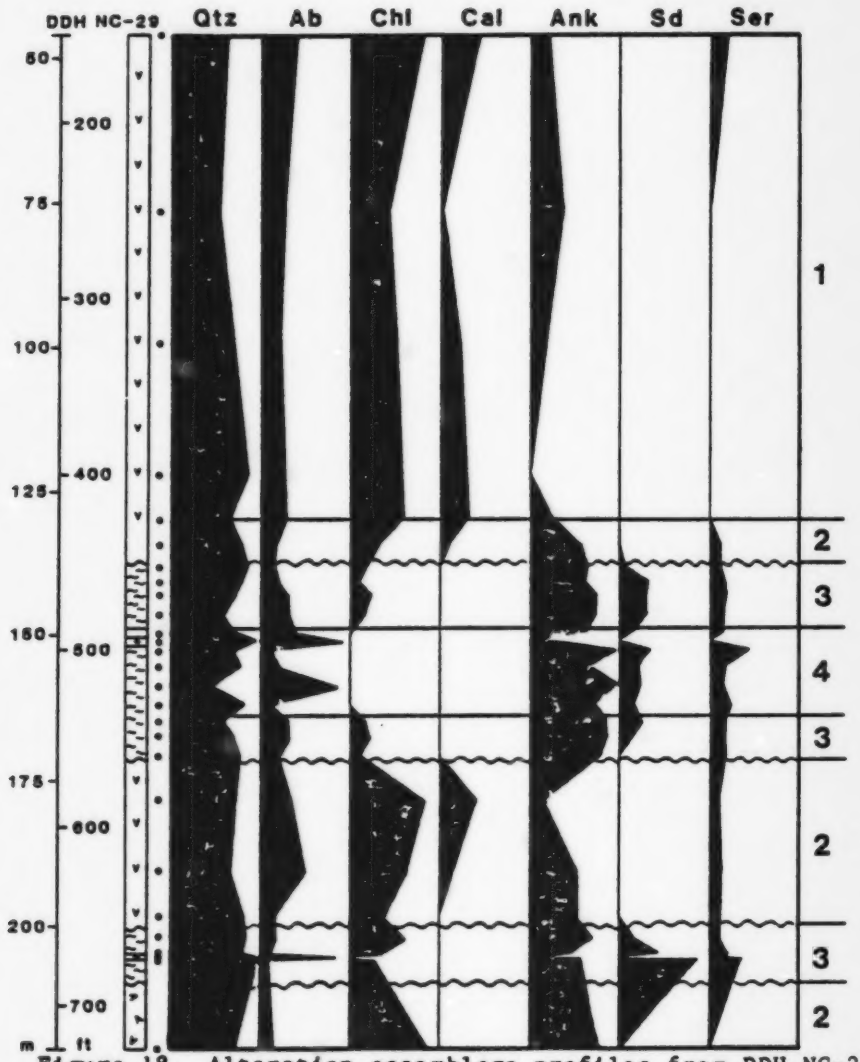

Figure 18. Alteration assemblage profiles from DDH NC-29 illustrating the spatial relationships between hydrothermal alteration and deformation at Cameron Lake. Data correspond to X-ray diffraction peak heights normalized to quartz. Absolute peak heights for quartz are used. Shear zone boundaries are indicated by the fault symbols. The gold-bearing zone is centred on 500 ft. In conjunction with core logging and petrography, four symmetrical alteration zones are defined based on these data. The assemblages characteristic of these zones include: 1) Quartz-albite-chlorite-calcite-ankerite-epidote-actinolite, 2) Quartz-albite-ankerite-sericite-chlorite-calcite-rutile, 3) Quartz-albite-ankerite-sericite-siderite-chlorite-pyrite-rutile, 4) Quartz-albite-ankerite-ankerite-sericite-siderite-pyrite-rutile. The latter assemblage is spatially associated with pyritic, quart-albite breccia-veins. Within the gabbroic rocks Fe-rich magnesite is developed in contrast to the Mg-rich siderite in the basalts. Dots correspond to sample locations. Quartz = Qtz, Albite = Ab, Chlorite = Chl, Calcite = Cal, Ankerite = Ank, Siderite = Sd, Sericite = Ser. Mineral abbreviations after Kretz (1983).

assemblage 3 is similar to that in the basaltic rocks except for the occurrence of magnesite rather than siderite and the absence of pyrite and gold-enrichment. Although sheared basaltic rocks adjacent to the contact may locally contain anomalous Au values the gabbroic rocks themselves have not yet shown significant concentrations. The gabbroic rocks commonly display "speckled" textures resulting from the contrast between coarse-grained carbonate and chlorite. An emerald green mica is locally present in the sheared gabbroic rocks which envelop narrow (<1 m) quartz-feldspar porphyry dykes. A dull red hematitic staining is also locally present.

Alteration assemblage 4 occurs in sheared basaltic rocks spatially associated with the breccia-veins (Figure 18). It is characterized by the absence of calcite and chlorite, and the presence of ankerite, siderite, sericite and pyrite (Plates 2a, 2b, and 4e). This type of alteration is equivalent to the pervasive carbonate-sericite-pyrite alteration mapped on surface and described in drill core. The term "pervasive" will be retained in further discussion. This alteration assemblage contains high grades of Au (300 ppm to 1200 ppm) and generally occurs in the centre of the high strain zones. The breccia-veins consist of foliated, pervasively altered rock fragments in a quartz-albite-rich matrix (Plates 4f, 4g, and 4h).

5.1 Petrography of Sulfide Minerals in the Altered Rocks.

Thirty-four polished thin sections of pyrite-rich rocks from the deposit were studied of which fifteen are considered representative of the sheared, pervasively altered, basaltic rocks; the remainder are representative of breccia-veins (Table III). No systematic differences

in mineralogy or textures of the opaque minerals from these two rock types were recognized except for a higher average pyrite content in the breccia-veins.

Though pyrite rarely exceeds 10% of any sample, it is the most abundant sulfide constituting greater than 98 modal percent of the opaques. Pyrite occurs as subhedra to euhedra less than 2mm in size. A striking feature of all coarser-grained pyrite are sieve textures (Plate 5a), resulting from inclusions of silicate and carbonate gangue, rutile, chalcopyrite, lesser gold and pyrrhotite, and rare hematite and magnetite (Plates 5b, 5d, and 5f). Sieve textures may result from pyrite nucleation in a pre-existing solid medium (Frater, 1985). Growth involves the impingement and inclusion of silicate and carbonate minerals of the host rocks. The concentric arrangement of inclusions within pyrite indicate growth zoning (Plate 5a) (Craig and Vaughan, 1981; Edwards, 1965; Ramdohr, 1969). A process may be envisaged involving sequential pulses of sulfur-bearing fluids circulating through the rocks which result in successive coatings of pyrite. The inclusion of all other sulfide phases within pyrite suggests contemporaneous precipitation.

Cataclastic deformation of pyrite is common in deformed sulfide ores (Craig and Vaughan, 1981; Edwards, 1965). Fracturing and brecciation resulting in pull-aparts and broken grains post-date sulfidation at Cameron Lake (Plates 6a, 6b, and 6c). Brittle deformation appears to be favoured by coarser grain sizes and may result in the apparent macroscopic "ribbon" textures commonly observed in deformed breccia-veins and pyritiferous, pervasively altered rocks (Plates 2f, 2h, and 2i). Pull aparts in sieve-textured, euhedral,

Table III. Summary of sulfide petrography: mineralogy and textures.

		PYRITE															GOLD						CHALCOPYRITE						RUTILE					
			TEXTURES								INCLUSIONS																							
Sample #	Rk Ty	%	E	S	A	Brx	Rxt	Anl	Slv	Au	Cop	Rt	Mag	Po	Hem	Gan	Inc	Fxt	Ani	Plt	Fre	Prf	Inc	Frx	Ani	Plt	Fre	Prf	Inc	Eng	Dis	Psd	Hem	Gold
NC-15-226	Phy	1	X						X	X	X	X				X	X						X			X	X		X	X		X		0,14
NC-15-409	Phy	1			X				X		X	X	X	X	X	X							X				X	X	X			X	X	tr
NC-15-424	Phy	4	X			X			X	X	X	X	X	X		X	X						X				X	X	X	X		X		0,05
NC-15-483	Phy	1	X			X			X		X	X		X		X							X				X	X	X	X		X	X	0,09
NC-22-429	Phy	3		X					X			X				X										X	X		X	X		X		0,82
NC-22-475	Phy	1		X					X		X	X				X							X			X			X	X		X		0,72
NC-22-503	Phy	1	X	X				X	X	X	X	X			X	X	X			X	X		X		X		X		X	X		X		0,22
NC-22-504	B-vein	3	X	X		X		X	X	X	X	X				X	X				X		X	X	X		X		X	X		X		0,22
NC-22-508	Phy	2	X					X	X	X	X	X				X	X	X	X	X			X	X	X		X		X	X	X			0,56
NC-22-530	B-vein	10	X	X			X	X	X	X	X		X	X		X	X	X	X	X	X	X	X	X	X	X	X	X			X			0,16
NC-43-782	Phy	9	X	X			X	X	X		X	X	X			X							X							X	X			tr
NC-43-792	Phy	1	X	X			X	X	X		X	X		X		X							X				X	X	X			X		0,05
NC-43-804	B-vein	1	X						X			X		X		X													X	X		X	X	1,35
NC-43-808	B-vein	2	X						X	X		X		X		X	X				X								X	X		X		2,33
NC-43-812	Phy	1	X						X		X					X								X		X	X	X				X		tr
NC-22-545	Phy	3	X			X			X		X	X	X	X	X	X	X						X	X		X	X	X	X			X		0,01
NC-7-54	Phy	10	X	X	X		X	X	X	X	X		X		X	X	X		X	X			X		X				X	X		X		0,57
NC-29-490	B-vein	1	X	X					X	X	X					X	X						X						X	X	X		X	0,92
NC-29-495	Phy	4	X			X		X	X	X	X	X		X		X	X						X		X				X		X			0,08
NC-29-519	Phy	5	X	X	X			X	X	X	X	X	X	X		X	X		X		X		X		X				X	X		X		0,66

Legend: (Rk Ty), rock type; (B-vein), breccia-vein; (Phy), phyllonite; (%), percent pyrite; (E), euhedral; (S), subhedral; (A), anhedral; (Brx), brecciated; (Rxt), recrystallized; (Anl), annealed; (Slv), sieve cores; (Au), gold; (Cop), chalcopyrite; (Rt), rutile; (Mag), magnetite; (Po), pyrrhotite; (Hem), hematite; (Gan), gangue; (Fxt), fractures; (Plt), plated; (Fre), free in silicate matrix; (Prf), pressure fringes; (Enq), enqulfed by pyrite grain boundaries; (Dis), disseminated; (Psd), pseudomorphing limonite; (Gold), in troy oz/ton; Mineral abbreviations after Kretz (1983).

Table III (continued). Summary of sulfide petrography: mineralogy and textures.

			PYRITE																													
			TEXTURES								INCLUSIONS							GOLD						CHALCOPYRITE					RUTILE				
Sample #	Rk Ty	%	E	S	A	Brx	Rxt	Ani	Slv		Au	Cop	Rt	Mag	Po	Hem	Gan	Inc	Fxt	Ani	Plt	Fre	Prf	Inc	Frx	Ani	Plt	Fre	Prf	Inc	Eng	Dis	Psd	Hem	Gold
D4-1A	B-VEIN	2	X						X		X	X	X		X		X	X						X	X		X	X	X	X	X		X		11000
D4-1B	B-VEIN	3	X	X		X			X		X	X	X		X		X	X						X				X	X	X	X	X		1880
D4-2A	B-VEIN	5	X	X	X				X		X	X	X		X		X	X	X					X	X		X			X	X		X	12200
D4-2B	B-VEIN	2	X							X	X	X	X	X	X		X	X						X	X		X	X		X	X		X	1800
D4-2C	B-VEIN	7	X	X		X			X		X	X	X				X	X	X			X	X	X	X			X		X	X		X	15000
D4-2D	B-VEIN	6	X			X			X		X	X	X		X		X	X	X					X	X		X	X		X	X		X	15000
D4-XY3	B-VEIN	4	X			X	X		X		X	X	X				X	X				X		X	X		X	X	X	X	X		X	13000
D4-YZ3	B-VEIN	5	X			X			X		X	X	X				X	X				X		X	X		X	X	X	X	X		X	13000
D4-XZ3	B-VEIN	3	X				X		X			X	X				X					X	X	X			X	X	X	X	X		X	13000
D4-5A	B-VEIN	1	X	X					X		X	X	X				X	X						X						X			X	1200
D4-6A	B-VEIN	1	X						X			X	X	X			X							X						X	X		X	1960
D4-6B	B-VEIN	2	X	X		X			X		X	X	X	X			X	X						X						X	X		X	1950
D4-6C	B-VEIN	1	X						X		X	X	X	X			X							X			X	X		X	X		X	X	4000
D4-6D	B-VEIN	2	X						X		X	X	X	X			X	X						X			X	X	X	X			X	X	4000

Legend: (Rk Ty), rock type; (B-vein), breccia-vein; (Phy), phyllonite; (%), percent pyrite; (E), euhedral; (S), subhedral; (A), anhedral; (Brx), brecciated; (Rxt), recrystallized; (Ani), annealed; (Slv), sieve cores; (Au), gold; (Cop), chalcopyrite; (Rt), rutile; (Mag), magnetite; (Po), pyrrhotite; (Hem), hematite; (Gan), gangue; (Fxt), fractures; (Plt), plated; (Fre), free in silicate matrix; (Prf), pressure fringes; (Eng), engulfed by pyrite grain boundaries; (Dis), disseminated; (Psd), pseudomorphing ilmenite; (Gold), in ppb; Mineral abbreviations after Kretz (1983).

pyrite grains occur perpendicular to cleavage in the carbonates and silicates and fibre growth in pressure fringes adjacent to pyrite (Plates 6e, 6f, and 6g).

Rare epitaxial overgrowths on pyrite form euhedral, rectangular grains with sieve-textured centres and inclusion-free ends. These grains are invariably associated with quartz-carbonate pressure fringes (Plate 5e). Such textures are considered to form by mass transfer processes which involve the removal of material from areas of high mean stress and redeposition elsewhere (Kerrich, 1979). In this case, pyrite is redeposited in the low pressure region at the crystal matrix interface, perpendicular to the shortening direction. Due to inhomogeneous strain patterns around the crystal, grain growth is unimpeded in an area of extension, and the overgrowths are relatively inclusion-free. Similar textures produced by mass transfer have been discussed by McClay and Ellis (1984). The anomalous anisotropy of the pyrite may be due to deformation by dislocation processes.

Some pyrite euhedra have inclusion-free rims. Coarser pyrite aggregates may show annealed grain boundaries and triple junctions defined by trapped blebs and rods of chalcopyrite and rare gold (Plates 5c and 5d). These aggregate textures are interpreted to result from post-tectonic, static recrystallization.

Annealing and grain growth generally destroy those textures indicative of earlier deformation (McClay and Ellis, 1984); however, in pyrite-rich samples from Cameron Lake, evidence of prior deformation is preserved. Plates 6d and 6h clearly illustrate cases where coarse pyrite was brecciated prior to static recrystallization and the development of inclusion-free rims.

Chalcopyrite is common and occurs as inclusions within pyrite, as blebs and rods along annealed grain boundaries and fractures in pyrite, plated on pyrite euhedra and as anhedral masses in the carbonate-silicate matrix and pressure fringes (Plates 5a, 5c, 5d, 5h, and 6a). The association of chalcopyrite, pyrrhotite, and gold is common. Chalcopyrite is often localized with quartz and ankerite in pressure fringes adjacent to pyrite grains suggesting mobilization of chalcopyrite by mass transfer.

Gold in pyrite-rich samples has several modes of occurrence:

1) inclusions within pyrite grains (Plate 5b);
2) blebs along annealed grain boundaries and in fractures within pyrite (Plates 5d and 5h);
3) coatings on pyrite grains (Plate 5g);
4) interstitial grains to pyrite within the carbonate-silicate matrix (Plate 5g);
5) free grains in quartz-ankerite-sericite pressure fringes;
6) free grains in the quartz-rich matrix between breccia fragments.

The gold grains are generally anhedral, and as large as 50 microns in size. There is a strong association of sulfide minerals with gold. Textural evidence suggests that gold precipitation was contemporaneous with, and may have even persisted after pyrite formation.

Rutile is present in all the samples studied. It is generally associated with pyrite, occurring as ragged inclusions, and engulfed masses along pyrite grain boundaries. Skeletal, trellis-textured aggregates are also present (Plate 7e). Textural evidence suggests that rutile formed as pseudomorphs of ilmenite lamellae which

themselves had exsolved from titanomagnetite (cf. Rumble, 1976). Magnetite is common in the unaltered basalts near the deposit but is distinctly absent from zones of alteration and gold-pyrite mineralization. Replacement textures indicate that rutile occurs at sites of pyrite nucleation and growth (Plates 7f and 7g).

Hematite occurs as small bladed euhedra interstitial to pyrite, as inclusions within and plating pyrite, and associated with rutile (Plate 7h).

In summary, mineralogical and textural evidence indicates that the precipitation of gold is most closely related to pyrite precipitation rather than the more extensive carbonitization and sericitization. Deposition of gold occurred in a dynamic environment; deformation clearly predates and postdates gold-pyrite mineralization. Furthermore, sulphide nucleation appears, in part, to have occurred on primary iron oxides within the host rock.

6.0 Lithogeochemistry.

Samples were collected from the deposit for lithogeochemical analysis:

(i) to identify the trace elements associated with gold;

(ii) to supplement and assist in the interpretation of petrographic and mapping data;

(iii) to provide some insight into the chemical processes operative during alteration.

A geochemical profile through the deposit was obtained by sampling DDH NC-29. This hole was chosen for several reasons. First the rocks in both the hanging wall and footwall adjacent to the gold-bearing, sheared, pervasively altered rocks were originally both basaltic. Secondly, gold shoots in the hanging wall and footwall to the main zone of gold enrichment are absent. Thirdly, horses of unaltered, weakly deformed rocks which commonly occur within broad zones of shearing are not present in this part of the deposit. Finally, thin (1 m) quartz-feldspar porphyry dykes intrude the sheared, pervasively altered rocks, as well as the deformed contact between the basalt and gabbroic sill.

6.1 Sampling and Analytical Proceedures.

Material sampled outside the shear zone, in DDH NC-29, provided composite samples obtained by selecting several homogeneous, vein-free, 4 to 5 cm pieces of BQ core over a total core length of 1 to 2 m. Samples representing the sheared, pervasively altered, gold zone were obtained from the assay pulps which represent complete composite samples of split core over lengths averaging about 1.2 m.

Nine specimens of breccia-vein were collected from six different

vein structures exposed on surface. Polished slabs, and polished thin sections corresponding to these samples were retained for mineralogical and textural studies.

The analytical data (Appendix IV) were grouped according to rock type (basalt, gabbro and quartz-feldspar porphyry dykes) and the basalts were subdivided into least altered and pervasively altered rock sub-types. None of the samples could be considered unaltered. Breccia-veins were grouped as a distinct rock type.

The concentrations of Ag, As, Au, B, Ba, Be, Bi, Cd, Co, Cr, Cu, Hg, Li, Mo, Ni, Pb, Rb, Sb, Se, Sn, Sr, Ta, Te, U, V, W, and Zn were determined by a variety of techniques (Appendix 2). Major element analyses of SiO_2, Al_2O_3, total Fe as Fe_2O_3, FeO, MgO, CaO, Na_2O, K_2O, TiO_2, P_2O_5, MnO, CO_2, and S, and loss on ignition were also obtained. Analytical work was performed by Bondar - Clegg and Company Limited, Ottawa.

6.2 Interpretation of Results.

The Jensen diagram (Jensen, 1976) (Figure 19) was used to classify the rocks from the deposit. All of the least altered as well as pervasively altered volcanic rocks, plot within the high-iron tholeiitic basalt field. The high Mg content of the gabbroic intrusion in the footwall of the deposit is unusual and not recognized regionally or even along strike within the same unit. Quartz-feldspar porphyry dyke rocks classify as calc-alkaline dacites and rhyolites. Half of the breccia-veins plot within the cluster of high-iron tholeiitic basalts while several appear to define a trend of decreasing Fe, Ti, and Mg relative to Al.

Figure 19. Jensen cation plot of samples taken from the Cameron Lake deposit. Half filled squares are weakly altered basalt, solid squares are pervasively altered basalts, and diamonds are breccia-veins. Triangles are gabbro, and circles are quartz-feldspar porphyry dikes.

Figure 20 illustrates lithogeochemical and trace element profiles based on the data from DDH NC-29 (intersection: 17.4 m grading 0.26 oz/ton Au) and breccia veins from surface (Au ranging from 1200 to 15,000 ppb). There is a tight zone of gold enrichment which correlates with the distinct pervasively altered, strongly foliated rocks. CO_2 and CaO reflecting carbonate content, and K_2O and S reflecting sericite and pyrite contents respectively, are high in this zone. The CO_2-rich rocks form an extremely broad halo around the deposit; they are also characteristic of the barren shear zone at the contact of the mafic volcanics and the gabbroic sill in the footwall. High K_2O values are also diagnostic of both shear zones, but its distribution is less extensive than that of CO_2. S shows the strongest correlation with Au in the pervasively altered shear zone. It is absent from the shear zone in the footwall which lacks gold concentrations. Two peaks in Au content occur, one associated with a breccia-vein (note high corresponding silica) and another correlated with extremely high pyrite content indicated by high S.

Figure 19 and 20 illustrate that even in pervasively altered rocks, concentrations of SiO_2, Al_2O_3, TiO_2, MgO, and total iron as Fe_2O_{3T} are approximately equal to those in the least altered basalts. The MgO content of the gabbroic sill in the footwall to the deposit is double that of the basalts, and much higher than would be expected in rocks of gabbroic composition.

Two quartz-feldspar porphyry (QFP) dykes occur in DDH NC-29, one within the gold zone and the other within the shear at the gabbroic-basalt contact. The compositions of the dykes are similar. The gold content of the QFP in the altered zone although anomalous (150 ppb) is

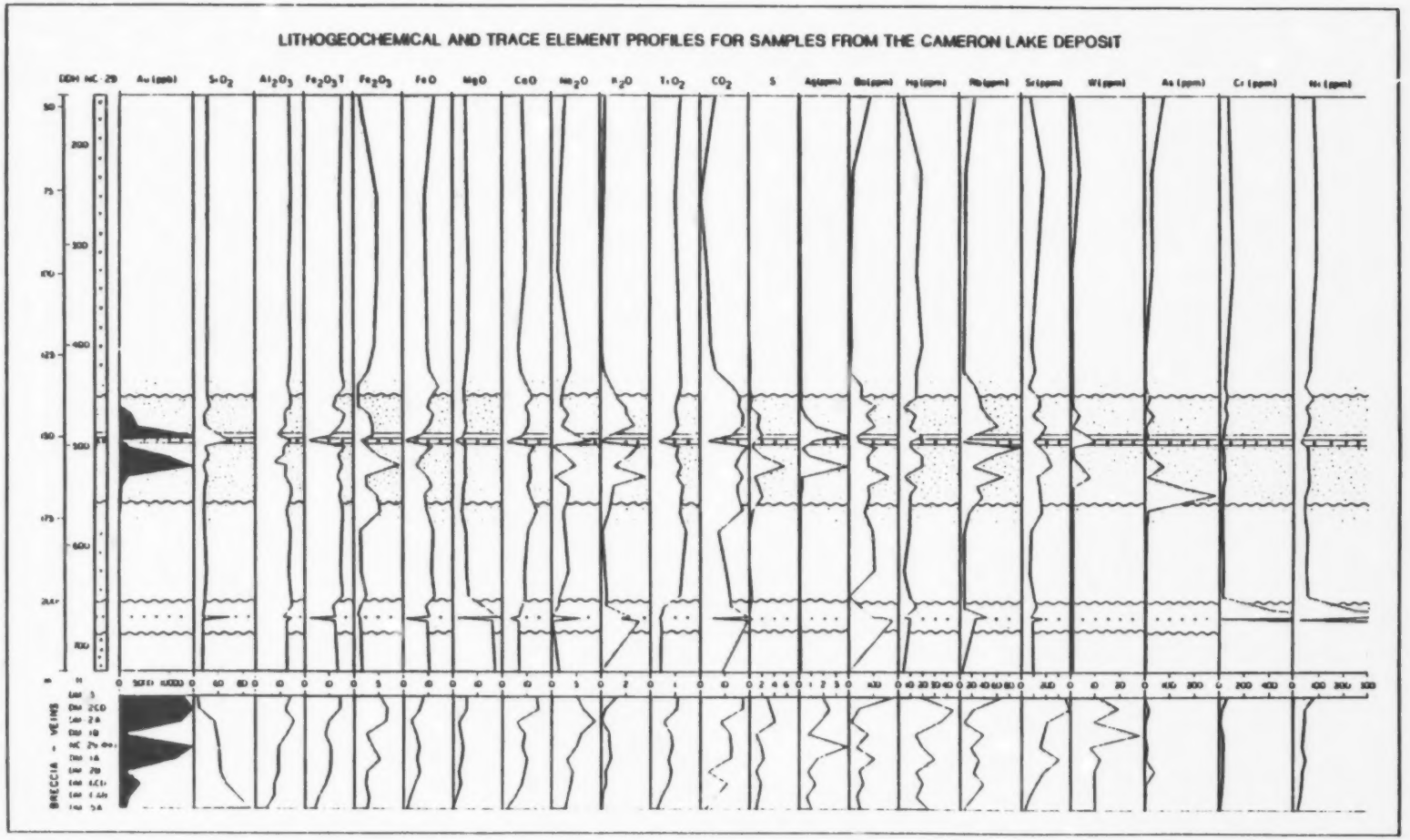

Figure 20. Lithogeochemical profiles for samples taken from DDH NC-29 and breccia veins at surface which illustrate the broad alteration envelopes which surround the gold deposit and the dilution effect of silica in the breccia-veins. Analyses of major oxides recalculated to 100% (volatile free).

much less than the surrounding rocks. This supports the contention that the QFP dykes postdate the formation of the deposit and that anomalous gold concentrations stem from the inclusion of sheared, pervasively altered rock fragments (Plate 7d) during intrusion.

In Figure 20 the samples of breccia-vein material are arranged in order of increasing silica. As the silica content of the breccia-veins increases gold and all the major element concentrations tend to decrease. This suggests a dilution of altered wall rocks with SiO_2.

Of the trace elements studied only seven, Ag, As, Ba, Hg, Rb, Sr, and W, correlate positively with gold (Figure 20). Ag, Ba, Rb, Sr, and W are enriched in both the altered basalts and the breccia-veins. Ag has a strong correlation with gold, and has a maximum value of 4.2 ppm; it occurs alloyed with the gold. Ba is also associated with gold and has a maximum value of 161 ppm, which is only about twice background levels. W shows a weak but positive correlation with gold and has a maximum value of 28 ppm. Both Rb and Sr are related to the mineralization and have maxima of 107 ppm and 410 ppm respectively. Arsenic behaves erratically within the zone of gold enrichment, and even though maximum values do not correspond to highest gold concentrations it is considered to be related to the ore forming processes. Hg exhibits a maximum value of 45 ppm in the breccia-veins which is at best only twice the background in both the unaltered and altered basalts.

Cr and Ni contents, although not indicative of gold zones, are useful in distinguishing rock types (Figure 20). The gabbroic sill in the footwall to the deposit has Cr contents ranging from 407 to 1369 ppm and Ni values from 244 to 411 ppm which, coupled with high MgO

content are compatible with Kaye's (1973) proposed relationship of these rocks to mafic-ultramafic intrusions to the north.

Figure 21 consists of scatter plots of the lithogeochemical data. CO_2 and SiO_2 were chosen as parameters upon which to base this discussion. Field and petrographic observations suggest that two styles of alteration and veining are dominant, the first characterized by pervasive carbonatization and the second by quartz-albite-rich breccia-veins accompanied by sulfidation. There is no indication of primary SiO_2 variation in the basaltic rocks (Figure 20).

CO_2 correlates positively with Au, S, K_2O and CaO in the basalts and is a function of degree of alteration (Figure 21a, 21b, 21c, and 21d). The breccia veins show similar trends; however the data must be interpreted with caution. If the two types of alteration were sequential, then the pervasively altered basaltic rocks may have been carbonatized prior to their inclusion as fragments within the breccia-veins. The CO_2 versus SiO_2 diagram (Figure 21e) illustrates this point. In basalt, silica displays no systematic variation with carbonatization; however, the breccia-veins never have CO_2 values which exceed those of the most altered basalts, and CO_2 has a negative correlation with silica. Since quartz is present in the form of a vein matrix this relationship may be thought of as simply a dilution of pervasively carbonatized basalt. In other words, the more vein matrix (SiO_2), the fewer pervasively altered rock fragments and therefore lower levels of CO_2, K_2O, and CaO.

These trends are clearly reflected in all data plotted against SiO_2. Silica shows no systematic variation related to carbonatization and sericitization of the basalts and the negative correlations exist

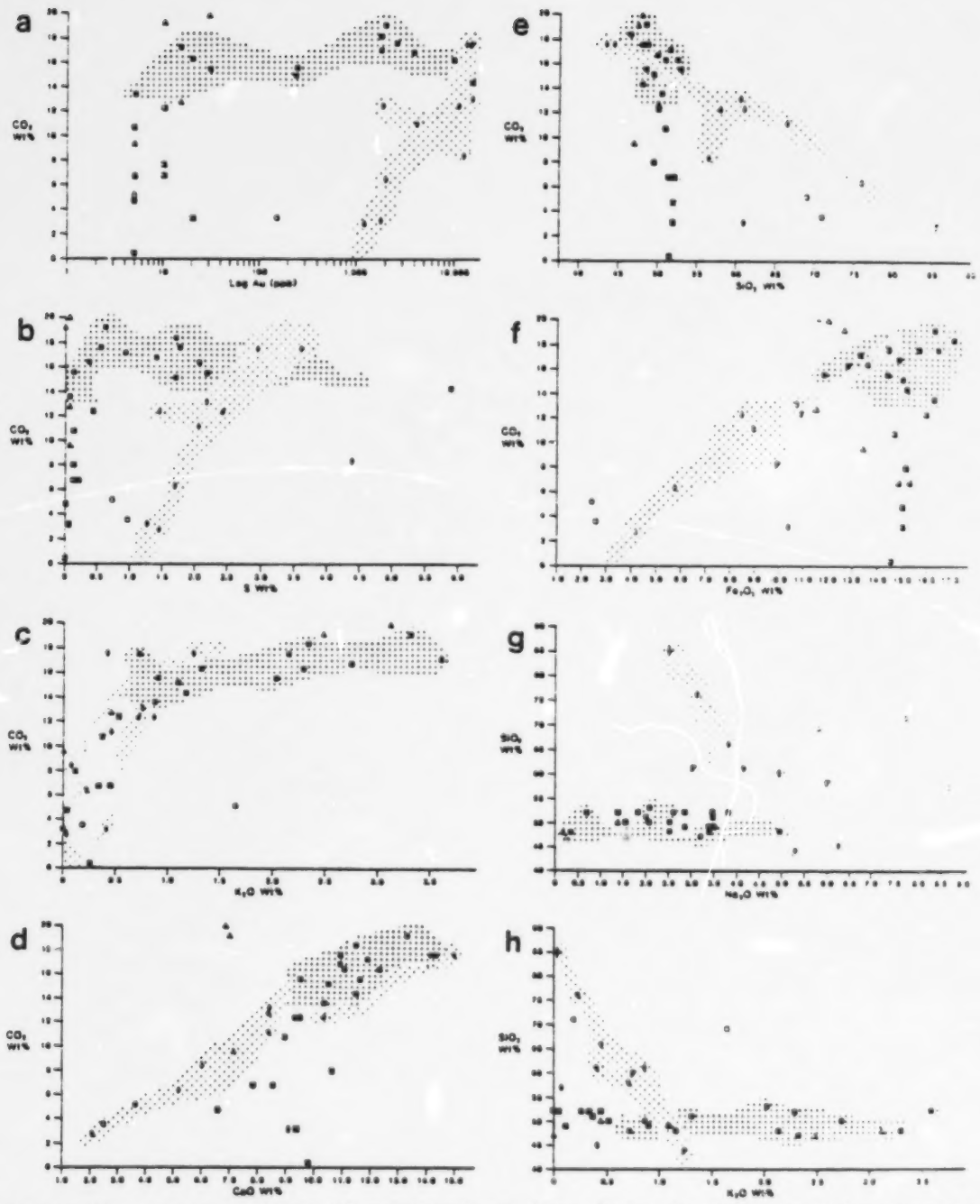

Figure 21. Scatter plots of geochemical data from the Cameron Lake deposit. (A) CO_2 against Log Au. (B) CO_2 against S. (C) CO_2 against K_2O. (D) CO_2 against CaO. (E) SiO_2 against CO_2. (F) CO_2 against Fe_2O_3. (G) SiO_2 against Na_2O. (H) SiO_2 against K_2O. Half filled squares are weakly altered basalt, solid squares are pervasively altered basalts. Diamonds are breccia-veins, circles are quartz-feldspar porphyry dykes, and triangles are gabbros. Fields are specified for weakly altered basalts (light dots), pervasively altered basalts (dark dots), and breccia veins (crosses).

among CO_2, Na_2O, and K_2O data (Figures 21e, 21g, and 21f).

Several inferences about gold precipitation may be made in light of these data. Within the breccia-veins the highest Au and S values are associated with the lowest silica values (Figures 21a and 21b). Consequently the presence of pervasively altered rock fragments within the breccia-veins seems critical in terms of providing sites for sulfidation and Au precipitation. The highest gold grades are found in those breccia-veins containing the greatest percentage of fragments and in the wall rocks adjacent to the veins. However, a quartz vein of the same generation lacking breccia fragments may still contain gold (Figures 21a and 21b). As CO_2 values approach zero, Au and S do not, but rather reach minima of 1 percent S and 1,000 ppb Au. This is compatible with observations that Au and pyrite do locally occur within the siliceous vein matrix.

Since iron shows no positive correlation with that of CO_2 (Figure 21f) the Fe component in ankerite and siderite must have been derived from the alteration of pre-existing Fe-rich minerals in the basalts rather than being introduced with CO_2.

Na_2O in the basalts displays a wide range of values totally independent of SiO_2 content and degree of alteration. Within the breccia-veins Na_2O displays a higher concentration than in any of the basalts, but has a negative correlation with silica in the veins (Figure 21g). This is compatible with the localized occurrence of albite in the quartz-rich matrix of the breccia-veins which contain the highest percentage of included wall rock.

K_2O values within the least siliceous and therefore most inclusion rich breccia-veins (Figure 21c) are approximately equal to those

transitional from least altered to pervasively altered basalt. If sericitization occurred prior to breccia-vein formation, the silica-poor veins might be expected to have much higher K_2O values similar to those occurring in the most altered rocks. One possible explanation for this apparent inconsistency may be that during breccia-vein development, K_2O was locally mobilized immediately adjacent to veins and within included fragments. This is supported by petrographic observations and XRD data on breccia-veins which indicate that the breccia fragments contain less modal sericite than their pervasively altered host rocks.

In summary, geochemical data on rock specimens from the deposit indicate the following: (1) The pervasively altered rocks of the CLSZ are the metasomatized and sheared equivalents of the enveloping basaltic and gabbroic rocks, (2) Variable but significant concentrations of Ag, Au, Ba, Rb, Sr, W, CO_2, CaO, K_2O, and S were added to the basaltic rocks during alteration and enrichments of Au, Ag, Ba, Hg, Rb, Sr, W, SiO_2, Na_2O, and S occur in the breccia-veins, (3) The basaltic rocks appear to have been carbonatized prior to brecciation and the inclusion of altered rock fragments into the veins, (4) Iron was not introduced with the hydrothermal fluid and consequently the Fe component in both carbonate minerals and pyrite must have been derived from the alteration of pre-existing Fe-rich minerals in the basalts.

7.0 Discussion.

7.1 Significance of the Cameron Lake Shear Zone.

The relationship between the Cameron Lake Shear Zone and regional geological features has not yet been established. Schwerdtner et al., (1979) showed that within the Kakagi Lake greenstone terrain shortening by continuous deformation is due to diapirism during emplacement of the surrounding batholiths; however, as they point out, this does not account for any discontinuous deformation such as faulting. Blackburn (1980) suggested that the thick succession of calc-alkaline pyroclastic rocks (Kakagi Lake Volcanics) which overlie an equally thick succession of tholeiitic basaltic flows (Snake Bay and Katimiagamak Volcanics) southwest of the Pipestone-Cameron Fault (Figure 1) is missing northeast of the fault and probably removed by erosion, indicating that the northeast side is upthrown on the fault. This would imply a correlation between the Kakagi Lake Volcanics and the Rowan Lake Volcanics; however this has not been demonstrated.

Based on the occurrence of a rotated block of felsic volcanic rocks adjacent to the Pipestone-Cameron Fault, Davies and Morin (1976) suggested that offset was dextral. The compilation of regional geology shown in Figure 2 further illustrates this geometric relationship of the orientation of lithological contacts and the fault. The consistent transposition of rock units into the plane of the fault implies dextral movement. There are components of dextral shear within the CLSZ which occurs at a low angle to the Pipestone-Cameron Fault. These observations are compatible with the CLSZ representing a splay from the Pipestone-Cameron Fault. In addition the CLSZ may in part represent a

tectonic slide (Hutton, 1979) associated with flexural slip folding on the Shingwak Lake Anticlne. Davies and Morin (1976) described zones of extensive carbonatization and shearing which occur at the contact of a peridotite sill and intermediate to felsic pyroclastic rocks in the Kakagi Lake greenstone terrain, which they attibuted to flexural slip folding.

Wade (1985) showed that displacement on the Monte Cristo Shear Zone has a significant dip slip component with the south side having moved up relative to the north; however, he also noted the presence of sinistral sense folds of the shear fabric whose hinge line orientations are similar to those of measured stretching lineations. In addition Wade (1985) postulated the presence of a brittle fault on the south side of the shear zone. Given the respective orientations of the CLSZ (315/70^{o} N) and MCSZ (246/80^{o} N) the possibility of contemporaneous deformation exists. Whether this deformation initiated the two shear zones as a conjugate set, or merely reactivated one or both of them is purely speculative.

The specific relationship between the CLSZ and other structural features in the Rowan Lake greenstone terrain remains equivocal until further studies on these structures are completed.

7.2 Structural Control of the Cameron Lake Deposit.

As shown by previous workers, most of the gold occurrences in the Cameron-Rowan Lakes area occur in the mixed Cameron Lake Volcanic succession near the transition from a lower tholeiitic volcanic succession (Rowan Lake Volcanics). However, this stratigraphic control does not necessarily imply primary, syngenetic gold enrichment as suggested by Blackburn and Janes (1983). Most of the gold

occurrences in the Cameron-Rowan Lakes area occur in zones of high strain, near lithologic contacts. The contrasting competency of mafic flows, intermediate to felsic pyroclastic rocks and intrusive rocks characteristic of the Cameron Lake Volcanics could easily explain the location of shear zones. Thus the high frequency of gold occurrences within the Cameron Lake Volcanics may be due to the presence of these shear zones and represent a structural rather than stratigraphic control.

Stuctural controls are recognized as major influences on gold deposit geometry (Bouchard et al., 1984; Fernandez et al., 1979; Guha et al., 1983; Henderson, 1983; Hoffman, 1981; Graves and Zentilli, 1982; Poulsen, 1983; Poulsen et al., 1986; Robert et al., 1983). It has been shown that the paragenesis, geometry, and mechanics of vein formation at Cameron Lake are related to deformation in the enveloping CLSZ. Furthermore, the geometry of the deposit, gold zones, and individual shoots may be interpreted simply with respect to the structure of the shear zone.

The importance of breccias in metallic mineral concentrating processes has been recently reviewed by Warnaars et al. (1985), Scherkenbach et al. (1985), Nelson and Giles (1985), Hedenquist and Henley (1985), Ohle (1985) and others (Economic Geology, Volume 8, Number 6). Little attention has been devoted to ore-related breccias which occur in Archean lode-gold deposits. Breccias constitute a specific ore type within the Timmins mining camp; Karvinen (1980, 1982) interpreted them as exhalitive vent-breccias and integral parts of his genetic model for gold deposition. Breccia-veins are reported to occur in the Red Lake mining camp (MacGeehan and Hodgson, 1982), the Val d'Or

area (Robert et al., 1983), and the San Antonio Mine in Manitoba (K.H. Poulsen, personal communication, 1985) but little work has been done in assessing their significance.

At Cameron Lake the highest contents of gold occur in breccia-veins. It has been shown that the breccia-veins formed during progressive deformation along the CLSZ during transition from ductile cleavage development to brittle processes. The change from ductile to brittle behavior may have been the result of local increases in fluid pressure as has been suggested by Kerrich et al. (1979), Phillips (1972), and Raybould (1974).

7.3 Alteration in Gold-bearing Rocks.

The four alteration assemblages which envelop the auriferous rocks of the CLSZ are similar to those recognized in basaltic rocks of other Archean gold camps (Colvine et al., 1985; Fyon and Crocket, 1982; Fyon, et al., 1983; Kerrich, 1983; Phillips and Groves, 1983; Smith and Kesler, 1985; Whitehead et al., 1981).

Carbonate alteration is an extremely common process in areas where gold has been precipitated from hydrothermal solutions. Carbonatization is a function of temperature and mole fraction, XCO_2, in the introduced fluid, and the carbonate minerals precipitated are obviously related to the availability of Ca, Mg, and Fe in the host rocks (Whitehead et al., 1981). Harte and Graham (1975) have shown that in metabasaltic rocks containing epidote, chlorite, and actinolite, calcite will form before dolomite or ankerite at lower XCO_2. Fyon et al., (1983) have shown that in altered ultramafic rocks from the Timmins camp, the stability fields for calcite, dolomite, and magnesite, respectively, correlate with increasing CO_2 content as well

as MgO/MgO + CaO in the rocks. Since complete solid solution is possible between magnesite and siderite (Deer et al., 1966), similar relationships probably exist in rocks containing more Fe and less Mg. Therefore the presence of Fe- and Mg-rich carbonates are considered indicative of higher intensities of alteration.

At Cameron Lake the distibution of carbonates and alteration assemblages indicates that the areas of most intense alteration occur in the central part of the CLSZ. Ankerite- and siderite-bearing assemblages occur in the core of the CLSZ, where fluid flux was greatest. The enveloping calcite-bearing assemblages in the undeformed host rocks to the deposit reflect lower XCO_2. This is a function of either lower gold-bearing hydrothermal fluid/ rock ratios, or mixing and dilution of the hydrothermal fluid with other types of water present in the host rocks.

Carbonate-rich rocks in the Cameron Lake area are widespread, but are not necessarily indicative of gold-enrichment. It has been shown that gold is more closely associated with pyrite, both in the breccia-veins and adjacent rocks, than with carbonates. Pyrite appears to have nucleated on rutile intergrowths interpreted as pseudomorphs after ilmenite exsolution lamellae in magnetite. Magnetite, although an abundant accessory i' the host rocks to the deposit, is rarely present within the altered g - : ring zones. Furthermore it has been shown that iron contents in the pervasively altered rocks and their basaltic precursors are similar and that there was no net increase in total iron associated with gold-pyrite mineralization. These data suggest that the fluid-wall rock reactions which led to gold deposition involved sulfidation of the Fe-bearing minerals, especially magnetite. Similar

observations have been made by Kerrich et al. (1977) and Kerrich (1983), who have shown that gold-bearing fluids are of sufficiently low oxidation potential to reduce ferric to ferrous iron in ore grade schists adjacent to gold-quartz veins.

7.4 Gold Transport and Precipitation.

Fyfe and Henley (1973), Helgeson and Garrels (1968), Kerrich and Fryer (1981), Kerrich and Fyfe (1981), and Kerrich (1983) inferred that gold is transported as chloride complexes, carbonyl complexes or both (eg. $HAu(Cl)_2$, $HAu(HCO_3)_2$) and precipitation occurred primarily in response to decreases in temperature, pressure, and carbonate fixation during fluid-wall rock interaction (i.e. carbonatization). However, Seward (1984) has proposed that gold travels as a bisulfide complex at slightly alkaline conditions which is consistent with available data on the physical and chemical characteristics for the fluids implicated in gold transport, and the experimental stabilities of the complexing ligands. From his experimental results, Seward (1984) showed that gold precipitation may be accomplished by any of the processes of boiling, precipitation of metal sulfides, dilution of the fluid, decrease in pH or oxidation potential of the transporting fluid. The precipitating reactions always involve the removal of sulphur from the fluid by reaction with Fe-silicates or oxides to produce pyrite (Phillips and Groves, 1983).

$$FeO \text{ (in silicate)} + HAu(HS)_2 + 1/4O_2 = Au + FeS_2 + 3/2H_2O$$

$$Fe_3O_4 + 3HAu(HS)_2 + 1/4O_2 = 3Au + 3FeS_2 + 9/2H_2O$$

Gold transport by and deposition from bisulfide complexes is compatible with the distinctive elemental associates commonly found in gold ores (Phillips and Groves, 1984). High concentrations of Au, Sb,

Bi, Hg, As, W, and B and corresponding low concentrations of Ag, Cu, and Zn relative to crustal abundances occur in a number of deposits (Kerrich and Fryer, 1981; Kerrich, 1983). Phillips and Groves (1983) have argued that the enriched elements all form weakly charged cations which complex selectively with large polarizable ligands such as bisulfide ions. If chloride complexes had been involved elemental ratios close to those of crustal abundances should be typical, as seen in volcanogenic base metal sulfide deposits for example. Furthermore, the solubility of gold as bisulfide complexes is affected by a much broader range of natural environments than chloride complexes, which is consistent with the wide range of diverse local environments associated with Archean gold deposits (Phillips and Groves, 1984).

7.5 Model For Gold Precipitation at Cameron Lake.

At Cameron Lake, ductile deformation and shear zone development occurred in a mechanically heterogeneous succession of rocks (Cameron Lake Volcanics), closely associated in time with greenschist facies metamorphism. The shear zones became paths of higher permeability. Fluids rich in CO_2 + K carrying Au as bisulfide or mixed ligand complexes gained access to the zone, ascending due to thermal and fluid pressure gradients (Figure 22). Field relationships suggest that widespread, pervasive carbonatization and sericitization occurred during ductile deformation, followed by local brittle deformation, the formation of breccia-veins, and sulfidation. As carbonatization proceeded, the fluid may have become enriched but not saturated in S and Au. Pervasive carbonatization strengthened the rock relative to its mafic precursor promoting local competancy contrast (Colvine et al., 1985). This, coupled with high hydrothermal fluid

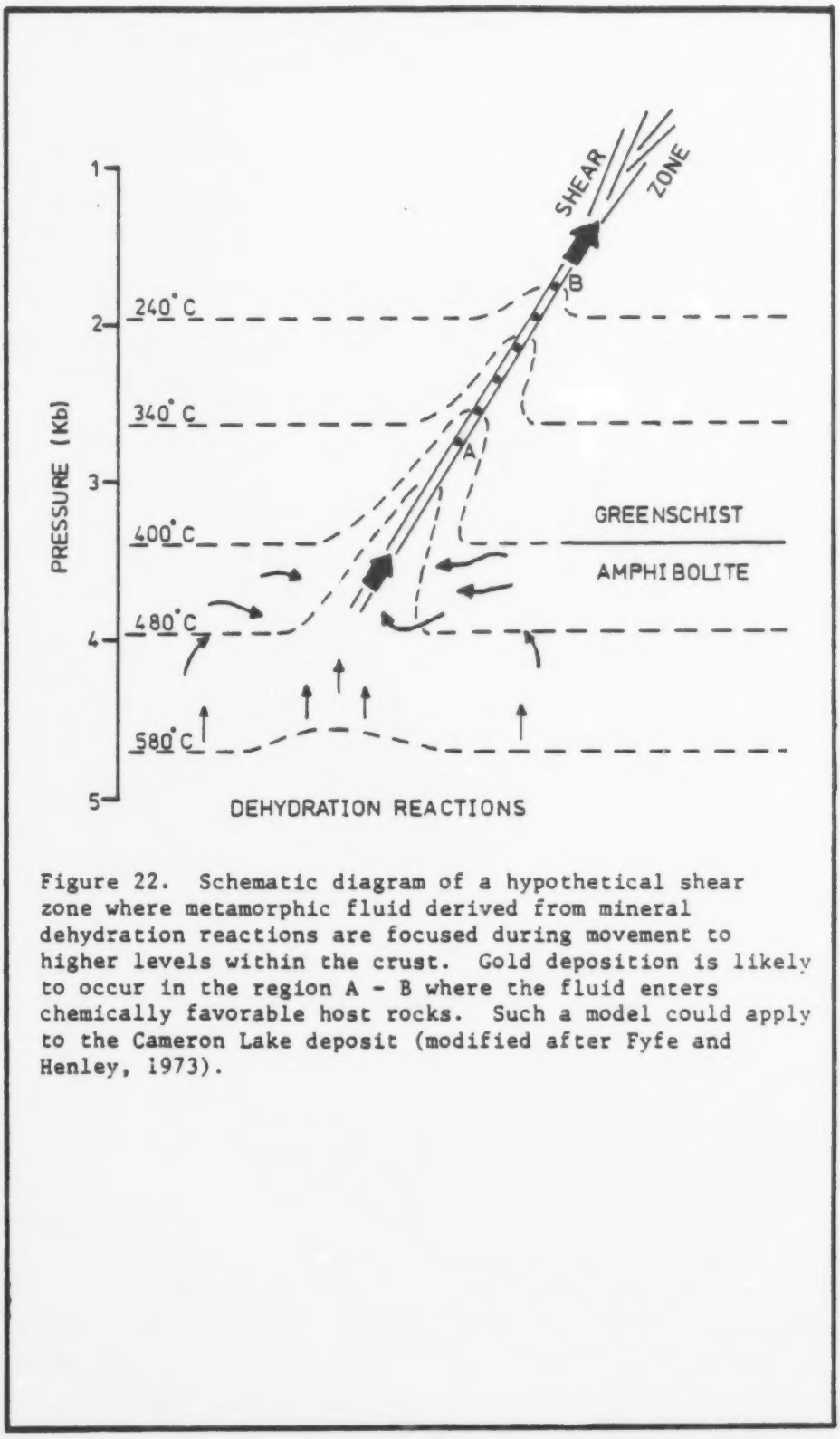

Figure 22. Schematic diagram of a hypothetical shear zone where metamorphic fluid derived from mineral dehydration reactions are focused during movement to higher levels within the crust. Gold deposition is likely to occur in the region A - B where the fluid enters chemically favorable host rocks. Such a model could apply to the Cameron Lake deposit (modified after Fyfe and Henley, 1973).

overpressures, resulted in brittle failure.

Rapid fracturing and brecciation formed a permeable conduit enhancing gold-bearing hydrothermal fluid flux. The rapid drop in pressure associated with formation of the breccia-veins promoted effervescence of the fluid, lowering gold solubility. CO_2-rich gas moved rapidly upward and the fluid remaining became saturated with respect to a S-bearing phase and Au. Brecciation increased the rock surface area exposed to the hydrothermal fluid, enhancing the rate of metasomatism and gold precipitation. Gold complexes with sulfur-bearing species became unstable and precipitation occurred when these fluids lost sulfur species by reaction with the iron-rich tholeiitic rocks to form pyrite. This model is compatible with changes in the composition of the hydrothermal fluids (Colvine et al., 1984), which may have been initially CO_2 + K rich and later CO_2 + H_2O + S rich; gold precipitation was most significant from the latter.

8.0 Conclusions.

1) The Cameron Lake gold deposit occurs in mafic volcanic rocks of the Cameron Lake Volcanics and occurs in the discordant, brittle-ductile Cameron Lake Shear Zone, which may be a splay of the Pipestone-Cameron Fault. Near the deposit strain was localized adjacent to contacts of basaltic and gabbroic rocks because of competancy contrast.

2) The localization of gold-bearing solutions occurred in response to the development of oblique, bedding-controlled sympathetic splays to the CLSZ; this also appears to control the geometry of the deposit.

3) The deposit is essentially of the vein-type associated with a large, symmetric, hydrothermal alteration zone. Alteration assemblages

are the product of intense carbonatization and variable degrees of sericitization and sulfidation of basaltic rocks.

4) The alteration assemblage associated with the highest grades of gold consists of quartz-albite-ankerite-siderite-sericite-pyrite-rutile.

5) The alteration is chemically expressed by the relative addition of major amounts of CO_2, K, Ca, and S, and minor amounts of Au, Ag, As, B, Rb, Sr, and W to the basaltic rocks.

6) Carbonatization and sericitization appear to have occurred early, followed by the formation of breccia-veins accompanied by sulfidation and gold precipitation.

7) Alteration, veining and gold mineralization occurred contemporaneously with deformation in the CLSZ under greenschist facies metamorphic conditions.

9.0 Selected Bibiliography.

Allison, I. and Kerrich, R. 1979. History of deformation and fluid transport in shear zones at Yellowknife. In Procedings of Gold Workshop, Yellowknife District, Northwest Territories. Edited by R.D. Morton, pp. 202-222.

Archibald, G.F. 1984. Cameron Lake gold property, northwestern Ontario, report on exploration activities. Unpublished company report, Nuinsco Resources Limited, 6 p.

Archibald, G.F. 1985. Summary report on 1985 diamond drilling program, Cameron Lake gold zone. Unpublished company report, Nuinsco Resources Limited, 7 p.

Beach, A. 1975. The geometry of en-echelon vein arrays. Tectonophysics, Volume 28, pp. 245-263.

Beard, R.C., and Garratt, G.L. 1976. Gold deposits of the Kenora-Fort Frances Area, Districts of Kenora and Rainy River. Ontario Division of Mines, MDC 16, 46 p. Accompanied by Chart A, scale 1:253,440, or 1 inch to 4 miles.

Bell, A.M. 1981. Vergence: an evaluation. Journal of Structural Geology, Volume 3, Number 3, pp. 197-202.

Berthe, D., Choukroune, P., and Jegouzo, P. 1979. Orthogneiss, mylonite and non-coaxial deformation of granites: the example of the South Amorican Shear Zone. Journal of Structural Geology, Volume 1, pp. 31-42.

Blackburn , C.E. 1980. Towards a mobilist tectonic model for part of the Archean of northwestern Ontario. Geoscience Canada, Volume 7, Number 2, pp. 64-72.

Blackburn, C.E. 1982. Geology of the Manitou Lakes Area, District of Kenora, (stratigraphy and petrochemistry). Ontario Geological Survey Report 223, 61 p. Accompanied by map 2476, scale 1:50,000.

Blackburn, C.E., and Janes, D.A. 1983. Gold deposits in Northwestern Ontario. In The Geology of Gold in Ontario. Edited by A.C. Colvine. Ontario Geological Survey Miscellaneous Paper 110, pp. 194-210.

Blackburn, C.E. and Hailstone, M.R. 1984. The geological environment of gold mineralization, Cameron-Rowan Lakes, N.W. Ontario. Paper Presented at the Ontario Geological Survey Geoscience Research Seminars, December 6-7, 1983, Toronto, Ontario, 13 p.

Clifford, P.M., Crocket, J.H. and Fueten F. 1983. Distribution and localization of gold in Meguma Group rocks, Nova Scotia. Part 1: structural effects and pressure solution - prelimenary results. In Current Research, Part B, Geological Survey of Canada, Paper 83-1B, pp. 279-283.

Colvine, A.C. (Editor) 1983. The Geology of Gold in Ontario. Ontario Geological Survey Miscellaneous Paper 110, 278 p.

Colvine, A.C., Andrews, A.J., Cherry, M.E., Durocher, M.E., Fyon, A.J., Lavigne, M.J., Jr., Macdonald, A.J., Marmont, S., Poulsen, K.H., Springer, J.S. and Troop, D,G. 1984. An integrated model for the origin of Archean lode gold deposits. Ontario Geological Survey, Open File Report 5524, 98 p.

Craig, J.R. and Vaughan, D.J. 1981. Ore microscopy and ore petrography. John Wiley and Sons Inc., New York, 406 p.

Crocket, J.H., Clifford, P.M., Fueten F. and Kabir, A 1983. Distribution and localization of gold in Meguma Group rocks, Nova Scotia. Part 2: implications of background geochemistry and cleavage development - preliminary results. In Current Research, Part B, Geological Survey of Canada, Paper 83-1B, pp. 285-290.

Davis, D.W., Blackburn, C.E. and Krogh, T.E. 1982. Zircon U-Pb ages from the Wabigoon-Manitou Lakes region, Wabigoon Subprovince, northwest Ontario. Canadian Journal of Earth Sciences, Volume 19, Number 2, pp. 245-266.

Davis, D.W. and Trowell, N.F. 1982. U-Pb zircon ages from the eastern Savant Lake-Crow Lake metavolcanic-metasedimentary belt, northwestern Ontario. Canadian Journal of Earth Sciences, Volume 19, Number 4, pp. 868-877.

Davis, D.W. and Edwards, G.R. 1982. Zircon U-Pb ages from the Kakagi Lake area, Wabigoon Subprovince, northwest Ontario. Canadian Journal of Earth Sciences, Volume 9, Number 6, pp. 1235-1245.

Davies, J.C. 1973. Geology of the Atikwa Lakes Area, District of Kenora. Ontario Divison of Mines, GR 111, 57 p. Accompanied by map 2273, scale 1 inch to 1/2 mile.

Davies, J.C. and Morin, J.A. 1976. Cedartree Lake area, District of Kenora. Ontario Division of Mines, GR134 52 p. Accompanied by Map 2319, scale 1 inch to 1/2 mile.

Deer, W.A., Howie, R.A. and Zussman, J. 1966. An introduction to the rock forming minerals. John Wiley and Sons Inc., New York, 528 p.

Dickson, J.A.D. 1965. A modified staining technique for carbonates in thin section. Nature, Volume 205, Number 497, 587 p.

Edwards, A.B. 1965. Textures of the ore minerals. The Australian Institute of Mining and Metallurgy, Melbourne, 242 p.

Edwards, G.R. 1980. Geology of the Schistose Lake Area, District of Kenora. Ontario Geological Report 194, 67 p. Accompanied by map 2421, scale 1:31,680 or 1 inch to 1/2 mile.

Etheridge, M.A., Wall, V.J., and Vernon, R.H. 1983. The role of the fluid phase during regional metamorphism and deformation. Journal of Metamorphic Geology, 1 (Part 3), pp. 205-226.

Etheridge, M.A., Wall, V.J., Cox, S.F., and Vernon, R.H. 1984. High fluid pressures during regional metamorphism and deformation: implications for mass transport and deformation mechanisms. In Journal of Geophysical Research, Volume 89, Number B6, pp. 4344-4358.

Esson, D.W. 1982. Report on property of Lockwood Petroleum Inc. in the Cameron-Beggs Lakes Area, District of Kenora, Ontario. Unpublished company report, Lockwood Petroleum, 30 p.

Frater, K.M. 1985. Mineralization at the Golden Grove Cu-Zn deposit, Western Australia. II: Deformation textures in the opaque minerals. Canadian Journal of Earth Sciences, Volume 22, Number 1, pp. 15-26.

Fyfe, W.S. and Henley, R.W. 1973. Some thoughts on chemical transport processes, with particular reference to gold. Miner. Sci. Engng., Volume 5, Number 4, pp. 151-172.

Fyon, J.A., Crocket, J.H. and Schwarcz, H.P. 1983. Magnesite abundance as a guide to gold mineralization associated with ultramafic flows, Timmins area. Journal of Geochemical Exploration, Volume 18, pp. 245-266.

Fyon, J.A. and Crocket, J.H. 1982. Gold exploration in the Timmins District using field and lithogeochemical characteristics of carbonate alteration zones. In Geology of Canadian Gold Deposits. Edited by R.W. Hodder and W. Petruk, CIM Special Volume 24, pp. 113-129.

Golding, S.D. and Wilson, A.F. 1983. Geochemical and stable isotope studies of the No. 4 lode Kalgoorlie, Western Australia. Economic Geology, Volume 78, pp. 438-450.

Graves, M.C., and Zentilli, M. 1982. A review of the geology of gold in Nova Scotia. In Geology of Canadian Gold Deposits. Edited by R.W. Hodder, and W. Petruk, CIM Special Volume 24, pp. 233-242.

Guha, J., Archambault, G., and Leroy, J. 1983. A correlation between the evolution of mineralizing fluids and the geochemical development of a shear zone as illustrated by the Henderson 2 Mine, Quebec. Economic Geology, Volume 78, pp. 1605-1618.

Harte, B. and Graham, C.M. 1975. The graphic analysis of greenschist to amphibolite mineral assemblages in metabasites. Journal of petrology. Volume 16, Part 2, pp. 347-370.

Hedenquist, J.W. and Henley, R.W. 1985. Hydrothermal eruptions in the Waiotapu geothermal system, New Zealand: their origin, associated breccias and relation to precious metal mineralization. Economic Geology, Volume 80, pp. 1640-1668.

Helgeson, H.G. and Garrels, R.M. 1968. Hydrothermal transport and deposition of gold. Economic Geology, Volume 63, pp. 622-635.

Henderson, J.R. 1983. Analysis of structure as a factor controlling gold mineralization in Nova Scotia. In Current Research, Part B, Geological Survey of Canada, Paper 83-1B, pp. 13-21.

Higgins, M.W. 1971. Cataclastic Rocks. United States Geological Survey, Professional Paper 683, 97p.

Hobbs, B.E., Means, W.D., and Williams, P.F. 1976. An outline of structural geology. John Wiley and Sons Inc., New York, 571 p.

Hodder, R.W. and Petruk, W. (Editors) 1982. Geology of Canadian Gold Deposits. Canadian Institute of Mining and Metallurgy, Special Volume 24, 286 p.

Hunter, A.D. 1981. Report on the exploration activities in 1981 and proposed diamond drilling in 1982. Unpublished company report, Nuinsco Resources Limited, 10 p.

Hunter, A.D. 1984. Cameron Lake gold property, northwestern Ontario: report on 1983 exploration activities. Unpublished company report, Nuinsco Resources Limited, 27 p.

Hunter, A.D. 1985. Cameron Lake: another reason to re-evaluate old gold showings. Canadian Mining Journal, April, pp. 45-48.

Hunter, A.D., Curtis, L.W. and Melling, D.R. 1984. The Cameron Lake gold deposit, northwestern Ontario: pioneering in a dormant gold camp. (Abstract) Canadian Institute of Mining and Metallurgy, Bulletin, Volume 77, Number 863, pp. 60.

Hutton, D.H.W. 1979. Tectonic slides: a review and reappraisal. In Earth Science Reviews, Volume 15, pp. 151-172.

Jensen, L.S. 1976. A new cation plot for classifying subalkalic volcanic rocks. Ontario Division of Mines, Miscellaneous Paper 66, p. 22.

Karvinen, W.O. 1982. Geology and evolution of gold deposits, Timmins area, Ontario. In Geology of Canadian Gold Deposits. Edited by R.W. Hodder and W. Petruk, Canadian Institute of Mining and Metallurgy, Special Volume 24, pp. 101-112.

Karvinen, W.O. 1980. Geology and evolution of gold deposits, Timmins area, Ontario. In Genesis of Archean, Volcanic Hosted Gold Deposits. Edited by E.G.Pye and R.G. Roberts, Ontario Geological Survey Miscellaneous Paper 197, pp. 29-46.

Kaye, L. 1973. Rowan Lake Area, District of Kenora. Ontario Division of Mines, Preliminary Map 381, scale 1 inch to 1/4 mile.

Keays, R.R. and Scott, R.B. 1976. Precious metals in ocean-ridge basalts: implications for basalts as source rocks for gold mineralization. Economic Geology, Volume 71, Number 4, pp. 705-720.

Kerrich, R. 1983. Geochemistry of gold deposits in the Abitibi Greenstone Belt. Canadian Institute of Mining and Metallurgy, Special Volume 27, 75 p.

Kerrich, R., and Allison, I. 1978. Vein geometry and hydrostatics during Yellowknife mineralization. Canadian Journal of Earth Sciences, Volume 15, pp. 1653-1660.

Kerrich, R. and Allison, I. 1978. Flow mechanisms in rocks. Geoscience Canada, Volume 5, Number 3, pp. 109-118.

Kerrich, R. and Fryer, B.J. 1981. The separation of rare elements from abundant base metals in Archean lode gold deposits: implications of low water/rock source regions. Economic Geology, Volume 76, pp. 160-166.

Kerrich, R. and Fyfe, W.S. 1981. The gold - carbonate association: source of CO_2, and CO_2 fixation reactions in Archean lode gold deposits. Chemical Geology, Volume 33, pp. 265-294.

Kerrich, R., Fyfe, W.S. and Allison, I. 1977. Iron reduction around gold-quartz veins, Yellowknife District, Northwest Territories, Canada. Economic Geology, Volume 72, pp. 657-663.

Kerrich, R. and Hodder, R.W. 1982. Archean lode gold and base metal deposits: chemical evidence for base metal fractionation into independent hydrothermal reservoirs. In Geology of Canadian Gold Deposits. Edited by R.W. Hodder, and W. Petruk, Canadian Institute of Mining and Metallurgy, Special Volume 24, pp. 144-160.

Kretz, R. 1983. Symbols for rock forming minerals. American Mineralogist, Volume 68, pp. 277-279.

Kwong, Y.T.J. and Crocket, J.H. 1978. Background and anomalous gold in rocks of an Archean greenstone assemblage, Kakagi Lake Area, Northwestern Ontario. Economic Geology, Volume 73, pp. 50-63.

Ludden, J.N., Daigneault, B., Robert, F. and Taylor, R.P. 1984. Trace element mobility in alteration zones associated with Archean Au lode deposits. Economic Geology, Volume 79, pp. 1131-1141.

MacGeehan, P.J. and Hodgson, C.J. 1982. Environments of gold mineralization in the Cambell Red Lake and Dickenson Mines, Red Lake District, Ontario. In Geology of Canadian Gold Deposits. Edited by R.W. Hodder and W. Petruk, Canadian Institute of Mining and Metallurgy, Special Volume 24, pp. 184-207.

Mackasey, W.O., Blackburn, C.E. and Trowell, N.F. 1974. A regional approach to the Wabigoon-Quetico Belts and its bearing on exploration, in Northwestern Ontario. Ontario Division of Mines, Miscellaneous Paper 58, 30 p.

McClay, K.R., and Ellis, P.G. 1984. Deformation of pyrite. Economic Geology, Volume 79, pp. 400-403.

Melling, D.R. and Watkinson, D.H. 1985. The Cameron Lake deposit: introductory discussion and field guide. Institute on Lake Superior Geology, 31st Annual Meeting, Kenora, Ontario, pp. 1-11.

Melling, D.R., Watkinson, D.H., Chorlton, L.B. and Poulson, K.H. 1985a. The influence of shear zone geometry and vein paragenesis on gold-pyrite mineralization at Cameron Lake, northwestern Ontario. Institute on Lake Superior Geology, 31st Annual Meeting, Kenora, Ontario, Abstracts with Program, pp. 55-56.

Melling, D.R., Watkinson, D.H. Poulson, K.H. and Chorlton, L.B. 1985b. The geological setting and genesis of the Cameron Lake gold deposit (Grant 193 pp. 136-150). In Geoscience Research Grant Program, Summary of Research 1984-1985, edited by V.G. Milne, Ontario Geological Survey, Miscellaneous Paper 127, 246 p.

Mitcham, T.W. 1974. Origin of breccia pipes. Economic Geology, Volume 69, pp. 412-413.

Nelson, C.E., and Giles, D.L. 1985. Hydrothermal eruption mechanisms and hot spring gold deposits. Economic Geology, Volume 80, Number 6, pp. 1633-1639.

Northern Miner 1983a. Cameron Lake gold rush builds momentum. The Northern Miner, June 23, Volume 69, Number 16, pp. 1, 21.

Northern Miner 1983b. Cameron Lake find spurs Kenora District. The Northern Miner, October 20, Volume 6, Number 33, pp. B12-B13.

Ohle, E.L. 1985. Breccias in Mississippi Valley-type deposits. Economic Geology, Volume 80, pp. 1736-1752.

Phillips,G.N. and Groves, D.I. 1984. An epigenetic origin for Archean banded iron-formation-hosted gold deposits. Economic Geology, Volume 79, pp. 162-171.

Phillips, G.N. and Groves, D.I. 1983. The nature of Archean gold-bearing fluids as deduced from gold deposits of western Australia. Journal of the Geological Society of Australia, Volume 30, pp. 25-39.

Phillips, W.J. 1972. Hydraulic fracturing and mineralization. Journal of the Geological Society of London, Volume 138, pp. 337-359.

Price, N.J. 1975. Fluids in the crust of the Earth. Sci. Prog., Volume 62, pp. 59-87.

Poulsen, K.H. 1983. Structural setting of vein-type gold mineralization in the Mine Centre-Fort Francis Area: implications for the Wabigoon Subprovince. In The Geology of Gold in Ontario. Edited by A.C. Colvine, Ontario Geological Survey Miscellaneous Paper 110, pp. 174-180.

Poulsen, K.H., Ames, D.E., and Galley, A.G. 1985. Gold mineralization in the Star Lake pluton, La Ronge belt, Saskatchewan: a preliminary report. In Current Research, Part A, Geological Survey of Canada Paper 86-1A, pp. 205-212.

Pye, E.G. and Roberts, R.G. (Editors) 1980. Genesis of Archean, Volcanic Hosted Gold Deposits. Ontario Geological Survey, Miscellaneous Paper 97, 175 p.

Ramdohr, P., 1969. The ore minerals and their intergrowths. Pergamon Press, Oxford, 1174 p.

Ramsay, J.G. 1967. Folding and fracturing of rocks. McGraw-Hill Book Company, New York, 586 p.

Ramsay, J.G.1980a. The crack-seal mechanism of rock deformation. Nature, Volume 284, pp. 135-139.

Ramsay, J.G. 1980b. Shear zone geometry: a review. Journal of Structural Geology, Volume 2, pp. 83-99.

Ramsay, J.G. and Graham, R.H. 1970. Strain variation in shear belts. Canadian Journal of Earth Sciences, Volume 7, pp. 786-813.

Ramsay, J.G. and Huber, M.I. 1983. The techniques of modern structural geology volume 1: strain analysis. Academic Press, New York, 307 p.

Raybould, J.G. 1974. Ore textures paragenesis and zoning in the lead-zinc veins of mid-Wales. Trans. Inst. Mining Met., Volume 83, pp. B112-B119.

Robert, F., Brown, A.C. and Audet, A.J. 1983. Structural control of gold mineralization at the Sigma Mine, Val d'Or, Quebec. CIM Bulletin, Volume 76, Number 850, pp. 72-80.

Robert, F. and Brown, A.C. 1984. Progressive alteration associated with gold-quart-tourmaline veins at the Sigma Mine, Abitibi Greenstone Belt, Quebec. Economic Geology, Volume 79, pp. 393-399.

Roering, C. 1968. The geometrical significance of natural en-echelon crack arrays. Tectonophysics, Volume 5, pp. 107-123.

Rumble, D. 1976. Oxide minerals. Mineralogical Society of America, Short Course Notes, Volume 3, pp. Hg1-Hg100.

Sawkins, F.J. 1969. Chemical brecciation, an unrecognized mechanism for breccia formation. Economic Geology, Volume 64, pp. 613-617.

Schwerdtner, W.M., Stone, D., Osadetz, K., Morgan, J. and Scott, G.M. 1979. Granitoid complexes and the Archean tectonic record in the southern part of northwestern Ontario. Canadian Journal of Earth Sciences, Volume 16, pp. 1965-1977.

Scherkenback, P.A., Sawkins, F.J., and Seyfried, W.E., Jr. 1985. Geologic, fluid inclusion, and geochemical studies of the mineralized breccias at Cumobabi, Sonora, Mexico. Economic Geology, Volume 80, pp. 1566-1592.

Seward, T.M. 1984. The transportation and deposition of gold in hydrothermal systems. Gold 82 - Proceedings of the International Symposium, Zimbabwe: Roterdam, Balkema Publications, pp. 165-181.

Shearman, D.J., Mossop, G., Dunsmore, H. and Martin, M. 1972. Origin of gypsum veins by hydraulic fracture. Trans. Int. Mining Met., Volume 81, pp. B149-B155.

Sibson, R.H. 1977. Fault rocks and fault mechanisms. Journal of the Geological Society of London, Volume 133, pp.191-213.

Sibson, R.H., Moore, J.McM., and Rankin, A.H. 1975. Seismic pumping - a hydrothermal transport mechanism. Journal of the Geological Society of London, Volume 131, pp. 653-659.

Simpson, C. 1983. Strain and shape-fabric variations associated with ductile shear zones. Journal of Structural Geology, Volume 5, Number 1, pp. 61-72.

Simpson, C., and Schmid, S.M. 1983. An evaluation of criteria to deduce the sense of movement in sheared rocks. Geological Society of America Bulletin, Volume 94, pp 1281-1288.

Smith, D.R., McNutt, R.H. and Clifford, P.M. 1973. Nature and origin of sialic pyroclastic rocks at Kakagi Lake, Northwestern Ontario. Canadian Journal of Earth Sciences, Volume 10, pp. 538-550.

Smith, T.J. and Kesler, S.E. 1985. Relation of fluid inclusion geochemistry to wall rock alteration and lithogeochemical zonation at the Hollinger-McIntyre gold deposit, Timmins, Ontario, Canada. Canadian Institute of Mining and Metallurgy Bulletin, Volume 78, Number 876, pp. 35-46.

Studemeister, P.A. 1983. The redox state of iron, a powerful indicator of hydrothermal alteration. Geoscience Canada, Volume 10, Number 4, pp. 189-194.

Thompson, J.E. 1935. Geology of the Rowan-Straw Lakes Area. Ontario Department of Mines, Volume 44, Part 4, pp. 1-28.

Trowell, N.F., Blackburn, C.E., Edwards, G., and Bartlett, J.R. 1977. Savant Lake-Crow Lake special project, Districts of Thunder Bay and Kenora. In Summary of Field Work 1977 by The Geological Branch. Edited by V.G. Miline, O.L. White, R.B. Barlow, and J.A. Robertson, Ontario Geological Survey, Miscellaneous Paper 75, pp. 29-50.

Trowell, N.F., Blackburn, C.E. and Edwards, G.R. 1980. Preliminary synthesis of the Savant Lake-Crow Lake Metavolcanic-Metasedimentary Belt, Northwestern Ontario, and its bearing upon mineral exploration. Ontario Geological Survey, Miscellaneous Paper 89, 30 p. Accompanied by Chart A.

van der Pluijm, B.A. 1984. An unusual 'crack-seal' vein geometry. Journal of Structural Geology, Volume 6, pp. 593-597.

Wade, M.P.G. 1985. A kinematic study of the Monte Cristo Shear Zone, northwestern Ontario. Unpublished B.Sc. thesis, Carleton University, 59 p.

Walker, S.D. and Cregheur, P. 1982. The Chadbourne Mine Noranda, Quebec: a gold bearing breccia. In Geology of Canadian Gold Deposits. Edited by R.W. Hodder and W. Petruk, CIM Special Volume 24, pp. 58-62.

Warnaars, F.W., Holmgren, C.D., and Barassi, F.S. 1985. Porphyry copper and tourmaline breccias at Los Bronces - Rio Blanco, Chile. Economic Geology, Volume 80, pp. 1544-1565.

Whitehead, R.E.S., Davies, J.F., Cameron, R.A. and Duff, D. 1981. Carbonate, alkali and arsenic anomalies associated with gold mineralization, Timmins area. Ontario Geological Survey, Miscellaneous Paper 98, pp. 318-333.

APPENDIX I

Analytical data for samples from the Cameron - Rowan Lakes area.

FIGURE 23 - SEE BACK POCKET

ANALYTICAL DATA FROM BLACKBURN FOR THE CAMERON-ROWAN LAKES AREA.

SAMPLE #	SiO_2	Al_2O_3	Fe_2O_3	FeO	MgO	CaO	Na_2O	K_2O	TiO_2	P_2O_5	MnO	H_2O+	H_2O-	CO_2	S	Total
RL1	52.8	15.5	1.66	8.53	6.42	7.45	2.41	1.45	0.91	0.16	0.18	1.10	0.33	0.10	0.01	98.8
RL2	63.9	13.2	0.95	4.67	3.21	4.01	1.94	1.28	0.67	0.15	0.09	2.44	0.41	2.90	0.01	99.8
RL3	52.2	16.2	2.61	7.73	5.21	6.27	4.02	0.28	1.05	0.19	0.17	2.64	0.35	0.40	0.01	99.3
RL4	48.2	14.0	3.10	9.98	7.11	10.4	0.91	0.04	1.08	0.10	0.20	3.10	0.30	0.10	0.05	98.7
RL5	45.9	15.0	2.70	9.90	5.76	12.7	1.74	0.06	0.92	0.08	0.22	2.46	0.28	1.90	0.08	99.7
RL6	48.3	14.3	3.10	9.66	7.84	9.03	1.39	0.01	1.02	0.08	0.17	2.83	0.36	0.90	0.01	99.0
RL7	48.4	15.1	3.29	8.29	6.47	12.2	0.95	0.01	0.74	0.06	0.19	2.14	0.32	0.65	0.10	98.9
RL8	47.8	15.1	2.76	8.05	5.92	13.8	1.54	0.05	0.75	0.06	0.18	2.28	0.29	1.10	0.06	99.8
RL8-D	47.8	15.0	2.47	8.13	5.86	13.7	1.63	0.05	0.75	0.06	0.18	2.28	0.29	1.00	0.08	99.3
RL9	50.0	13.8	3.67	8.94	6.22	9.95	2.18	0.02	1.06	0.09	0.19	2.23	0.34	0.30	0.11	99.1
RL10	47.4	14.6	2.30	10.4	7.46	8.97	2.33	0.23	1.17	0.10	0.21	3.26	0.48	0.10	0.13	99.1
RL11	50.3	17.2	3.37	6.60	3.29	12.0	1.19	0.01	0.87	0.07	0.19	2.48	0.38	2.00	0.26	100.2
RL12	46.2	18.5	2.96	8.05	4.35	10.1	2.48	0.01	1.02	0.07	0.27	3.12	0.37	1.90	0.22	99.6
RL13	49.1	16.7	3.06	6.20	4.67	12.0	1.43	0.01	0.86	0.08	0.20	2.57	0.33	2.00	0.07	99.3
RL14	53.4	15.1	1.99	7.08	6.57	7.09	3.84	0.15	0.89	0.16	0.18	2.09	0.35	0.10	0.02	99.0
RL15	47.6	14.7	2.70	10.6	6.92	10.5	1.47	0.02	1.01	0.08	0.22	2.59	0.30	0.10	0.10	98.9
RL16	49.2	15.9	3.23	7.08	3.11	12.4	1.32	0.01	0.96	0.07	0.31	2.50	0.23	3.50	0.14	100.0
RL17	46.9	15.6	1.60	9.74	2.96	9.67	2.20	0.45	1.19	0.09	0.33	3.71	0.30	5.80	0.12	100.7
RL17-D	46.8	15.6	1.00	9.74	2.95	9.60	2.37	0.45	1.19	0.10	0.32	3.63	0.31	5.70	0.11	99.9
RL18	49.0	16.1	4.88	6.68	2.85	11.9	1.32	0.01	1.22	0.09	0.24	2.41	0.25	2.20	0.07	99.2
RL19	52.8	16.4	2.64	7.89	7.23	4.90	2.04	0.01	0.97	0.18	0.16	4.10	0.40	0.30	0.01	100.0

Data obtained from C.E. Blackburn, Regional Geologist, Kenora Mining Division, Ministry of Development and Mines.

ANALYTICAL DATA FOR SAMPLES FROM THE ROWAN LAKE AREA.

Sample #	Au*	B	Hg	Cu	Zn	Co	Ni	Cr	Ag	V	As	W	Sb	Li	Ba	Rb	Sr
LNM-3				12	49	31	21	4	0.5		5	10	5				
LNM-5				1	62	24	17	7	0.5		5	10	5				
LNM-6				2	108	7	3	3	0.5		5	10	5				
LNM-7				1	36	2	1	1	0.5		5	10	5				
TS-2				150	96	61	125	213	0.5		5	10	5				
TS-3				59	63	18	34	37	0.5		5	10	5				
TS-6				138	104	56	158	265	0.5		5	10	5				
TS-7				14	35	6	12	13	0.5		5	10	5				

Analyses reported in ppm except for * which is given in ppb.
Samples collected by D.R. Melling.
Analyses performed by Bondar-Clegg and Company Limited, Ottawa.
See Appendix II for detection limits and methods.

ANALYTICAL DATA FOR SAMPLES FROM THE ROWAN LAKE AREA.

SAMPLE #	SiO_2	Al_2O_3	Fe_2O_3	FeO	MgO	CaO	Na_2O	K_2O	TiO_2	P_2O_5	MnO	CO_2	S	LOI	Total
L-84-01	57.80	17.70	6.60	3.82	3.91	6.51	3.70	1.09	0.57	0.13	0.10			3.15	101.26
L-84-02	54.20	14.70	8.71	6.32	3.55	6.93	3.88	0.31	0.82	0.22	0.14			4.75	98.21
L-84-03	75.90	11.80	3.40	2.41	0.34	1.22	5.17	0.76	0.28	0.10	0.04			0.60	98.95
L-84-04	49.50	14.20	11.40	7.45	5.89	12.10	2.00	0.06	0.72	0.11	0.17			2.70	98.86
L-84-05	49.30	14.60	10.70	7.75	5.48	10.00	2.85	0.06	0.85	0.17	0.22			5.30	99.53
L-84-06	45.00	14.10	14.90	10.35	7.78	10.90	1.85	0.08	1.02	0.14	0.20			2.10	98.13
L-84-07	60.10	16.90	6.46	4.74	1.51	3.28	3.33	2.49	0.66	0.21	0.14			2.75	97.83
L-84-08	53.50	15.80	10.90	7.31	4.79	4.43	4.77	1.06	0.98	0.30	0.20			2.00	98.74
L-84-09	61.82	16.60	5.47	3.75	1.59	3.48	4.61	1.61	0.79	0.34	0.12			2.10	98.53
L-84-10	51.00	16.10	11.30	7.87	6.38	9.34	2.14	0.53	0.93	0.26	0.20			2.90	101.07
LNM-3	58.70	12.20	11.40		2.28	8.99	1.30	0.02	1.15	0.35	0.10			3.00	99.49
LNM-5	59.70	15.70	8.02		2.58	6.03	4.61	0.19	0.89	0.27	0.10			1.55	99.64
LNM-6	62.30	17.50	6.20		1.56	3.40	6.55	0.71	0.76	0.36	0.11			1.65	101.10
LNM-7	74.60	12.10	2.46		0.24	1.58	5.25	1.42	0.29	0.07	0.06			2.05	100.12
TS-2	48.60	14.00	14.30		7.78	9.87	2.60	0.09	1.03	0.07	0.20			3.15	101.69
TS-3	61.00	14.20	6.58		3.52	2.31	5.40	0.28	0.78	0.18	0.07			3.55	97.87
TS-6	44.70	15.10	13.00		6.62	11.80	0.89	0.01	0.87	0.28	0.22			6.35	99.83

Values reported in weight percent.
Fe_2O_3 is total iron.
LOI determined at 850°C.
Totals calcuated using major oxides and LOI; CO_2 and S were excluded.
LNM and TS series collected by D.R. Melling.
L-84-01 to L-84-10 collected by P.L. Jones, Nuinsco Resources Limited.
Analyses performed by Bondar-Clegg and Company Limited, Ottawa.
See Appendix II for detection limits and methods.

ANALYTICAL DATA FOR SAMPLES FROM THE CAMERON LAKE AREA.

Sample #	Au*	B	Hg	Cu	Zn	Co	Ni	Cr	Ag	V	As	W	Sb	Li	Ba	Rb	Sr
DM-84-01				1	57	30	129	377	0.5		11	10	5				
DM-84-02				22	54	9	28	34	0.5		5	10	5				
DM-84-03				13	95	20	62	78	0.5		5	10	5				
DM-84-04				14	122	67	135	153	0.5		5	10	5				
DM-84-05				9	64	3	53	6	0.5		5	10	5				
DM-84-11				176	98	61	159	234	0.5		5	10	5				
DM-84-12				73	121	62	188	273	0.5		5	10	5				
DM-84-13				73	113	57	177	235	0.5		5	10	5				
DM-84-16				176	104	62	156	208	0.5		5	10	5				
DM-84-17				164	157	66	64	33	0.5		5	10	5				
DM-84-20				215	126	71	101	67	0.5		5	10	5				
DM-84-21				46	98	31	76	126	0.5		5	10	5				
NC-81-1146				1	109	97	515	806	0.5	114	5	10	5				
NC-33-135				18	73	13	29	37	0.5		5	10	5				

Analyses reported in ppm except * which is given in ppb.
Samples collected by D.R. Melling.
Analyses performed by Bondar-Clegg and Company Limited, Ottawa.
See Appendix II for detection limits and methods.

ANALYTICAL DATA FOR SAMPLES FROM THE CAMERON LAKE AREA.

SAMPLE #	SiO_2	Al_2O_3	Fe_2O_3	FeO	MgO	CaO	Na_2O	K_2O	TiO_2	P_2O_5	MnO	CO_2	S	LOI	Total
DM-84-01	48.80	18.30	6.61		7.75	9.27	4.34	0.57	0.55	0.18	0.13			3.55	100.05
DM-84-02	48.90	14.10	3.75		2.32	14.90	4.60	0.60	0.39	0.20	0.13			11.45	101.34
DM-84-03	63.20	14.80	6.34		3.67	1.13	1.19	2.56	0.61	0.21	0.15			3.85	97.71
DM-84-04	44.70	13.40	14.30		6.00	7.16	2.70	0.03	1.12	0.16	0.27			8.80	98.64
DM-84-05	72.00	11.80	2.67		0.44	1.62	5.08	1.00	0.25	0.14	0.05			3.25	98.30
DM-84-11	43.70	15.80	10.50		4.45	13.50	3.31	0.04	0.90	0.17	0.19			9.05	101.61
DM-84-12	48.00	14.70	12.80		8.96	8.96	1.88	0.34	0.85	0.18	0.22			3.55	100.44
DM-84-13	49.20	15.40	14.10		7.47	6.02	2.33	0.13	0.91	0.15	0.23			3.65	99.59
DM-84-16	46.50	14.10	12.60		6.09	12.50	1.25	0.01	0.84	0.12	0.20			4.55	98.75
DM-84-17	49.60	13.00	16.70		6.70	8.22	1.78	0.01	1.54	0.23	0.22			3.55	101.54
DM-84-20	47.00	13.90	15.10		3.98	8.42	2.13	0.76	1.17	0.11	0.28			8.60	101.45
DM-84-21	57.90	15.00	8.18		4.37	3.36	5.04	0.78	0.79	0.25	0.10			6.05	101.82
NC81-1146	43.40	11.70	11.40		15.60	5.04	2.37	0.11	0.32	0.06	0.16	2.54		7.05	97.21
NC-33-135	51.60	13.10	4.10		1.60	12.20	3.02	1.58	0.41	0.22	0.10			11.60	99.53

Values reported in weight percent.
Fe_2O_3 is total iron.
LOI determined at 850°C.
Totals calculated using major oxides and LOI; CO_2 and S were excluded.
Samples collected by D.R. Meiling.
Analyses performed by Bondar-Clegg and Company Limited, Ottawa.
See Appendix II for detection limits and methods.

ANALYTICAL DATA FROM BLACKBURN FOR THE CAMERON-ROWAN LAKES AREA.

SAMPLE #	Au	B	Hg	Cu	Zn	Co	Ni	Cr	Ag	V	As	W	Sb	Li	Ba	Rb	Sr
RL1				65	100	40	115	270	1	200				25	440		300
RL2				110	110	25	60	270	1	100				6	160		200
RL3				110	85	30	40	145	1	200				10	120		300
RL4				135	110	45	75	255	1	300				10	60		200
RL5				165	115	50	120	285	1	250				10	50		150
RL6				65	60	45	60	305	1	300				15	30		150
RL7				120	90	45	115	330	1	200				8	30		250
RL8				140	90	45	120	340	1	200				5	50		150
RL8-D				140	90	45	120	340	1	200				5	50		150
RL9				150	100	40	65	220	1	250				8	30		200
RL10				120	105	45	100	200	1	250				10	70		100
RL11				125	95	50	160	335	1	200				10	30		200
RL12				110	115	55	170	355	1	250				8	40		150
RL13				165	95	50	150	305	1	200				6	40		200
RL14				80	105	35	90	235	1	200				6	110		100
RL15				155	110	50	85	270	1	250				4	30		150
RL16				165	95	50	100	275	1	250				4	50		150
RL17				115	120	45	95	225	1	200				10	110		100
RL17-D				115	120	45	95	225	1	200				10	110		100
RL18				120	105	45	90	240	1	250				6	20		250
RL19				6	110	40	95	180	1	150				10	40		300

Data obtained from C.E. Blackburn, Regional Geologist, Kenora Mining Division, Ministry of Northern Development and Mines.

ANALYTICAL DATA FROM GOODWIN FOR THE CAMERON-ROWAN LAKES BELT.

SAMPLE #	SiO_2	Al_2O_3	Fe_2O_3	FeO	MgO	CaO	Na_2O	K_2O	TiO_2	P_2O_5	MnO	H_2O^+	CO_2	LOI	Total
231	52.50	16.65	4.44	6.28	3.85	7.65	3.57	1.29	0.84	0.18	0.10	1.50	0.31		99.16
232	51.00	15.80	4.45	6.32	4.25	9.55	4.13	0.52	0.86	0.16	0.21	1.62	0.93		99.80
233	49.75	15.30	2.00	8.56	5.90	10.35	2.02	0.24	0.67	0.17	0.19	2.41	1.67		99.23
234	47.85	15.35	5.55	6.96	5.40	10.40	2.40	0.30	0.92	0.23	0.20	2.73	1.07		99.36
235	46.8	14.2	2.77	9.74	3.93	11.90	1.25	0.00	1.07		0.23			8.09	99.98
236	45.5	15.0	3.02	10.6	4.70	9.39	1.62	0.11	0.81		0.34			7.90	98.18
237	45.8	15.1	3.09	9.64	8.09	7.28	2.14	0.12	0.94		0.20			6.11	98.51
238	49.5	16.10	2.06	8.72	7.00	7.00	3.17	0.50	0.85	0.23	0.20	2.95	2.06		100.34
239	48.40	15.65	3.00	7.88	5.20	9.65	3.25	0.16	0.79	0.17	0.19	2.97	1.73		99.04
240	47.65	15.25	3.40	6.72	4.55	11.35	3.66	0.25	0.75	0.17	0.19	2.36	2.95		99.25
241	46.05	15.65	2.70	9.16	6.85	8.35	2.51	0.27	0.79	0.27	0.25	4.19	3.44		100.48
242	48.60	14.40	3.60	7.68	6.40	9.00	2.78	0.10	0.92	0.23	0.20	3.54	1.73		99.18
243	49.0	15.9	1.06	12.18	6.30	4.66	1.22	0.40	1.03		0.17			8.82	100.74
244	54.7	16.8	2.25	6.57	4.77	6.34	3.68	0.18	1.09		0.17			4.39	100.94
245	75.5	12.3	0.56	1.93	0.05	1.19	3.92	1.34	0.23		0.05			1.81	98.86
246	53.6	13.8	1.16	6.65	4.30	7.75	2.47	0.83	0.73		0.12			9.05	100.46
247	55.7	15.8	2.64	6.80	3.32	5.92	3.77	0.56	1.11		0.15			4.13	99.90
248	56.4	15.6	2.88	5.15	4.83	3.75	4.61	0.58	0.63		0.13			5.61	100.17
249	59.6	15.8	0.81	5.22	2.51	4.19	4.85	0.75	0.88		0.15			4.74	99.50
250	74.3	14.7	0.34	1.07	0.05	1.12	3.90	2.02	0.13		0.04			2.30	99.97
251	54.9	16.1	2.46	6.74	6.28	5.41	2.77	0.14	0.73		0.18			3.95	99.66
252	51.8	15.1	4.51	9.02	3.38	10.7	2.18	0.12	0.25		0.24			3.50	100.80
253	50.0	14.8	2.70	7.09	5.29	11.7	3.14	0.12	0.70		0.21			5.20	100.95
254	56.3	15.3	1.28	7.22	5.16	4.48	3.12	0.47	0.78		0.13			7.01	101.25
255	53.5	15.2	2.67	8.22	3.82	4.58	3.37	0.82	1.12		0.30			6.79	100.39
256	78.5	11.8	0.15	2.34	0.26	1.20	1.48	2.14	0.30		0.60			2.02	101.39
257	51.1	15.8	1.58	7.02	4.50	9.35	1.79	0.52	0.71		0.13			8.17	100.67

Data obtained from C.E. Blackburn, Regional Geologist, Kenora Mining Division, Ministry of Northern Development and Mines.

ANALYTICAL DATA FROM GOODWIN FOR THE CAMERON-ROMAN LAKES AREA.

SAMPLE #	Au	B	Hg	Cu	Zn	Co	Ni	Cr	Ag	V	As	W	Sb	Li	Ba	Rb	Sr
231				83	82	30	82	210	0.085	410					310		270
232				110	84	38	93	270	0.053	520					260		300
233				130	60	47	110	260	0.074	350					49		360
234				130	110	45	92	260	0.090	490					57		160
235				110	200	47	160	160	0.11	390					30		130
236				130	130	64	250	260	0.90	310					190		210
237				100	120	60	280	270	0.069	330					39		160
238				130	85	41	110	240	0.079	360					98		30
239				100	80	43	110	190	0.057	310					30		178
240				98	68	34	88	300	0.15	490					380		120
241				130	82	41	120	220	0.072	380					67		72
242				190	78	30	83	210	0.055	450					20		160
243				97	120	45	120	240	0.078	400					140		45
244				56	100	20	20	34	0.10	330					69		280
245				25	130				0.16						290		83
246				53	87	20	72	150	0.086	230					230		260
247				49	100	24	57	130	1.3	280					320		310
248				34	110	20	42	120	0.051	210					220		280
249				58	76	20	40	83	0.13	210					380		220
250				41	41				0.095						700		120
251				22	84	35	130	190	0.050	180					99		100
252				120	210	60	200	120	0.089	440					53		70
253				130	120	60	240	260	0.12	260					42		70
254				20	64	60	190	250	0.067	180					180		170
255				71	92	60	170	80	0.074	290					420		190
256				32	100	60	150	80	0.10	60					300		70
257				85	63	60	190	80	0.14	210					130		150

Data obtained from C.E. Blackburn, Regional Geologist, Kenora Mining Division, Ministry of Northern Development and Mines.

Appendix II

Detection limits and methods of chemical analysis.

Whole Rock.

Element	Extraction	Method	Lower Detection Limit	Variation at Detection Limit (% Relative)	Variation at 100X Detection Limit (% Relative)	Variation at 500X Detection Limit (% Relative)
SiO_2	Borate Fusion	DC Plasma Emm Spec	0.07%	±100%	±10%	±5%
Al_2O_{3t}	Borate Fusion	DC Plasma Emm Spec	0.01%	±100%	±10%	±5%
Fe_2O_3	Borate Fusion	DC Plasma Emm Spec	0.01%	±100%	±10%	±5%
FeO	H_2SO_4-$HCLO_4$-Boric	Titrametric	0.01%	±100%	± 5%	
MgO	Borate Fusion	DC Plasma Emm Spec	0.01%	±100%	±10%	±5%
CaO	Borate Fusion	DC Plasma Emm Spec	0.01%	±100%	±10%	±5%
Na_2O	Borate Fusion	DC Plasma Emm Spec	0.03%	±100%	±10%	±5%
K_2O	Borate Fusion	DC Plasma Emm Spec	0.03%	±100%	±10%	±5%
TiO_2	Borate Fusion	DC Plasma Emm Spec	0.01%	±100%	±10%	±5%
P_2O_5	Borate Fusion	DC Plasma Emm Spec	0.25%	±100%	±10%	±5%
MnO	Borate Fusion	DC Plasma Emm Spec	0.01%	±100%	±10%	±5%
LOI	850°C / 1000°C	Gravimetric	0.01%	±100%	± 1%	
CO_2	Phosphoric acid	Gravimetric	0.01%	±100%	± 5%	
S	HNO_3-$HCLO_4$-Br	Gravimetric	0.01%	±100%	± 2%	

Trace Elements.

Element	Extraction	Method	Lower Detection Limit	Variation at Detection Limit (% Relative)	Variation at 20X Detection Limit (% Relative)	Variation at 100X Detection Limit (% Relative)
Ag	HNO_3-HCL-$HCLO_4$-HF	DC Plasma Emm Spec	0.2 ppm	±100%	±25%	±15%
As	HNO_3-HCL-$HCLO_4$-HF	DC Plasma Emm Spec	5 ppm	±100%	±25%	±15%
Au	Aqua regia	Fire assay AA	5 ppb	±100%		± 5%
B	NaOH fusion	DC Plasma Emm Spec	1 ppm	±100%		±20%
Ba	HNO_3-HCL-$HCLO_4$-HF	DC Plasma Emm Spec	1 ppm	±100%	±25%	±15%
Be	HNO_3-HCL-$HCLO_4$-HF	DC Plasma Emm Spec	1 ppm	±100%	±25%	±15%
Bi	HNO_3-HCL-$HCLO_4$-HF	DC Plasma Emm Spec	1 ppm	±100%	±25%	±15%
Cd	HNO_3-HCL-$HCLO_4$-HF	DC Plasma Emm Spec	0.5 ppm	±100%	±25%	±15%
Co	HNO_3-HCL-$HCLO_4$-HF	DC Plasma Emm Spec	1 ppm	±100%	±25%	±15%
Cr	HNO_3-HCL-$HCLO_4$-HF	DC Plasma Emm Spec	1 ppm	±100%	±25%	±15%
Cu	HNO_3-HCL-$HCLO_4$-HF	DC Plasma Emm Spec	1 ppm	±100%	±25%	±15%
Hg	HNO_3-H_2SO_4-HCL-$KMNO_4$	Cold vapour AA	5 ppb	±100%		±10%
Li	HNO_3-HCL-$HCLO_4$-HF	DC Plasma Emm Spec	1 ppm	±100%	±25%	±15%
Ni	HNO_3-HCL-$HCLO_4$-HF	DC Plasma Emm Spec	1 ppm	±100%	±25%	±15%
Pb	HNO_3-HCL-$HCLO_4$-HF	DC Plasma Emm Spec	2 ppm	±100%	±25%	±15%
Rb	HNO_3-HCL-$HCLO_4$-HF	DC Plasma Emm Spec	8 ppm	±100%	±25%	±15%
Sb	HNO_3-HCL-$HCLO_4$-HF	DC Plasma Emm Spec	2 ppm	±100%	±25%	±15%
Se	HNO_3-HCL-$HCLO_4$-HF	DC Plasma Emm Spec	5 ppm	±100%	±25%	±15%
Sn	HNO_3-HCL-$HCLO_4$-HF	DC Plasma Emm Spec	1 ppm	±100%	±25%	±15%
Sr	HNO_3-HCL-$HCLO_4$-HF	DC Plasma Emm Spec	1 ppm	±100%	±25%	±15%
Ta	HNO_3-HCL-$HCLO_4$-HF	DC Plasma Emm Spec	8 ppm	±100%	±25%	±15%
Te	HNO_3-HCL-$HCLO_4$-HF	DC Plasma Emm Spec	3 ppm	±100%	±25%	±15%
U	HNO_3-HCL-$HCLO_4$-HF	DC Plasma Emm Spec	2 ppm	±100%	±25%	±15%
W	HNO_3-HCL-$HCLO_4$-HF	DC Plasma Emm Spec	1 ppm	±100%	±25%	±15%
Zn	HNO_3-HCL-$HCLO_4$-HF	DC Plasma Emm Spec	1 ppm	±100%	±25%	±15%

Gold analyses using 10g sample weight, fire assay Pb collection and atomic emmission spectroscopy.

Appendix III

Photographic plates.

Plate 1. Photographs of polished core samples representing the major stratigraphic units encountered in drilling at Cameron Lake.

All photos are at the same scale; scale bar equals 3 cm.

Plate 1a. NC-97-328 Medium-grained gabbro located in the footwall of the deposit. Rock consists primarily of plagioclase, pyroxene, quartz, and chlorite. Light coloured skeletal grains are rutile.

Plate 1b. NC-36-435 Least-altered aphanitic, weakly amygdaloidal pillowed basalt. Note thick selvage (0.7mm) and chilled margins which have been altered to chlorite. White mineral within selvage is ankerite.

Plate 1c. NCX-29-498 Incipiently altered, aphanitic, weakly amygdaloidal pillowed basalt, typical of the least deformed rocks occurring at the fringes of the gold-bearing hydrothermally altered zones. Light crystals are rhombohedral ankerite, locally termed "carbonate rhomb" alteration. Less altered character of the chlorite selvages probably reflects primary textural/compositional differences due to equilibration with sea water during quenching. Note the more intense cleavage development in comparison with sample NC-36-435.

Plate 1d. NC-36-110 Medium-grained "black-spotted" basalt. This rock forms a distinctive unit characterized by its grain-size and irregular shaped dark chlorite clots interpreted as amygdules. Light whispy patches are epidote.

Plate 1e. NC-28-234 Aphanitic amygdaloidal basalt. Amygdules contains an infilling assemblage of quartz-calcite-chlorite commonly rimmed with epidote. Note epidote veinlet cutting core.

Plate 1f. NC-48-215 Aphanitic, amygdaloidal framework-supported pillow breccia. Amygdules are composed chiefly of quartz and chlorite. Matrix is predominantly chlorite and epidote. Note more intense foliation development compared to the "black spotted" flow (NC-36-110).

Plate 1g. NC-28-146 Aphanitic, amygdaloidal, matrix-supported pillow breccia. Intense bleaching of fragments is interpreted as the result of early (primary) carbonatization unrelated to ore-forming processes. Note the foliation development and fragments displaying portions of selvages.

Plate 1h. NC-71-55 Epiclastic rock containing volcanic fragments and rip up clasts of fine-grained muddy sediment. Note the bedding laminations in the large elongate fragment (lower right hand corner) and fold structures (upper right hand corner).

Plate 1i. NC-71-44 Epiclastic rock containing siliceous volcanic fragments (white) and rip up clasts of fine-grained graphitic sediment. Note the bedding laminations in the larger elongate fragments.

Plate 1j. NC-70-139 Interlayered, heterolithic, felsic lapilli-ash tuff and fine-grained ash tuff.

Plate 1k. NC-33-111 Massive, monolithologic, intermediate lapilli-crystal tuff. Note large feldspar-phyric lapilli fragment (left center) and the crystal component in ash-size fraction.

Plate 1l. NC-X7-250 Massive, monolithologic mafic crystal tuff which may represent a more distal facies of sample NC-33-11 (Plate 1k). White euhedral and broken crystals are feldspar.

Plate 1m. NC-1-39 Bedded, heterolithic, intermediate lapilli-crystal tuff. Sample contains both aphyric and feldspar-phyric fragments. Euhedral, stubby and lath-shaped crystals in lapilli and ash matrix are feldspar.

Plate 1n. NC-1-48 Fine-grained bedded volcanic sediment. Euhedral crystals consist of cubic pyrite and ankerite rhombs.

Plate 1o. NC-1-38 Bedded, heterolithic, intermediate lapilli-crystal tuff. Sample contains both aphyric and feldspar-phyric fragments. Euhedral, stubby and lath-shaped crystals in lapilli and ash matrix are feldspar.

Plate 1p. NC-43-902 Quartz-feldspar porphyry. Sample is veined by quartz, plagioclase, and ankerite. Note quartz eyes, plagioclase phenocrysts, and pervasively altered, foliated fragments included within the porphyry (arrow).

Plate 1

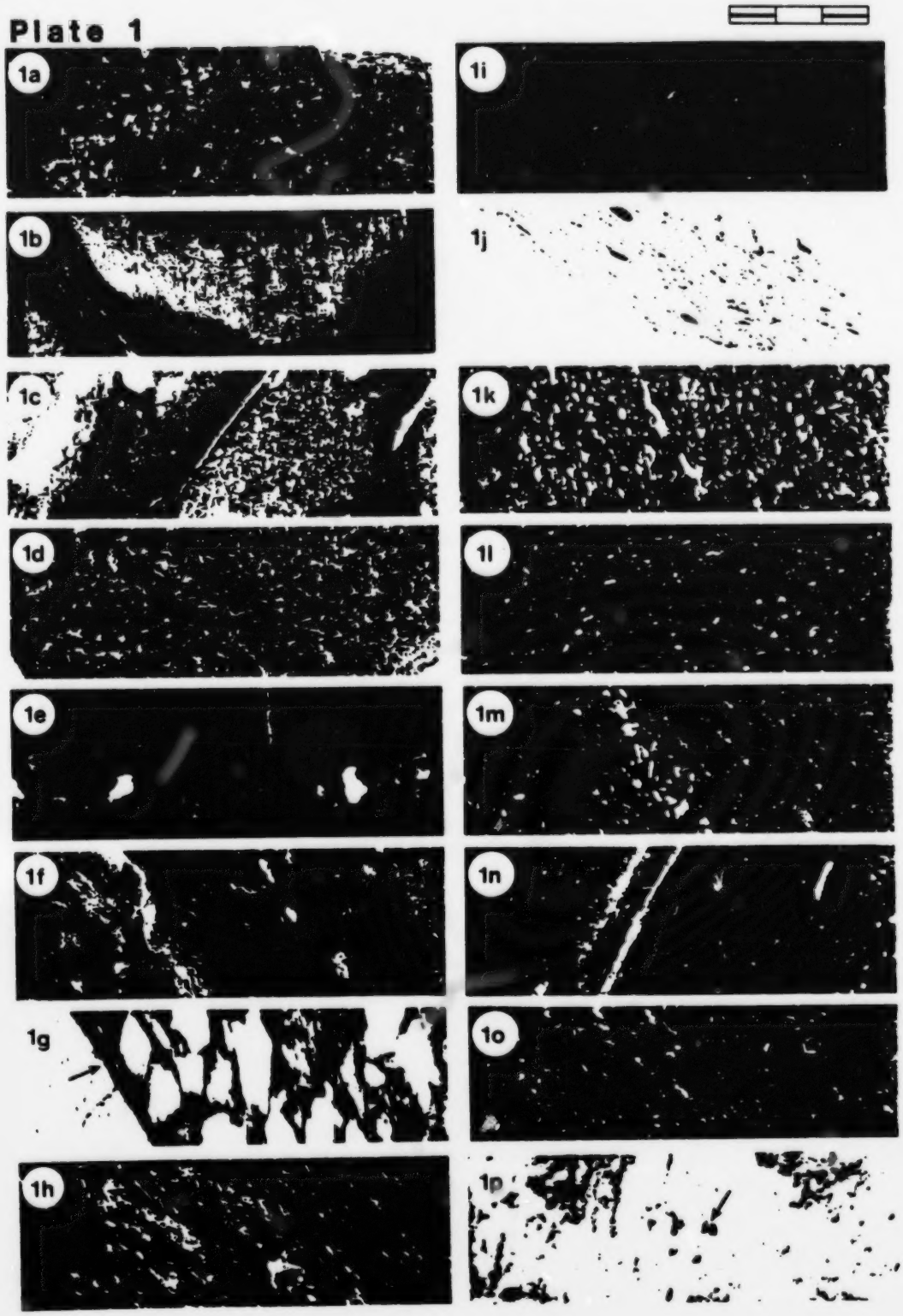

Plate 2. Photographs of polished core samples and rock slabs of altered rocks and breccia-veins encountered in drilling and on surface at Cameron Lake.

All photos of core are at the same scale; scale bar equals 3 cm. For the rock slab photos, scale card divisions are in centimetres.

Plate 2a. NC-11-121 Pervasively altered, pyritiferous basalt of the CLSZ. Note the dark pressure fringes associated with brecciated pyrite and prominent foliation.

Plate 2b. NC-16-432 Pervasively altered, sheared rock cut by a type 1, buckled quartz-ankerite vein. Note the dark pressure fringes associated with the brecciated pyrite and the cleavage approximately axial planar to the buckles. Note that the ankerite in the vein nucleates on the vein margins adjacent to the carbonatized host rock.

Plate 2c. DM-1A Breccia-vein from the discovery outcrop containing elongate angular fragments of pervasively altered basalt. Note the absence of pyrite within the vein matrix and the asymmetric distribution of ankerite which is concentrated on only one side of the fragments.

Plate 2d. NC-11-33 Breccia-vein containing angular fragments of pervasively altered basalt. Note the pyrite rimming the inner margins of the fragments. The *in situ* nature of the breccia is indicated by two adjacent fragments which were veined prior to brecciation.

Plate 2e. Discovery outcrop Gradational contact of a breccia-vein. Note the elongate fragment only slightly detached from the vein margin (arrow).

Plate 2f. North trench Moderately deformed breccia-vein. Individual fragments are difficult to identify, and pyrite is concentrated in thin seams (arrows). Note the type 3 vein cutting the sample.

Plate 2g. NC-11-113 Breccia-vein containing sub-angular, equant fragments of pervasively altered basalt.

Plate 2h. NC-24-564 Moderately deformed breccia-vein. Note the ribbon texture beginning to develop due to the brecciation of pyrite (arrow).

Plate 2i. NC-105-761 Breccia-vein cut by a type 3 vein. Note the coarse clots of hematite and chlorite which occur with quartz.

Plate 2j. NC-20-391 Thin breccia-vein containing frame-work supported, elongate, pervasively altered rock fragments. Note the type 3 veins which cut the breccia-vein but not the pervasively altered, foliated rocks.

Plate 2k. DM-6C Breccia-vein from the blood trench containing framework supported, elongate, pervasively altered fragments. Locally, quartz fibres occur oriented perpendicular to fragment boundaries.

Plate 21. DM-6A Breccia-vein from blood trench exhibiting ribbon texture defined by elongate pyritic seams (arrows). Note the cross-cutting type 3 veins.

Plate 2

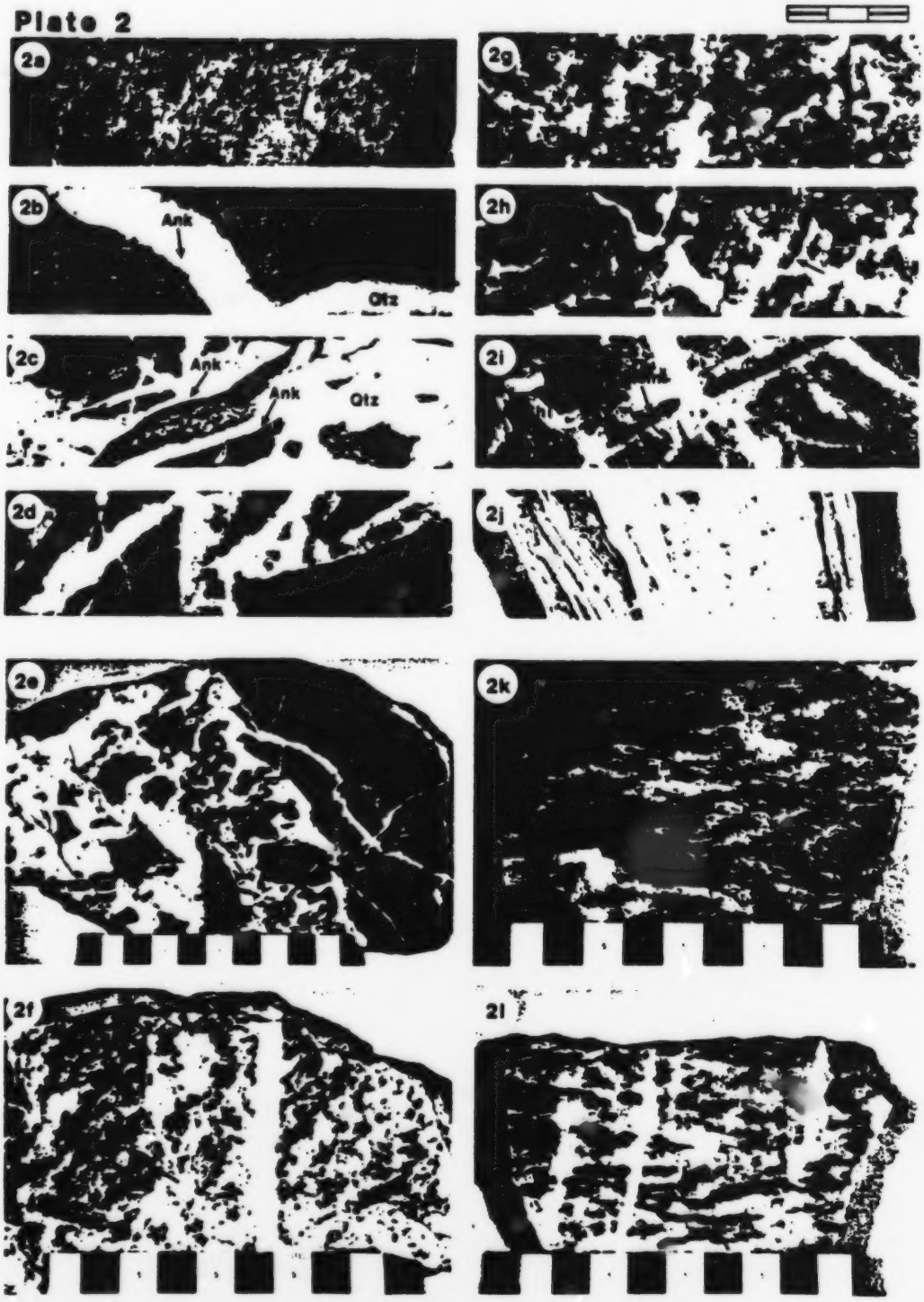

Plate 3. Photographs of deformed rocks and vein types exposed in the excavated outcrops at Cameron Lake.

Plate 3a. Discovery outcrop Weakly deformed pillowed basalt within and near the boundary of the CLSZ. Note the crenulated selvage (right centre). Aspect ratio is about 2:1.

Plate 3b. Discovery outcrop Moderately deformed pillowed basalt within the CLSZ. Note intense cleavage development. Aspect ratios are about 7:1.

Plate 3c. Discovery outcrop Type 1 buckled vein. Note the median seam of ankerite and cleavage axial planar to the buckles. Vein is boudinaged to the left of the scale card.

Plate 3d. Discovery outcrop Type 1 buckled vein. Note the median seam of ankerite and pointed vein termination (right centre). The vein is Z-folded to the right of the scale card.

Plate 3e. Discovery outcrop Breccia-vein containing pervasively altered, angular fragments. Note the sharp vein margin contacts and asymmetry of cleavage with respect to the veins.

Plate 3f. Island trench Breccia-vein occurring oblique to cleavage within the pervasively altered, basaltic rocks.

Plate 3g. North trench An array of type 3 quartz-carbonate-chlorite-hematite-gold veins cutting a breccia-vein. Note the recessive pits in the breccia-vein caused by the weathering of pervasively altered basaltic fragments. A quartz-feldspar porphyry dike intrudes the breccia-vein (bottom of photo).

Plate 3h. North trench Close up of a type 3 vein cross-cutting the breccia-vein in Plate 3g. Note the internal quartz fibres normal to the vein walls.

Plate 3

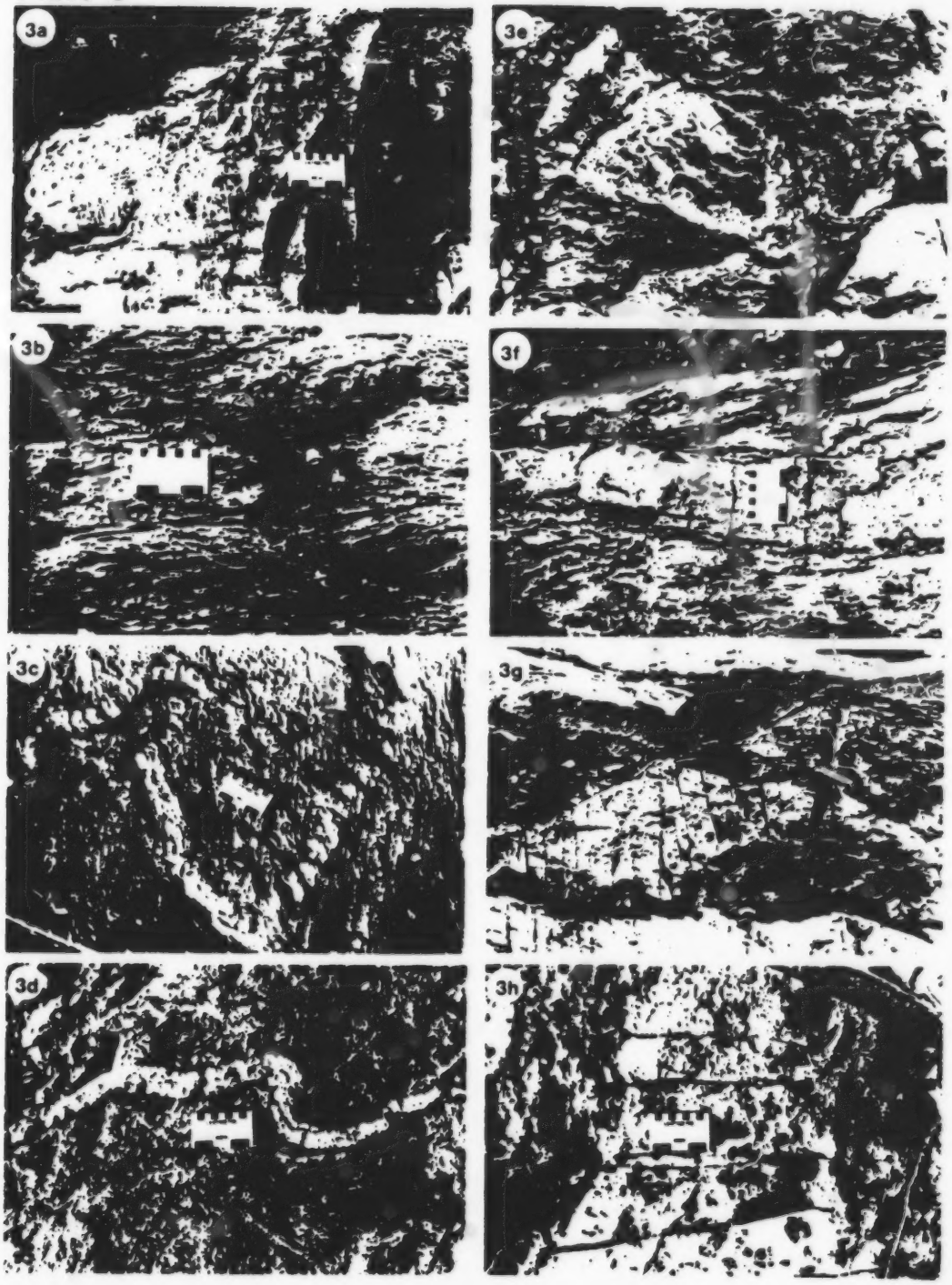

Plate 4. Photomicrographs of altered basaltic rocks in thin sections.

Plate 4a. NC-27-174 Least altered "black spotted" basalt. Dark irregular patch, interpreted as an amygdule, is infilled with chlorite, epidote, and actinolite. Note the large euhedral albite lath. Crossed nicols. Bar scale = 0.4 mm.

Plate 4b. NC-110-142 Disseminated cabonate rhomb alteration characteristic of asemblage 2. Note the large euhedral ankerite porphyroblasts, sericite replacing chlorite, and lack of foliation. Crossed nicols. Bar scale = 0.4 mm.

Plate 4c. NC-16-545 Alteration assemblage 3. Note the intense foliation defined by sericite (light) and chlorite (dark). Sericite appears to replace chlorite. Ankerite is present in the groundmass and as large euhedral porphyroblasts. Crossed nicols. Bar scale = 0.4 mm.

Plate 4d. NC-16-545 Overview of Plate 4c showing a relic porphyroclast now altered to an aggregate of chlorite, ankerite and sericite (lower left). Crossed nicols. Bar scale = 1.6 mm.

Plate 4e. NC-22-530 Ankerite-quartz veinlet cutting pervasively altered rocks of assembage 4. Note the buckled, dismembered character of the vein. Crossed nicols. Bar scale = 1.6 mm.

Plate 4f. NC-29-480 Breccia-vein. Pervasively altered basaltic fragment surrounded by vein matrix. Fragment is defined by fine-grained, high relief ankerite and pyrite euhedra. Plane polarized light. Bar scale = 0.4 mm.

Plate 4g. NC-29-480 Same as Plate 4f but illustrating the medium-grained quartz and albite which make up the vein matrix. Quartz is locally recystallized. Crossed nicols. Bar scale = 0.4 mm.

Plate 4h. NC-43-782 Beccia-vein. Note the medium-grained quartz-albite vein matrix separating two pervasively altered basaltic fragments. Crossed nicols. Bar scale = 1.6 mm.

Plate 4

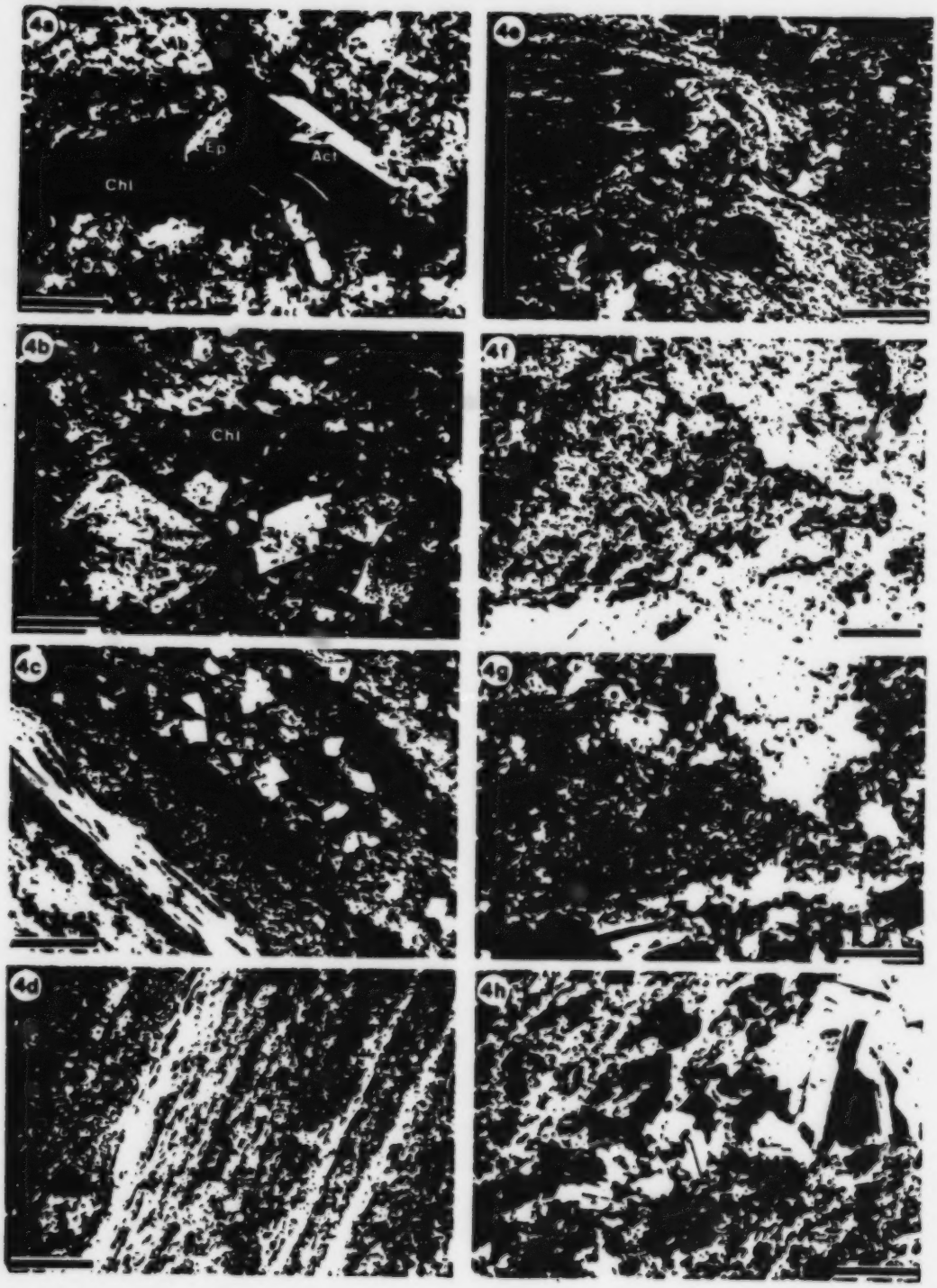

Plate 5. Photomicrographs of sulfides, oxides and gold in polished sections.

Plate 5a. DM-XY3 Euhedral sieve-textured pyrite. Note the concentric arrangement of inclusions within the pyrite grain which indicate growth zoning. Chalcopyrite occurs in the pressure fringe (upper left). Reflected light. Bar scale = 0.4 mm.

Plate 5b. NC-22-530 Subhedral to euhedral, sieve-textured pyrite grain. Inclusions consist of gangue, magnetite, chalcopyrite and gold. Note the higher concentration of inclusions in the centre of the grain, relative to the grain boundary rims. Reflaected light. Bar scale = 0.1 mm.

Plate 5c. NC-22-530 Subhedral, sieve-textured, annealed pyrite grains. Note the well developed triple junction trapping rods of chalcopyrite along the pyrite grain boundaries. Pyrite rims are relatively inclusion-free. Reflected light. Bar scale = 0.2 mm.

Plate 5d. NC-22-530 Annealed grain boundary between adjacent euhedral pyrite grains. Note the blebs of chalcopyrite and gold which define the annealed grain boundary between the grains. Pyrite rims are relatively inclusion free. Pyrrhotite inclusions are also present. Reflected light. Bar scale = 0.2 mm.

Plate 5e. DM-XY3 Rare epitaxial over-growth on pyrite. Note the rectangular form, sieve-textured centre and inclusion free ends. Also note the associated pressure fringe containing chalcopyrite plated on pyrite. Reflected light. Bar scale = 0.4 mm.

Plate 5f. NC-22-530 Anhedral pyrite containing a large inclusion of gold associated with chalcopyrite. Reflected light. Bar scale = 0.2 mm.

Plate 5g. NC-22-530 Free gold occurring in the silicate-ankerite matrix and plating on pyrite. Note chalcopyrite infilling large fracture (right). Similar irregular grain boundaries in pyrite are suggestive of brecciation. Reflected light. Bar scale = 0.2 mm.

Plate 5h. NC-22 530 Gold and chalcopyrite infilling a fracture in pyrite. Reflected light. Bar scale = 0.2 mm.

Plate 5

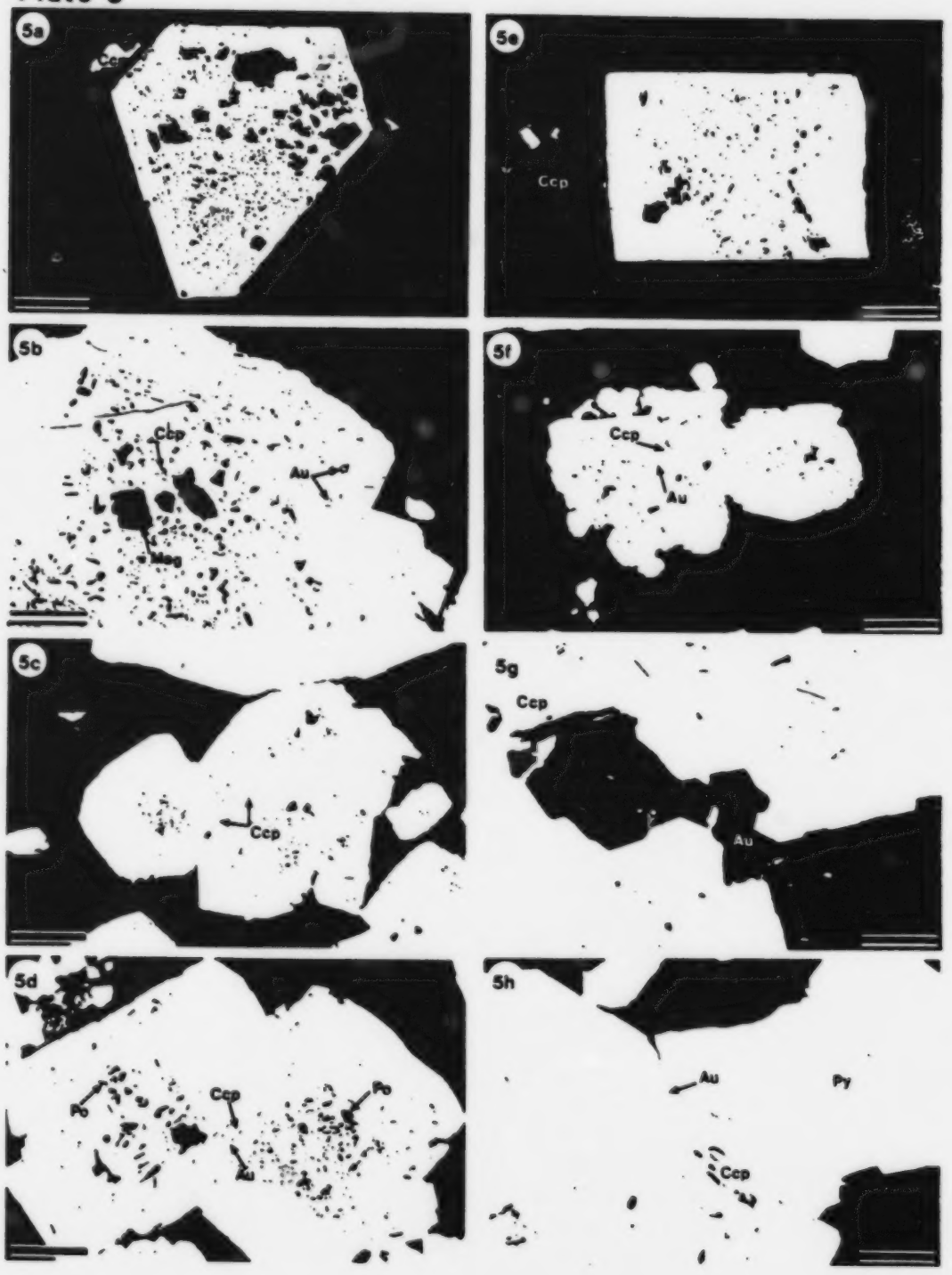
5a
Ccp
5e
Ccp
5b
Ccp
Au
Mag
5f
Ccp
Au
5c
Ccp
5g
Ccp
Au
5d
Po
Ccp
Po
Au
5h
Au
Py
Ccp

Plate 6. Photomicrographs of deformation textures in sulfides in polished sections.

Plate 6a. DM-YZ3 Brecciated, euhedral, sieve-textured pyrite. Note the extensive pressure fringe linking the detached part to the parent pyrite crystal. Chalcopyrite has been mobilized into the pressure fringe and plates the pyrite grain. Reflected light. Scale bar = 0.4 mm.

Plate 6b. DM-YZ3 Pull apart within a euhedral, seive-textured pyrite grain. Note the pressure fringes on opposite ends of the pyrite grain and the weak concentric arrangement of inclusions within the grain. Reflected light. Scale bar = 0.4 mm.

Plate 6c. DM-YZ3 Brecciated sieve-textured pyrite with pressure fringes linking fragments. Reflected light. Scale bar = 0.4 mm.

Plate 6d. Nc-22-530 Irregular sieve-textured pyrite grains with relatively inclusion-free grain boundary rims. This is interpreted as resulting from static recrystallization which post-dates brecciation. Reflected light. Scale bar = 0.2 mm.

Plate 6e. DM-YZ3 Same as plate 6a but illustrating the quartz-ankerite-sericite pressure fringe in transmitted light. Crossed nicols. Scale bar = 0.4 mm.

Plate 6f. DM-YZ3 Same as plate 6b but illustrating the quartz-ankerite-sericite pressure fringe in transmitted light. Crossed nicols. Scale bar = 0.4 mm.

Plate 6g. DM-YZ3 Same as plate 6c but illustrating the quartz-ankerite-sericite pressure fringe in transmitted light. Crossed nicols. Scale bar = 0.4 mm.

Plate 6h. CL-67 Subhedral pyrite with sieve-textured centres. Similar irregular grain boundaries in the three central grains are suggestive of brecciation. Reflected light. Scale bar = 0.4 mm.

Plate 6

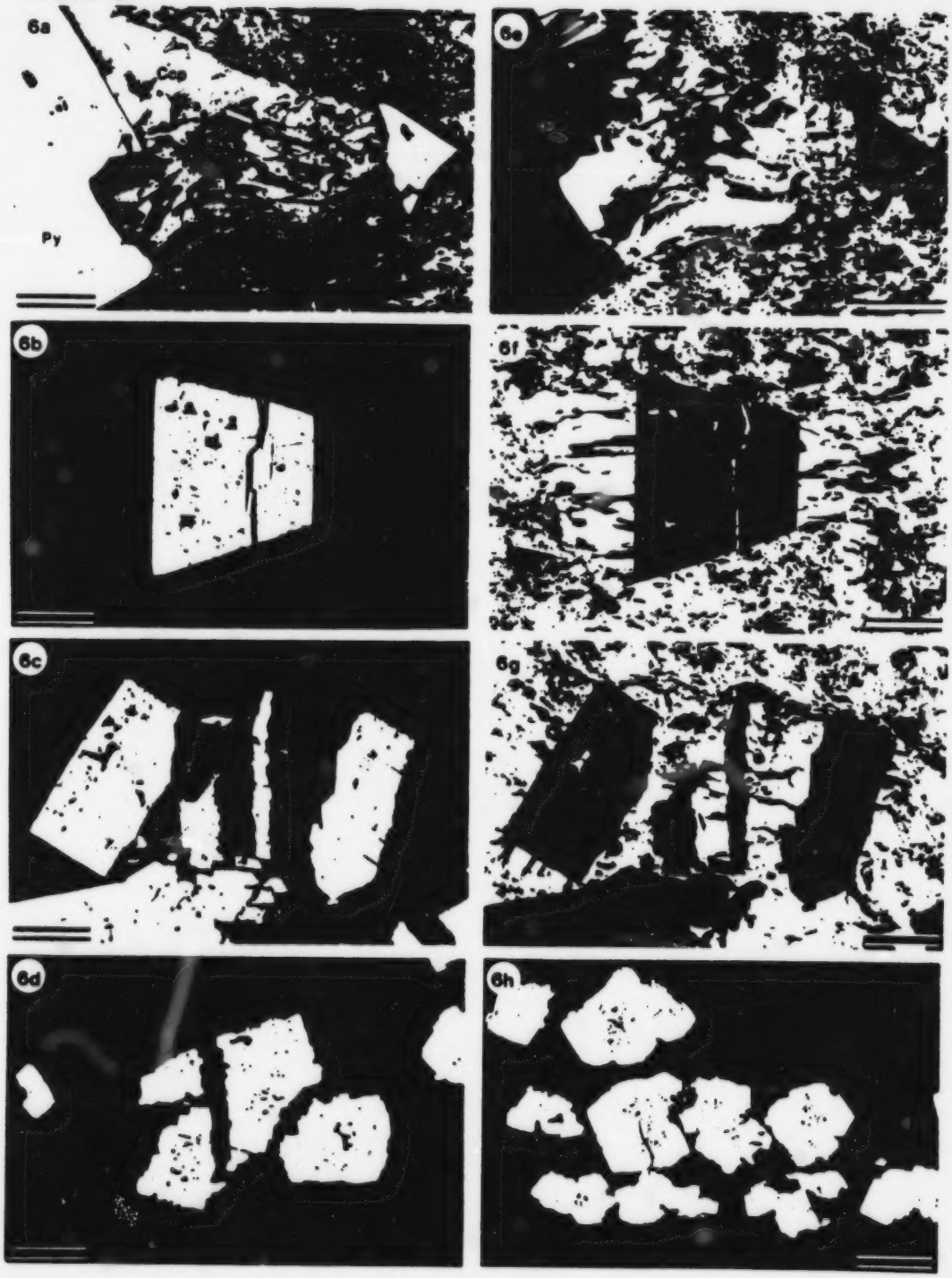

Plate 7. Photomicrogrphs of deformation textures, rutile intergrowths, and an inclusion in a quartz-feldspar porphyry dike.

Plate 7a. NC-43-782 Highly starined quartz grain in the matrix of a breccia-vein. Recrystallization occurred along deformation band boundaries. Note the undulatory, mosaic extinction. Crossed nicols. Bar scale = 1.6 mm.

Plate 7b. NC-43-782 Close-up view of Plate 7a. Crossed nicols. Bar scale = 0.4 mm.

Plate 7c. DM-6A Blood tench. Type 3 crack-seal vein. Note the quartz fibre growth normal to the vein margins and the included sliver of wall rock (lower right) in the vein. Infilling assemblage consists of quartz and ankerite. Crossed nicols. Bar scale = 1.6 mm.

Plate 7d. NC-43-902 Foliated, pervasively altered basaltic fragment included in a cross-cutting quartz-feldspar porphyy dike. Note the quartz-ankerite vein in the fragment which occurred prior to its incorporation within the dyke. This suggests that dyke emplacement post-dates alteration and gold enrichment. Crossed nicols. Bar scale = 0.1 mm.

Plate 7e. NC-22-475 Trellis-textured rutile pseudomorphing ilmenite exsolution lamellae displaying an inherited, ordered orientation. Reflected light. Bar scale = 0.1 mm.

Plate 7f. NC-7-54 Pyrite nucleating on trellis-textured rutile. Reflected light. Bar scale = 0.1 mm.

Plate 7g. NC-7-54 Pyrite grain engulfing rutile. Reflected light. Bar scale = 0.1 mm.

Plate 7h. DM-6D Blood trench. Pyrite euhedra containing engulfed rutile inclusion. Chalcopyrite and hematite are plated on pyrite. Reflected light. Bar scale = 0.1 mm.

Plate 7

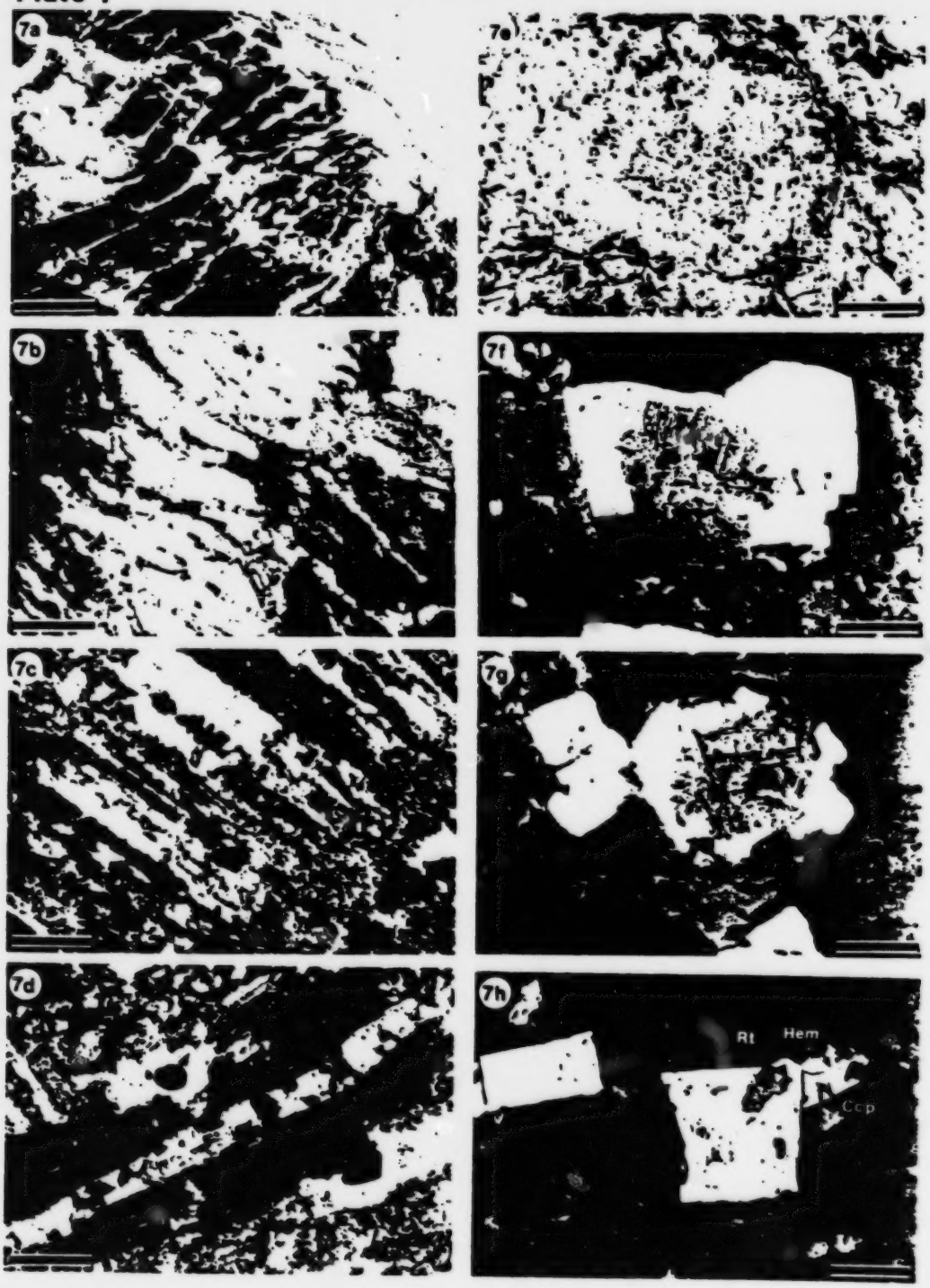

APPENDIX IV

Analytical data for samples taken from DDH NC-29 and breccia-veins on surface.

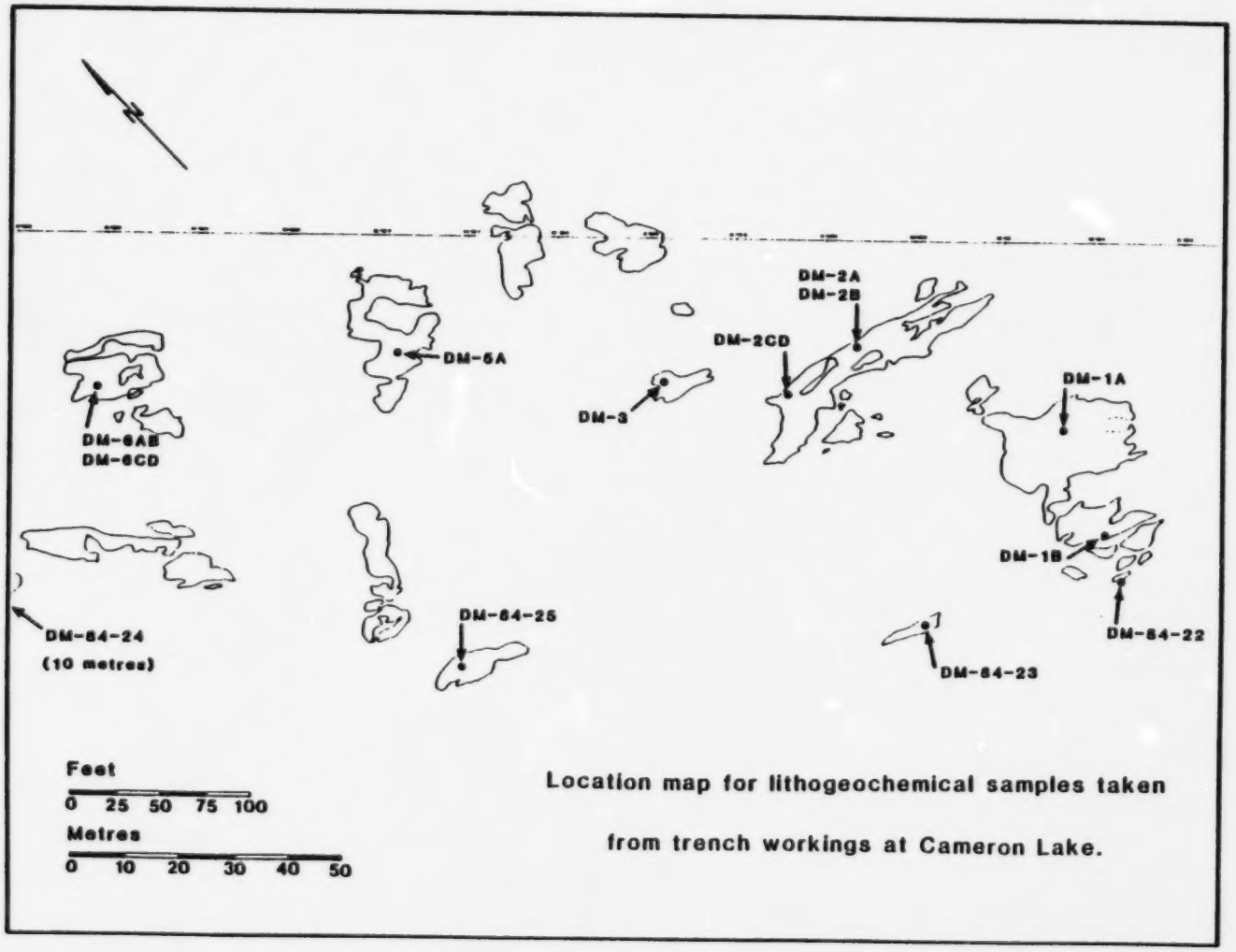

Figure 24. Location map of lithogeochemical sampling sites from trench workings.

ANALYTICAL DATA FOR SAMPLES TAKEN FROM DDH NC-29.

SAMPLE #	SiO_2	Al_2O_3	Fe_2O_3	FeO	MgO	CaO	Na_2O	K_2O	TiO_2	P_2O_5	MnO	CO_2	S	LOI	Total	Au
NC-29-150	45.60	12.30	13.60	11.27	4.93	7.53	2.55	0.40	1.11	0.07	0.20	6.70	0.12	10.10	98.34	10
NC-29-250	49.30	14.10	13.90	8.44	5.73	9.43	1.74	0.25	1.00	0.01	0.22	0.42	0.14	3.40	99.20	5
NC-29-325	47.30	12.50	13.70	8.44	5.96	8.52	1.28	0.01	1.02	0.21	0.20	3.34	0.05	6.65	97.15	20
NC-29-400	47.40	13.50	13.80	8.91	6.14	6.02	3.22	0.02	1.10	0.01	0.16	4.62	0.02	7.80	99.17	5
NC-29-425	46.60	12.70	13.40	9.68	4.98	7.07	3.43	0.03	1.11	0.01	0.20	6.70	0.15	8.90	98.43	5
NC-29-440	42.80	11.10	13.90	11.97	3.83	8.79	2.19	0.74	1.07	0.12	0.28	13.49	0.06	14.30	99.05	5
NC-29-452	42.10	12.00	10.60	8.83	4.00	10.20	1.67	1.08	0.93	0.12	0.14	16.28	0.36	17.35	100.19	20
NC-29-461	45.10	12.60	10.00	8.26	4.52	8.06	1.79	1.72	0.88	0.06	0.15	15.58	0.10	16.35	101.23	30
NC-29-468	39.80	9.94	13.60	9.96	4.38	8.99	2.85	1.78	0.88	0.20	0.28	17.73	1.74	17.65	100.35	2510
NC-29-468	38.50	9.78	14.10	10.30	4.57	9.50	2.67	1.92	0.91	0.22	0.29	18.27	1.69	18.30	100.06	1740
NC-29-480	42.00	10.50	12.50	8.89	4.75	9.17	1.80	2.31	0.95	0.01	0.18	16.95	1.35	16.30	100.47	3770
NC-29-490	53.70	8.34	9.61	5.73	3.71	7.54	4.48	0.68	0.80	0.07	0.15	13.03	2.13	13.65	102.73	15000
NC-29-495	66.60	13.58	2.38	0.92	1.06	2.34	7.32	0.16	0.32	0.05	0.03	3.42	0.94	3.80	97.64	150
NC-29-501	39.00	9.40	13.10	9.74	4.22	10.70	0.27	2.66	0.90	0.04	0.28	19.07	0.60	19.35	99.86	1980
NC-29-509	43.70	9.56	11.30	6.65	4.44	9.21	2.18	1.92	0.87	0.01	0.16	16.26	2.05	15.75	103.10	9670
NC-29-520	40.50	10.40	12.80	4.59	4.02	9.61	4.19	0.99	1.07	0.01	0.18	14.37	5.85	15.95	99.72	15000
NC-29-531	43.50	10.30	11.10	8.26	4.36	10.00	0.58	3.04	0.90	0.13	0.21	17.13	0.91	17.45	101.57	1765
NC-29-540	39.20	11.50	12.00	9.04	3.48	8.36	2.77	0.86	1.05	0.09	0.21	15.14	1.68	16.00	95.52	230
NC-29-549	41.10	12.50	12.20	7.50	3.68	9.82	2.85	0.77	1.07	0.17	0.23	15.71	2.14	16.00	100.39	240
NC-29-560	39.80	10.60	12.90	7.66	3.22	11.70	2.09	0.58	0.99	0.16	0.23	17.43	0.55	17.70	99.97	15
NC-29-585	44.30	13.20	13.60	11.12	4.67	9.55	2.59	0.09	1.29	0.13	0.19	7.84	0.12	10.80	100.41	10
NC-29-625	44.90	12.20	13.00	10.46	5.29	7.95	3.07	0.32	1.12	0.17	0.25	10.28	0.13	12.05	100.42	5
NC-29-650	43.40	12.70	14.00	10.70	5.79	8.16	1.38	0.45	1.05	0.01	0.22	12.24	0.39	13.80	100.96	10
NC-29-660	41.40	12.20	9.62	7.56	10.70	6.95	1.19	0.38	0.45	0.18	0.14	12.74	0.04	15.70	98.91	15
NC-29-671	38.00	9.25	10.20	8.58	14.50	5.67	0.21	1.98	0.34	0.01	0.16	19.18	0.01	21.25	101.57	5
NC-29-672	65.60	14.20	2.33	1.09	2.21	3.42	5.56	1.58	0.37	0.12	0.03	5.20	0.70	6.40	101.57	5
NC-29-674	37.50	10.10	9.42	7.62	12.50	5.38	0.14	2.44	0.35	0.11	0.16	19.90	0.07	20.75	98.85	30
NC-29-725	40.30	11.20	11.60	9.13	15.00	6.09	1.35	0.01	0.40	0.06	0.18	9.61	0.04	13.50	99.69	5

Values reported as weight % except * which is in ppb.
Fe_2O_3 is total iron.
LOI determined at 1000°C.
Totals calculated using major oxides and LOI; CO_2 and S were excluded.
Last three digits in sample number are depths measured in feet.
Samples collected by D.R. Melling.
Analyses performed by Bondar-Clegg and Company Limited, Ottawa.
See Appendix II for detection limits and methods.

ANALYTICAL DATA FOR SAMPLES TAKEN FROM DDH NC-29.

Depth	Au	B	Hg	Cu	Zn	Co	Ni	Cr	Ag	V	As	W	Sb	Li	Ba	Rb	Sr
NC-29-150	10	5	5	172	133	55	74	83	0.2	297	75	1	2	19	91	26	88
NC-29-250	5	18	20	192	160	58	90	97	0.2	327	34	4	9	7	20	10	191
NC-29-325	20	13	15	181	125	58	90	111	0.2	317	31	1	11	14	7	10	133
NC-29-400	5	7	20	211	81	54	68	63	0.2	337	<5	1	3	13	13	8	87
NC-29-425	5	5	15	212	146	57	64	56	0.2	330	<5	1	6	10	3	8	114
NC-29-440	5	20	15	143	111	38	48	50	0.2	255	<5	1	2	16	56	25	67
NC-29-452	20	43	15	159	105	51	79	72	0.2	270	22	1	4	8	51	33	155
NC-29-461	30	134	5	112	92	36	50	51	0.2	202	5	1	2	4	114	34	161
NC-29-468	2510	18	15	138	96	51	63	67	0.5	213	41	4	2	6	72	44	99
NC-29-468	1740	17	10	129	89	42	53	53	0.4	197	28	2	2	6	72	46	108
NC-29-480	3770	23	10	146	110	49	57	43	1.3	404	5	1	5	1	107	62	203
NC-29-490	15000	14	20	135	70	30	35	35	4.2	122	14	8	2	7	32	20	154
NC-29-495	150	16	10	3	38	8	28	15	1.2	17	5	10	5	1	46	8	99
NC-29-501	1980	10	10	152	105	46	52	33	0.4	299	5	1	7	1	110	107	154
NC-29-509	9670	21	20	171	102	46	52	40	0.8	244	20	1	3	1	77	57	206
NC-29-520	15000	34	20	137	98	48	53	40	4.2	260	80	5	7	1	80	22	242
NC-29-531	1765	30	<5	144	87	45	59	51	0.3	227	13	8	2	7	161	74	133
NC-29-540	230	32	15	158	93	49	58	34	0.3	278	144	1	3	8	79	28	151
NC-29-549	240	36	10	143	80	40	47	32	0.2	267	292	1	2	15	87	37	154
NC-29-560	15	31	10	176	79	36	43	30	0.2	281	13	1	15	6	68	16	165
NC-29-585	10	5	10	207	137	52	56	29	0.2	333	5	1	8	14	100	8	84
NC-29-625	5	5	5	139	124	41	51	36	0.2	300	5	1	11	11	105	8	70
NC-29-650	10	38	10	199	154	50	56	31	0.2	309	5	1	6	11	5	8	106
NC-29-660	15	20	15	1	92	49	244	407	0.2	144	5	1	4	15	50	8	134
NC-29-671	5	20	5	19	85	64	404	1369	0.2	112	5	1	5	18	98	45	79
NC-29-672	5	104	10	34	22	11	28	27	0.2	40	5	1	2	15	152	25	162
NC-29-674	30	28	10	28	87	60	388	721	0.2	131	5	1	5	8	180	26	95
NC-29-725	5	2	5	30	120	72	411	1123	0.2	116	5	1	2	17	5	5	105

Analyses reported in ppm except * which is given in ppb.
Last three digits of sample numbers are depths are measured in feet.
Samples collected by D.R. Melling.
Analyses performed by Bondar-Clegg and Company Limited, Ottawa.
See Appendix II for detection limits and methods.

ANALYTICAL DATA FOR SAMPLES TAKEN FROM GOLD-BEARING BRECCIA-VEINS OCCURRING AT SURFACE.

SAMPLE #	SiO_2	Al_2O_3	Fe_2O_3	FeO	MgO	CaO	Na_2O	K_2O	TiO_2	P_2O_5	MnO	CO_2	S	LOI	Total	Au*
DM-1A	53.40	8.12	9.60	4.52	3.42	9.04	2.68	0.75	0.64	0.04	0.16	12.30	2.39	11.50	97.75	11000
DM-1B	51.90	11.30	7.49	4.70	3.09	8.47	5.41	0.64	0.73	0.02	0.14	12.30	1.43	11.70	99.10	1880
DM-2A	52.00	14.34	9.10	2.87	2.14	5.58	8.00	0.08	0.50	0.01	0.08	8.34	4.35	7.30	98.22	12200
DM-2B	53.40	8.14	9.04	6.03	3.68	7.96	3.70	0.36	0.77	0.08	0.13	3.14	1.26	10.35	97.61	1800
DM-2CD	35.60	9.63	11.50	5.52	4.84	11.90	5.03	0.32	0.87	0.08	0.19	17.70	3.62	14.20	92.28	15000
DM-3	37.00	11.94	12.20	6.85	5.08	11.94	4.50	1.06	0.94	0.05	0.18	17.70	2.96	15.90	99.04	13000
DM-5A	78.60	4.29	3.76	1.20	0.75	1.93	2.36	0.04	0.26	0.13	0.06	2.94	1.43	2.70	94.41	1200
DM-6AB	71.80	6.78	5.40	2.33	1.81	4.84	2.98	0.22	0.46	0.18	0.10	6.46	1.68	6.20	100.42	1960
DM-6CD	58.10	6.97	7.84	4.15	2.82	7.35	3.39	0.40	0.67	0.07	0.17	11.20	2.01	9.50	96.83	4000

Values reported as weight % except * which is in ppb.
Fe_2O_3 is total iron.
LOI determined at 1000°C.
Totals calculated using major oxides and LOI; CO_2 and S were excluded.
Samples collected by D.R. Melling.
Analyses performed by Bondar-Clegg and Company Limited, Ottawa.
See Appendix II for detection limits and methods.

ANALYTICAL DATA FOR SAMPLES TAKEN FROM
GOLD-BEARING BRECCIA-VEINS OCCURRING AT SURFACE.

Sample #	Au*	B	Hg*	Cu	Zn	Co	Ni	Cr	Ag	V	As	W	Sb	Li	Ba	Rb	Sr
DM-1A	11000	13	30	106	70	33	48	30	1.5	237	5	12	5	1	107	32	259
DM-1B	1880	10	15	26	63	31	40	31	0.8	156	5	28	5	1	82	39	185
DM-2A	12200	7	35	24	52	43	47	11	1.8	36	12	10	5	1	11	8	211
DM-2B	1800	9	15	270	75	31	35	26	0.8	121	40	10	5	1	46	22	185
DM-2CD	15000	6	45	183	101	44	48	24	2.5	125	39	20	5	1	46	24	410
DM-3	13000	10	20	185	102	62	80	61	1.9	314	8	12	5	1	217	72	371
DM-5A	1200	14	20	10	23	13	17	9	1.0	23	5	10	5	1	50	8	35
DM-6AB	1960	13	15	41	41	20	25	17	0.6	90	6	10	5	1	36	24	69
DM-6CD	4000	12	25	96	70	30	32	26	1.3	165	5	10	5	1	57	39	120

Analyses reported in ppm except * which is given in ppb.
Samples collected by D.R. Malling.
Analyses performed by Bondar-Clegg and Company Limited, Ottawa.
See Appendix II for detection limits and methods.